

AN ABSTRACT OF THE THESIS OF

HAROLD RICHARD HOLBO for the DOCTOR OF PHILOSOPHY
(Name) (Degree)

in FOREST ENGINEERING
(HYDROLOGY) presented on 23 June 1972
(Major) (Date)

Title: THE ENERGY BUDGET OF A PUMICE DESERT

Abstract approved: *Lloyd W. Gay*
Lloyd W. Gay

The energy budget of a pumice desert surface was analyzed under clear skies during early, mid- and late summer periods. The pumice site is in the semi-arid plateau region of Central Oregon at an elevation of about 1500 meters. The flat pumice surface is approximately 250 hectares in extent, and is bordered by a sparse lodgepole pine forest. Energy budget components of net radiation, soil heat flux, sensible heat flux, and latent heat flux were evaluated for one clear day in each of the three measurement periods.

The daily energy budget totals were (cal/cm^2 day):

	<u>17 July 1969</u>	<u>13 August 1969</u>	<u>4 September 1969</u>
Net radiation	258	228	194
Soil heat flux	-7	-14	-2
Sensible heat flux	-197	-197	-180
Latent heat flux	-54	-17	-11

The most significant features of the pumice desert energy budget were: 1) Radiant energy transformed by the pumice surface (net

radiation) was approximately 60 percent of the amount measured over a nearby forested surface; 2) Energy transfer into the soil amounted to less than 3 percent of the energy supplied to the surface by net radiation, while surface temperatures varied through a 50°C range each day; 3) Sensible heat flux dissipated 85 percent of the net radiation supplied to the surface; and, 4) Evaporation at the pumice site averaged less than 0.05 cm per day, although the pumice beneath the dry surface layer remained moist.

A unique stability correction, ϕ , for the aerodynamic flux analysis of sensible or latent heat was developed to extend over the wide stability range found at the pumice site. The form of this correction during unstable conditions is:

$$\phi = (1 - 34\text{Ri})^{0.55},$$

where Ri is Richardson's stability parameter.

A method for estimating the uncertainty of the measurement system and of the resultant flux analyses was developed and applied to the results of this study. The average relative uncertainties of the net radiation and soil heat flux analyses were estimated to be less than 1 percent and 5 percent, respectively. The average uncertainty of the sensible heat flux analyses was estimated to be 3 percent when using an aerodynamic model, and 9 percent when using the Bowen

ratio model. The corresponding figures for latent heat flux are 25 percent with the aerodynamic model and 30 percent with the Bowen ratio model. The larger percentage uncertainties associated with latent heat are due in part to the small vapor pressure gradients near the pumice surface, relative to the measurement capabilities, and in part to the small values of the latent heat flux.

This study demonstrates the applicability of micrometeorological theory in characterizing complex microclimatological relationships by presenting them in a concise, comparable form through use of the energy budget.

The Energy Budget of a Pumice Desert

by

Harold Richard Holbo

A THESIS

submitted to

Oregon State University

in partial fulfillment of
the requirements for the
degree of

Doctor of Philosophy

June 1973

APPROVED:

Ray W. Gay
Associate Professor of Forest Engineering

George W. Brown in charge of major
Associate Professor of Forest Engineering

Patrick H. Cochran
Research Soil Scientist

William H. Ferrell
Professor of Forest Management

Shudson
Graduate Council Representative

William A. Davis
Head of Department of Forest Engineering

W. Hansen
Dean of Graduate School

Date thesis is presented 23 June 1972

Typed by Clover Redfern for Harold Richard Holbo

ACKNOWLEDGMENT

The work upon which this thesis is based was supported in part by funds provided by the U.S. Department of Interior, Office of Water Resources Research, as authorized under the Water Resources Research Act of 1964, and administered by the Water Resources Research Institute, Oregon State University. The field work was supported in part by the Pacific Northwest Forest and Range Experiment Station under Cooperative Agreement Supplement No. 58, FS-PNW-1203. The data handling, processing and analysis was supported in part by grants-in-aid from the Computer Center, Oregon State University.

TABLE OF CONTENTS

<u>Chapter</u>	<u>Page</u>
I. INTRODUCTION	1
The Problem	1
The Energy Flow Approach to the Study of Microclimate	2
Considerations in the Application of the Energy Budget	5
The Objective	6
II. FUNDAMENTAL CONSIDERATIONS OF THE ENERGY BUDGET	8
The Energy Budget at the Pumice Surface	8
System Definition	8
Principal Energy Budget Components	9
The Energy Budget Equation	13
Micrometeorological Relationships	13
Net Radiation Flux	14
Soil Heat Flux	17
Sensible and Latent Heat Fluxes	19
Summary	29
III. EXPERIMENTAL METHODS	30
Site Description	30
Measurement System Description	33
Data Acquisition	33
Instrumentation	35
Measurement System Performance	38
Mean Value Determination	40
Sensor Response	40
Frequency of Samples	41
The Psychrometer Response	43
Time Period of Analysis and Data Averaging	44
Averaging Periods	44
Numerical Integration	45
Gradient Approximation and Similarity	46
Summary	53
IV. ENERGY BUDGET RESULTS	54
The Uncertainty of Component Evaluation	55
The Stability Correction Function	58
Hourly and Daily Component Evaluation	63
Days of Analysis	63
Analytical Procedure	63
Tabulation of Results	64

<u>Chapter</u>	<u>Page</u>
Net Radiation	71
Soil Heat Flux	74
Sensible Heat Flux	80
Latent Heat Flux	84
Summary	85
V. CONCLUSIONS	86
The Applicability of Micrometeorological Relationships	86
The Bowen Ratio Model	87
The Aerodynamic Model	88
Analytical Uncertainties	89
Significant Features of the Energy Budget	90
Possibilities for Environmental Modification	92
Summary	93
BIBLIOGRAPHY	95
APPENDICES	102
Appendix I: Symbols and Definitions	102
Appendix II: Data Tabulation	105
Appendix III: Analytical Equations	109
Appendix IV: The Uncertainty of Measurement and Analysis	113

LIST OF TABLES

<u>Table</u>	<u>Page</u>
1. Overall system performance.	40
2. Average uncertainty of flux density evaluation.	56
3. Pumice surface energy budget by hour and day for 17 July 1969.	65
4. Pumice surface energy budget by hour and day for 13 August 1969.	66
5. Pumice surface energy budget by hour and day for 4 September 1969.	67
6. Daily integrals of the energy budget components.	71
7. Volumetric heat capacities for the pumice soil profile.	75
 <u>Appendix Table</u>	
II-1. Microclimate measurements at the pumice site, 17 July 1969.	106
II-2. Microclimate measurements at the pumice site, 13 August 1969.	107
II-3. Microclimate measurements at the pumice site, 4 September 1969.	108
IV-1. Performance specifications of the data acquisition system.	117

LIST OF FIGURES

<u>Figure</u>	<u>Page</u>
1. Aerial photograph of the pumice site taken in June 1954.	32
2. Instrumentation at the pumice site.	36
3. A representative midday windspeed profile from the pumice site.	48
4. A representative midday temperature profile from the pumice site.	49
5. A representative midday vapor pressure profile from the pumice site.	50
6. Relative similarity of properties at successive levels from the pumice surface.	52
7. A stability correction function fitted to analyses from the pumice site data.	59
8. Comparison of the stability correction function developed for the pumice site [$\phi = (1 - 34\text{Ri})^{0.55}$] to other forms appearing in the literature.	61
9. Pattern of energy budget components at the pumice site during 17 July 1969.	68
10. Pattern of energy budget components at the pumice site during 13 August 1969.	69
11. Pattern of energy budget components at the pumice site during 4 September 1969.	70
12. Soil temperature profiles during 17 July 1969 at the pumice site.	77
13. Soil temperature profiles during 13 August 1969 at the pumice site.	78
14. Soil temperature profiles during 4 September 1969 at the pumice site.	79

<u>Appendix Figures</u>	<u>Page</u>
IV-1. Uncertainty of voltage measurement.	120
IV-2. Pumice site ice bath data --4 September 1969.	123
IV-3. Measurement uncertainty of net radiation for an instrument having calibration coefficient, a , of $60 \text{ mV cm}^2\text{min/cal}$.	127

THE ENERGY BUDGET OF A PUMICE DESERT

I. INTRODUCTION

The pumice soils of the Central Oregon uplands are typically vegetated by lodgepole and ponderosa pine forests. The economic welfare of this region is dependent primarily upon this single natural resource. Timber harvesting and processing industries employ more than two-thirds of the industrial work force, according to a survey of the Industrial Development Research Council (1968). Most of the forest land is federally owned and managed; consequently, the government is the third largest employer in the region. Also, the region is renowned for its year-round recreational opportunities, which are based almost entirely on the forest lands, attracting many visitors for hunting, fishing, camping, skiing, hiking and sight-seeing.

The Problem

Scattered throughout this forested region are barren pumice deserts. These deserts are largely geological in origin (Horn, 1968), but their persistence to recent time is indicative that afforestation on them is achieved only slowly. Regeneration of areas cleared by logging is also observed to be difficult, and there is concern that mismanagement may result in the creation of more pumice deserts as a result of restricting factors in the environment.

The factors restricting tree establishment and growth in this region have been identified in a number of recent studies (Cochran et al., 1967; Hermann, 1968, 1970; Wagg and Hermann, 1962; Youngberg and Dryness, 1964). These studies point to several environmental or site factors which result in a severe microclimate at pumice surfaces. Hermann (1968) places environmental moisture as the most important limiting factor to successful seeding of pine in the region. Cochran et al. (1967) emphasize the thermal characteristics of the pumice soil as a dominant site factor influencing the microclimate, and thus tree establishment. The significance of these factors is clearly evident in these field studies, but as yet no practical solution to the problem of establishing and maintaining forests in this harsh microclimate has been advanced. Efforts at reducing the harshness of this microclimate have met with little success. Detailed studies of the microclimate of pumice surfaces in the region can therefore be justified on the basis of the value of the forest resource.

The Energy Flow Approach to the Study of Microclimate

The basic relationship between the microclimate and the flow of energy in the environment was demonstrated in 1927 by Geiger (1966). Because of this relationship the state of the environment is considered to be the consequence of the flows of energy by radiative, conductive, or convective processes, or by chemical transformation

(predominantly evaporation). The examination of these energy flows is fundamental to understanding the microclimate. Such understanding is essential for eventual modification of climatic factors at a given site.

The energy flow approach has been widely applied in the study of the environment of specific surfaces. The studies of Denmead (1969), Lemon (1965), McIlroy and Angus (1964), Rider and Robinson (1951), Tanner (1967), and Turner (1965) are but a few examples where energy flows have been evaluated as fundamental components of the microclimate.

In ecology, Gates (1965) has espoused the idea of characterizing the environment of a specific surface using energy flow relationships. He has suggested that energy relationships are useful in explaining the natural distributions of plants. This is not altogether unexpected, because large scale differences in plant production are commonly known to be correlated to regional climates, which in turn reflect the prevalent energy flows in the respective environments. On the micro-scale certain environmental factors, such as the moisture and thermal characteristics already mentioned, obviously have critical influences on plant establishment and on later growth and productivity. However, most attempts at quantifying these small scale influences have been incomplete because of the lack of fundamental information about the energy flow processes that have created the microclimate. It is a premise of this research that an examination of the energy flow

processes is basic to the evaluation of environmental influences at the microclimatological, or plant, level.

The potential of using energy flow information for silvicultural advantage has been widely recognized, and was specifically emphasized by Woods (1960). Most notable among the proponents of this approach to problems in forestry have been Baumgartner (1956), Miller (1955), Rauner (1960), and Reifsnyder and Lull (1965). The advantages of the energy flow approach include: 1) application to the field situation without alteration of the experimental surface; 2) a sensitivity suitable for short-term observations of environmental relationships; 3) the non-destructive nature of the technique, which allows repeated sampling at the same site; and, 4) direct comparison with other energy flow studies, owing to the fundamental nature of the analysis.

Inherent in the application of energy flow techniques is the desirability of treating the experimental surface as a system for which each of the energy flows are studied as components of an energy budget. An energy budget is an accounting of the incoming and outgoing energy flows, and the changes in energy storage by the system. Because energy is always conserved, the sum of these energy components for the system must be zero. Consequently, the energy budget is a convenient framework for microclimatological analysis.

Considerations in the Application of the Energy Budget

Despite the advantages of the energy budget, its application has met with varying success in the field. For many investigators, the major difficulties encountered in the energy budget approach have been associated with the need for relatively elaborate and expensive instrumentation (Namken et al. , 1968). Also, the more elaborate the instrumentation, the greater the expertise needed to acquire and handle the data collected.

The instrumentation requirements are large in energy budget studies because all of the major energy flows are being evaluated from measured values of representative properties in the environment. Since these properties change as the energy flows change in time, they must be repeatedly sampled throughout the day. The large amounts of data that are accumulated cause significant computational problems.

High expense and data handling problems are not the only difficulties encountered in the energy budget approach. The ready application of energy budget principles to many surfaces of practical interest is further restricted by limitations in theory and experimental design. For example, the scale and variability of forested surfaces create special difficulties in the application of energy flow analyses (Tanner, 1968). As a result, the majority of energy flow analyses have been based on data collected during clear weather periods over surfaces

that are large and flat. This has of course been necessary to facilitate the refinement and extension of the micrometeorological theory dealing with energy flow mechanisms. However, the analyses have seldom considered the total energy budget response of a natural surface over a wide range of environmental conditions (Webb, 1965; Lumley and Panofsky, 1964). This theoretical preoccupation is justified, but it is troublesome to those who are interested in specific microclimatological problems, and who view energy budget analysis as a tool to gain insight into environmental relationships. Fortunately, from a theoretical standpoint the pumice desert situation offers an excellent and unique experimental site on which to study environmental relationships pertinent to the problems of afforestation.

The Objective

The objective of this study is to evaluate the principal energy flows occurring at the pumice surface during the summer when environmental contrasts are greatest. The diurnal energy budget of this surface will be developed from micrometeorological observations made specifically for this purpose. These measurements will be examined to determine their suitability for the application of analytical relationships that have been proposed in the literature. These analytical relationships will also be tested for their applicability in representing the surface energy flows. And finally, the analytical errors

will be estimated from considerations of the adequacy of the measurements.

The information gained in this study will contribute to the solution of the problem of establishing and maintaining forests on the pumice soils in Central Oregon. It will provide a better understanding of the microclimatic conditions encountered by plants in similar harsh environments. The information will also be useful for comparison with similar analyses of other types of natural surfaces and for comparison with surfaces that have been modified to attempt environmental control.

II. FUNDAMENTAL CONSIDERATIONS OF THE ENERGY BUDGET

The purposes of this chapter are: 1) to identify the pumice desert surface as a system for energy budget analysis; 2) to define the principal components of the energy budget; and, 3) to develop micro-meteorological relationships for the evaluation of these components.

The Energy Budget at the Pumice Surface

System Definition

When dealing with energy budgets it is necessary to identify the system with which the energy components are to be associated. This is required to insure completeness of the energy budget analysis. Ideally, perfect correspondence should exist between the system as conceived by the investigator and the system as described by the measurements. Realization of this goal is foremost in the successful application of energy budget theory.

In the most general sense a system is a volume with prescribed boundaries. For microclimatological purposes the systems of most interest are at the earth's surface. Here the conservation of energy is chiefly the conservation of heat, with consideration of kinetic energy entering only as it influences the disposition of that heat. Energy budget, or energy conservation, theory requires any gains or losses of energy by a system to be balanced by a corresponding change in energy

content within the system.

Since there is no plant canopy at the pumice site, all of the energy exchange takes place at the pumice-atmosphere interface. The absence of a canopy allows the definition of the system to be simplified to a two-dimensional plane, eliminating the need to consider a three-dimensional, volumetric system. Since the plane has no finite thickness, there can be no lateral energy transfers through the sides of the system, neither can there be any contained energy. Evaluation of the energy budget thus becomes a problem of the evaluation of the budget components acting normal to the plane of the surface.

Principal Energy Budget Components

The principal energy budget components are becoming generally recognized to the extent that comprehensive, definitive treatments can be found in several recent texts (Sellers, 1965; Munn, 1966; Lowry, 1969). However, it will be helpful to define them from the perspective of this study.

The principal components of the energy budget are the result of the transfer of energy by the processes of radiation, conduction, and convection, or by chemical transformation, as occurs in the evaporation of water. The energy budget components may be defined relative to the operation of these processes at the surface.

Radiation is a process wherein heat transfer is accomplished by

electromagnetic phenomena. As a result, no intervening medium is required for radiant energy to be transferred from the surface. Radiation occurs as a result of the temperature of the surface. The spectral quality and intensity of the radiation varies with the temperature of the surface and with its relative ability to radiate. Radiative transfer rarely proceeds in one direction only, there being simultaneous transfer both away and toward the surface with other objects in the field of view. It is thus the net transfer of radiative energy which is of interest as an energy budget component.

The net transfer of radiation to the system is called net-radiation, symbolized Q^* .^{1/} It represents the difference between the incoming and outgoing flows of radiant energy. By convention, when the incoming radiation exceeds the outgoing radiation Q^* is considered positive. Net radiation is measured on the basis of a unit area of the system. It is also measured in terms of the prevailing rate of transfer per unit time, or flux. Consequently it is commonly called net radiation flux density, although the word flux is frequently used synonymously with flux density.

Conduction is a process by which heat transfer is accomplished by direct molecular interaction without displacement, and can occur

^{1/} Radiation symbols used correspond to the uniform terminology proposed in the 3rd Edition, Guide to Meteorological Instrument and Observing Practices, WMO-No. 8. TP. 3, World Meteorological Organization, Geneva, 1969.

within a single phase or between phases. Conductive heat transfer requires a medium and occurs in the direction of lower temperatures. The intensity of heat conduction varies with difference in temperature and with the thermal characteristics of the medium. Conduction is measured on the basis of a unit area of the system per unit time, i. e., a flux density. When conductive heat flux is directed toward the system it is considered positive.

The energy budget component wherein conduction performs the significant role is the soil heat flux, symbolized $G, \frac{2}{/}$ which accounts for the transfer of heat through the soil. The evaluation of G is made by the application of the principles of conductive heat transfer.

Conduction is also the controlling process for the transfer of heat from the surface to the air, but it is not the mode of transfer within the air itself. For this reason heat transfer in the air is evaluated using the principles of convective heat transfer.

Convection is a process by which heat transfer is accomplished by the displacement of molecules within a fluid. Convective heat transfer requires a medium and occurs in the direction of lower temperatures. The intensity of heat convection varies with difference in temperature and with the mechanism effecting displacement, or

$\frac{2}{/}$ This symbol for soil heat flux, or ground flux, was chosen to conform with the general practice followed in current journals. This consideration also govern the choice of symbols made throughout the text.

mixing, of the molecules of fluid. Mixing can be effected by buoyant forces, called free convection, or by winds, called forced convection. Convection is measured on the basis of a unit area of the system per unit time, or flux density. Convective heat flux directed toward the system is considered positive.

The energy budget component which involves the transfer of heat in the air by convection is the sensible heat flux, symbolized H . The term "sensible" implies the sensed temperature aspect of the analysis, although the same principle is used for G . However, the term "sensible" as used in the literature applies primarily to the analysis of convective heat transfer as an energy budget component.

The transformation of water between phases utilizes significant amounts of heat energy. Evaluation of this energy, the so-called latent energy, is necessary for the complete energy budget analysis if the water enters or leaves the system. Because the same convective mechanism which transports heat also transports water molecules, it is convenient to evaluate the flux density of water vapor as a convection process. This is readily converted to energy units by multiplication with the latent energy, λ , required to vaporize (or condense) the quantity of water transferred. Thus the energy budget component which involves the transformation energy of water is called latent heat flux and is symbolized λE . When the vapor flux is directed toward the system, λE is considered positive.

The Energy Budget Equation

Assembling the principal energy budget components, the basic energy budget equation can be written:

$$Q^* + G + H + \lambda E = 0, \quad [1]$$

the symbols having been defined as net radiation flux, soil heat flux, sensible heat flux, and latent heat flux, respectively. Standard units of these fluxes are calories per square centimeter per minute. Since all components cannot be of the same sign, that is, be acting in the same direction, the correct sign must be indicated from the relationships used for analysis. Because the pumice desert system is a two-dimensional surface, it is understood that the evaluation of these components is needed in the direction normal to the surface only.

Micrometeorological Relationships

The attainment of relationships permitting the evaluation of energy fluxes from micrometeorological measurements has been the objective of many investigations reported in the literature. The general form taken by these relationships is governed by knowledge of the mechanisms of energy transfer as adapted to the capabilities of instrumentation and data processing. This section presents a review of the fundamental relationships appropriate to the analyses of energy

fluxes for the pumice surface. The formulations assumed by these relationships for computational purposes are given in Appendix III.

Net Radiation Flux

The net radiation flux, Q^* , of plane surfaces is easiest of the energy budget components to measure. Instrumental developments in recent years have made the direct measure of Q^* a relatively straightforward procedure (Suomi et al., 1954; Funk, 1959; Fritschen, 1963). It is not the intent here to review the relationships governing the measurement of this component, which are summarized by Sellers (1965) and by van Bavel et al. (1963), but merely to include mention of net radiation flux for completeness.

It is often useful to examine net radiation in detail in order to determine certain characteristics or properties at the surface. The initial step in doing this is to expand the net radiation into a balance equation in which the contributing radiant energy fluxes are separately identified:

$$Q^* = K\downarrow + L\downarrow - K\uparrow - L\uparrow, \quad [2]$$

where K is used for the shortwave components and L for the long-wave. The incident solar radiation is represented by $K\downarrow$, while $L\downarrow$ is the incident atmospheric radiation, $K\uparrow$ is the reflected solar radiation, and $L\uparrow$ is the outgoing surface radiation. The solar

fluxes are characterized by wavelengths shorter than 4μ , and the longwave fluxes by wavelengths longer than 4μ . The signs affixed on the right side of Equation [2] take cognizance of the constant direction of these fluxes so that it is only necessary to determine their magnitude by measurement. The direction of Q^* , however, may go either positive or negative.

Albedo. The albedo, α , is an important surface characteristic because most of the energy dissipated at the surface originates from the conversion of solar radiation into longwave radiation or into non-radiant forms. Albedo is a proportional measure of the amount of solar radiation converted. It is directly determined by comparing the reflected shortwave radiation to that arriving at the surface of the system:

$$\alpha = K\uparrow / K\downarrow . \quad [3]$$

The albedo varies with the type of surface and with changes in the surface in time. It is a useful index for comparing the radiant response of different surfaces. Excepting for the wavelength-selective nature of the sensor, shortwave radiation is measured using instruments very similar in design to those used in measuring net radiation flux.

Surface Temperature. The outgoing longwave radiation, $L\uparrow$, originates for the most part at the surface, due to its temperature. Because this flux has longer wavelengths than solar radiation, it is

relatively easy to measure using appropriate radiometers. The outgoing longwave flux actually consists of three components: the outgoing surface radiation, L_g ; the reflected atmospheric radiation, r ; and, the outgoing atmospheric radiation, $A\uparrow$, which originates in the air layer between the surface and the measuring radiometer. Excepting in special instances as discussed by Funk (1960), this latter component can be disregarded, since it is relatively small. The reflected atmospheric radiation is also small, owing to the low reflectance of the surface to longwave radiation. For surfaces which may be slightly reflective the inclusion of r in $L\uparrow$ tends to partially correct for the correlated reduction in L_g . The result is that $L\uparrow$ primarily represents the surface radiation. Correspondingly, the surface temperature, TS , can be measured based on the amount of longwave radiant energy leaving the surface by employing the Stefan-Boltzmann law:

$$TS = (L\uparrow / \epsilon \sigma)^{1/4} - 273.16, \quad [4]$$

where ϵ is the longwave emissive ability of the surface (usually close to one), and σ is the Stefan-Boltzmann constant. The number 273.16 converts TS from degrees Kelvin to the more conventional Celsius scale.

If the other components in Equation [2] are measured it is seen that $L\uparrow$ can conveniently be obtained as a residual. The measure of

TS gotten by this technique is useful in the analysis of the soil heat flux. It may also be a singularly interesting micrometeorological property, particularly in extreme environments. This radiometric technique is preferred over contact measurement because of the difficulty in positioning temperature sensors in contact with the surface.

Soil Heat Flux

The basic equation for heat conduction in the soil can be developed using an energy conservation consideration of an incremental volume of soil (e. g. , van Wijk and de Vries, 1963). Since transfer is proceeding normal to the surface the applicable expression of this relationship is:

$$\partial G / \partial z = C(\partial T / \partial t), \quad [5]$$

where z is the distance from the surface, C is the volumetric heat capacity of the soil, T is the soil temperature, and t is time.

A solution for the soil heat flux density was obtained from Equation [5] by Carson (1961) by integrating the change in soil heat storage with time for small increments of depth beginning at the surface and ending at the point $z = 3d$, where d is the damping depth of the soil. The damping depth is a measure of the penetration of the diurnal temperature wave into the soil. Damping depths of 8 cm are typical for pumice soils (Cochran et al., 1967). The integral of Equation [5]

can be approximated by

$$G = \sum_{z=0}^{z=3d} C_i (\Delta T/2)_i \Delta z_i / \Delta t \quad [6]$$

In this equation $(\Delta T/2)_i$ is the mean temperature change across increment Δz_i for the i th layer of soil during time period Δt .

The mean temperature change may be calculated as

$$(\Delta T/2)_i = ((T_{t-1} - T_t)_{z_1} + (T_{t-1} - T_t)_{z_2}) / 2, \quad [7]$$

in which z_1 and z_2 indicate measurement levels at the boundaries of the soil layer increment Δz_i . Steady state is assumed when Δt is sufficiently long.

The volumetric heat capacity of each layer (C_i) must be estimated for each layer from soil samples taken at the site. The values are computed using the relationship (van Wijk and de Vries, 1963)

$$C_i = x_s C_s + x_w C_w + x_a C_a, \quad [8]$$

x being the volume fraction and C the volumetric heat capacity, respectively, of the soil (s), of the water (w), and of the air (a). Determinations of heat capacity and temperature must conform to the water content and horization of the soil profile.

Sensible and Latent Heat Fluxes

The evaluations of the sensible heat flux density, H , and the latent heat flux density, λE , are more involved than the measurement of net radiation or soil heat flux because the mechanism of transfer is substantially more difficult to characterize. Sensible and latent heat flux relationships may be grouped together because both are convective processes and are best characterized with respect to the turbulent action of the wind. In the development of certain analytical models that characterize these fluxes, it is useful to consider the momentum flux density, τ . The momentum flux is a measure of the kinetic energy imparted to the surface by the wind, causing mixing of the air. Therefore, the intensity of convective processes is related to τ .

The Eddy Transfer Equations. Physical models for the vertical transfer of momentum, sensible heat, and latent heat are based upon two principal assumptions. One is that the surface is homogeneous, with the resulting development of a predictable pattern of air flow. The other is that the transfer rates are constant between the surface and the level of flux evaluation, meaning that steady state conditions prevail. The models which result are known as the "eddy transfer" equations, because transfer is effected largely by the eddying motion of the air in turbulent flow. These equations are well known. The

forms used in this investigation are:

$$\tau = \rho K_M (\partial u / \partial z), \quad [9]$$

$$H = \rho C_p K_H [\partial (T_d + \Gamma z) / \partial z], \quad [10]$$

and

$$\lambda E = (\rho \lambda \epsilon / p) K_V (\partial e / \partial z). \quad [11]$$

In these equations the facility with which transfer may be accomplished is represented by the eddy diffusivities of momentum, heat, and vapor, and are shown as K_M , K_H , and K_V , respectively, while u , T_d , and e are the horizontal windspeed, dry-bulb or air temperature, and vapor pressure of water in the air. The vertical gradients of these properties are measures of the tendency for transfer to proceed, and establish the direction of the transfer. Constants are: the density of the air, ρ ; the specific heat of the air, C_p ; the adiabatic lapse rate (0.0001°C/cm), Γ ; the latent heat of vaporization, λ ; the ratio of the molecular weight of water to that of air, ϵ ; and the atmospheric pressure, p . These equations were derived for steady state conditions, so mean values of the properties must be used, with the effect of momentary fluctuations removed.

The Bowen Ratio Model. Equations [9], [10], and [11] are not readily applied as written since each contains an undefined eddy diffusivity term. They are generally applied in combination with other

known relationships. The most widely used combination relationship is attributed to Bowen (1926) and is formed by the ratio of Equation [10] with Equation [11], defining the "Bowen ratio," β :

$$\beta = \frac{H}{\lambda E} = \frac{\rho C_p \rho K_H \partial(T_d + \Gamma z) / \partial z}{\rho \lambda \epsilon K_V (\partial e / \partial z)} = \frac{C_p}{\lambda \epsilon} \left[\frac{\partial(T_d + \Gamma z)}{\partial e} \right] \quad [12]$$

The similarity of the eddy diffusivities as well as of the behavior of the gradients is implied by the elimination of these terms in the final form of the Bowen ratio. This is a widely accepted assumption.

Solutions for H and λE can now be obtained by substituting Equation [12] into the energy budget equation (Equation [1]). These solutions take the form,

$$H = -(Q^* + G)\beta / (\beta + 1), \quad [13]$$

and

$$\lambda E = -(Q^* + G) / (\beta + 1). \quad [14]$$

The Bowen ratio has the advantage that windspeed measurements are not required. It is important to note, however, that a solution for H independently of λE , or vice versa, is not possible.

The Aerodynamic Model. By employing the concept of a mixing length to effect transfer of an entity in turbulent flow Prandtl (1952) developed another relationship, besides Equation [9], for momentum transfer to rough surfaces:

$$\tau = \rho k^2 z^2 (\partial u / \partial z)^2 . \quad [15]$$

In this relationship k is an empirical constant determined from experiment to be 0.4. The eddy diffusivity for momentum in Equation [9] is thus defined as

$$K_M = k^2 z^2 (\partial u / \partial z), \quad [16]$$

which can be seen to vary with the windspeed gradient.

Equation [15] is strictly applicable only at times when sensible heat transfer is negligible. It has nonetheless proven to be a useful first approximation in estimating transfer because of the dominance of the wind in the transfer processes. The concept is applied in combination with the other transfer equations.

Eliminating τ between Equation [9] and [15] and then forming their ratio with Equation [10] provides a relationship for sensible heat transfer:

$$H = \rho C_p k^2 z^2 (\partial(T_d + \Gamma z) / \partial z) (\partial u / \partial z) (K_H / K_M) . \quad [17]$$

The corresponding relationship for latent heat transfer is:

$$\lambda E = (\rho \lambda \epsilon / p) k^2 z^2 (\partial e / \partial z) (\partial u / \partial z) (K_V / K_M) . \quad [18]$$

Although these relationships still contain the eddy diffusivity terms it has sometimes been assumed that $K_H / K_M = K_V / K_M = 1$. Based on this assumption, Equation [18] is essentially equal to the

evaporation formula first proposed by Thornthwaite and Holzman (1939). However, it has long been recognized that eddy diffusivity ratios involving K_M are seldom equal to unity. The stability of the atmosphere is important here.

Correction for Atmospheric Stability. The windspeed gradient, as incorporated in Equations [17] and [18], inadequately describes the intensity of the transfer process in the presence of a sensible heat flux (Panofsky, 1963). This inadequacy is brought about by the prevailing temperature gradient near the surface (Deacon, 1949). When this temperature gradient is away from a horizontal surface, i. e., the temperature decreases with distance upward, the surface air layer tends to be unstable due to buoyancy. Under these conditions energy (or mass) transfer is enhanced by vertical air movements which are not represented in the measurement of horizontal windspeed, and thus not assessable from it. The opposite condition is produced when the temperature increases with distance from the surface, with the suppression of the turbulent transfer as the more stable air restricts mixing in the layer near the surface.

Augmenting this effect, and in practice inseparable from it, is the preferred circumstance for heat or vapor transfer relative to momentum transfer in the presence of a temperature gradient (Priestley and Swinbank, 1947). This would indicate that the ratios

K_H/K_M and K_V/K_M (see Equations [17] and [18]) probably vary with atmospheric stability. Apparently, the value of this ratio is not always unity even when heat flux is negligible (Ellison, 1957). Panofsky (1965) has shown the ratio to become at least as large as 3 with increasing instability.

Clearly, a correction for stability is required before Equations [17] and [18] are useful estimators of the flux densities of H and λE . Fortunately, there is considerable evidence to suggest that K_H is equal to K_V (Dyer, 1967; Swinbank and Dyer, 1967; Denmead and McIlroy, 1970), which would indicate that a single correction function would serve for estimates of both H and λE .

Dimensional analysis has provided the Richardson number, Ri , (Richardson, 1920) as the appropriate correlating parameter to which the effects of atmospheric stability over horizontal surfaces can be related (Batchelor, 1953). The Richardson number is given by

$$Ri = (g/\theta_a)(\partial(T_d + \Gamma z)/\partial z)/(\partial u/\partial z)^2 \quad [19]$$

where g is the gravitational acceleration and θ_a is the average potential temperature of the air layer.

Correction terms proposed in the literature (e. g. Dyer, 1967; Paulson, 1970) have commonly been of the form

$$\phi = (1 - \alpha Ri)^Y, \quad [20]$$

where ϕ can be interpreted as including a correction for the wind-speed gradient as well as for the eddy diffusivity ratio, K/K_M . Values of the constants α and γ have varied widely, depending upon the particular experimental or theoretical criteria. It is apparent in Equation [20] that no correction is required when $Ri = 0$, that is, when there is no sensible heat flux. Further, the correction term becomes zero when $Ri = 1/\alpha$, implying a critical stability beyond which turbulent mechanisms (Equations [9] and [16]) may no longer be applicable (Ellison, 1957).

Because of the wide range of values which may be taken by the constants in Equation [20] it is not possible to select a formulation without some means of calibration. In some studies this has been done through the aid of an independent measure of H taking the form

$$\phi = H/\rho C_p k^2 z^2 (\partial(T_d + \Gamma z)/\partial z)(\partial u/\partial x). \quad [21]$$

An analogous correction form for λE can be developed if independent estimates of λE are available from, say, a lysimeter.

For this study it was necessary to adopt some other means of determining the stability correction formulation, since no independent measurement of H or λE could be obtained. To do this let Equation [1] be written as a defining equation for ϕ :

$$Q^* + G + \phi H + \phi \lambda E = 0, \quad [22]$$

in which H and λE are understood to be the uncorrected, aerodynamic estimates of the sensible and latent heat flux densities, respectively (Equations [17] and [18]; $K_H/K_M = K_V/K_M = 1$). By solving this equation for ϕ and correlating with Ri over a range of conditions the required values for the constants in Equation [20] can be obtained. This solution is in many respects equivalent to the Bowen ratio solution. Here, however, it serves as a means of deriving an appropriate correction function which can later be used with an aerodynamic model to estimate sensible heat flux independently of vapor pressure measurements. This is an advantage because of the difficulty in obtaining continuous, accurate vapor pressure measurements.

Boundary Layer Restrictions. At some distance from the surface the pattern of air flow begins to be influenced by adjacent surfaces, in addition to the underlying surface. The region between this level and the surface is called the boundary layer. To be representative of a specific surface it is necessary that flux evaluations be made from measurements which have been restricted to the boundary layer.

It is usually assumed that the boundary layer exceeds the level of the instrumentation, since its thickness is commonly found to be in the range of from 20 to 200 meters for many surfaces. However, this may not always be a valid assumption and can be tested. Using the flux density of momentum as a criteria for estimating the thickness of

in which H and λE are understood to be the uncorrected, aerodynamic estimates of the sensible and latent heat flux densities, respectively (Equations [17] and [18]; $K_H/K_M = K_V/K_M = 1$). By solving this equation for ϕ and correlating with Ri over a range of conditions the required values for the constants in Equation [20] can be obtained. This solution is in many respects equivalent to the Bowen ratio solution. Here, however, it serves as a means of deriving an appropriate correction function which can later be used with an aerodynamic model to estimate sensible heat flux independently of vapor pressure measurements. This is an advantage because of the difficulty in obtaining continuous, accurate vapor pressure measurements.

Boundary Layer Restrictions. At some distance from the surface the pattern of air flow begins to be influenced by adjacent surfaces, in addition to the underlying surface. The region between this level and the surface is called the boundary layer. To be representative of a specific surface it is necessary that flux evaluations be made from measurements which have been restricted to the boundary layer.

It is usually assumed that the boundary layer exceeds the level of the instrumentation, since its thickness is commonly found to be in the range of from 20 to 200 meters for many surfaces. However, this may not always be a valid assumption and can be tested. Using the flux density of momentum as a criteria for estimating the thickness of

the turbulent boundary layer, h , Lumley and Panofsky (1964) have derived the relationship

$$h = 2000\tau \quad [23]$$

Recalling the dependency of τ upon windspeed (Equation [19]) it is seen that h will be smallest during light winds. This relationship can thus be used to interpret the representativeness of the measurements during these times. Due to stability effects it should be noted that Equation [9] will underestimate τ when the surface is warmer than the air, and will tend to overestimate τ when the surface is colder.

The pattern of air flow also changes near the surface because of obstructions to the flow there. As a result it is necessary to restrict measurements to unaffected levels. The point at which the air flow is disrupted can be determined by the following procedure, which begins by writing Equation [15] for the windspeed gradient:

$$\partial u / \partial z = (\tau / \rho)^{1/2} / kz. \quad [24]$$

Throughout the boundary layer the steady state value of τ will be constant, and ρ and k are assumed constant. It is then apparent that as z is made small, near the surface, that $\partial u / \partial z$ becomes large, and would become indeterminate should z reach $z = 0$.

This does not happen due to surface roughness. Solving Equation [24]

for u predicts a logarithmic pattern to the windspeed distribution:

$$u = [(\tau/\rho)^{1/2}/k]\ln z + c. \quad [25]$$

Using observational data and plotting $\ln z$ as a function of u the constant c in this equation is found at the intercept where $u = 0$. The value of this intercept (c) is known as the roughness length, z_0 , and is a characteristic of the roughness elements on the surface.

Depending on the distribution and size of the roughness elements their effect on the windspeed gradient can be uniform, or they can produce flow perturbations to the extent that local gradients can be produced in the direction of the flow, parallel to the surface. Correspondingly, it is well to restrict instrumentation to distances well beyond the roughness length. When the surface is of uniform roughness Lettau (1959) recommends that measurements should be no closer than $5z_0$. If the roughness elements are widely dispersed Tanner (1963) suggests that it may be necessary to employ spatial averages for measurements as close as $5z_0$. At greater distances the pattern of the flow becomes more regular and predictable, however.

The roughness length will probably not be of critical significance in placing instruments at the pumice surface. Typical values for mown grass and other comparable surfaces are on the order of $0.1 \leq z_0 \leq 1$ cm (Sellers, 1965), far less than the closest level of

instrumentation used here (20 cm). However, the roughness length is a diagnostic characteristic of the surface. It also has an effect on boundary layer thickness.

Summary

This chapter has reviewed the fundamentals of energy budget micrometeorology as it relates to the pumice surface. The pumice surface has been defined as an energy conserving system, the principal energy components have been identified, and the governing micrometeorological relationships have been put forth to serve as the basis for the analysis of the energy budget.

III. EXPERIMENTAL METHODS

Two factors governed the selection of a pumice desert site for this investigation. First, consideration was given to sites where earlier research had been conducted relating to the problem of forest regeneration. The site selected for this study was included among those reported on by Wagg and Hermann (1962), and Hermann (1968, 1970). Second, consideration was given to the avoidance of theoretical limitations in micrometeorological analysis as might be imposed by insufficient size and uniformity of the surface. The pumice surface employed for this study satisfies these requirements.

The methods of data collection and handling employed for this investigation reflect current practice in energy budget micrometeorology. The primary objective of these methods was to provide data for energy budget analyses based upon the relationships detailed in the previous chapter. The methods considered here are concerned not only with field data acquisition and instrumentation but also with the evaluation of the adequacy of the measurements, the choice of an incremental time period for the analysis, and the suitability of the data for analysis by the proposed relationships.

Site Description

The pumice site selected for this study is located near Pine

Mountain, 55 kilometers southeast of Bend, Oregon. It is approximately 43°44' north latitude by 120°53' west longitude and at an elevation of 1500 meters above sea level. The region as a whole is arid, receiving perhaps 33 cm of precipitation annually (Hermann, 1968), primarily in winter as snow (Sternes, 1969). Summers are characterized by many successive days of clear skies. There is no period which could be regarded as frost free (Cochran, 1969).

This pumice desert is near the limit of the pine forests that characterize the eastern slopes of the Cascade Mountain Range. Sagebrush becomes the dominant vegetation further to the east. This desert opening is surrounded by a lodgepole pine (Pinus contorta Dougl.) forest having a small proportion of ponderosa pine (P. ponderosa Laws.). The area was logged for ponderosa pine in the 1920's (Wagg and Hermann, 1962). Some of the skid trails and roads made at that time are visible in the perimeter of the desert (Figure 1). The pumice surface is nearly barren, supporting less than about 5 percent coverage of low-growing subshrubs, forbs and grasses. The vegetative composition is similar to the pumice desert studied by Horn (1968).

The surface material on the pumice desert was probably deposited as part of the Newberry lava series, averages 71 cm in thickness, and is perhaps only 2,000 years of age (Youngberg and Dryness, 1964). Underlying this material is an older soil of finer

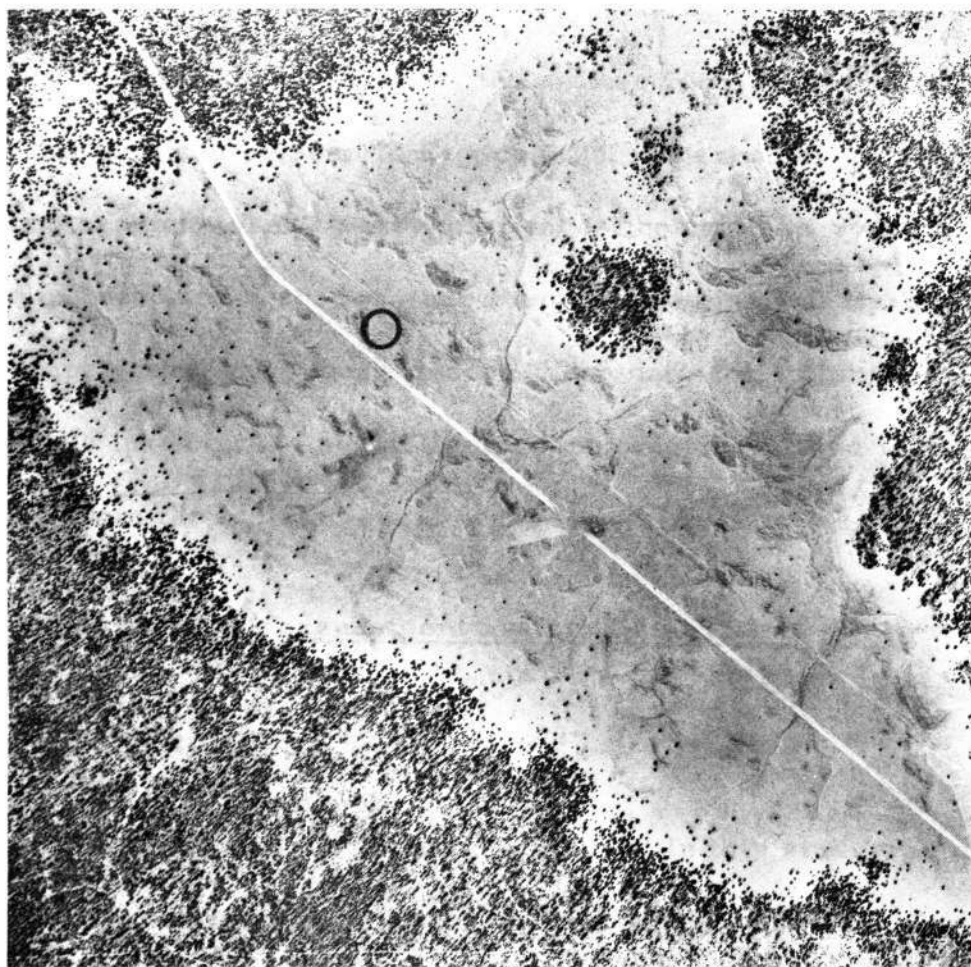


Figure 1. Aerial photograph of the pumice site taken in June 1954. Scale is approximately 200 m/cm. Road trends NW-SE.

loamy texture. Since deposition the pumice has apparently never been vegetated, although the surrounding forest is established on a similar surface.

Relief across the pumice desert is slight. Prevailing winds are from the north, as evidenced by the darker patches of wind sorted minerals that can be seen in Figure 1. The barren area totals about 250 hectares enclosed by irregular forest boundaries. An isolated stand of trees and a roadway are the only prominent features of the landscape within the pumice desert. The data collection point is within the circle inked on the aerial photograph (Figure 1), and is some 500 meters from the isolated stand of trees, which is to the east.

Measurement System Description

Data Acquisition

The data acquisition system employed in this study was developed for short term environmental and energy budget research (Gay, 1971a). The system has a high degree of resolution and is adaptable to making measurements on a wide range of micrometeorological instruments. The primary system components are a digital recorder,^{3/} a thermocouple reference junction,^{4/} and wind registers.^{5/} These were

^{3/} Vidar Corporation, Mountain View, California.

^{4/} Pace Engineering Company, North Hollywood, California.

^{5/} C.W. Thornthwaite Associates, Centerton, New Jersey.

mounted in an air conditioned trailer, which also served to transport the micrometeorological sensors, instrument supports, cables and other associated equipment to the site. A propane-fueled generator provided power in the field.

The digital recorder has several main parts: a 100 channel scanner; a clock; a digital voltmeter; and, a paper tape punch. At intervals commanded by the clock, the various sensors are sequentially connected to the voltmeter by the scanner for measurement and conversion to digital form. The time of record and the measured value of each input in the scan are punched on the paper tape. After the observation period the paper tape data is processed on the OSU computer.

The thermocouple reference junction provides a temperature stabilized comparison for up to 48 copper-constantan thermocouple channels. The reference temperature is regulated at 65° C to within very close tolerances, making possible precise temperature measurements with the digital recorder.

The wind registers were operated separately from the other system components and recorded photographically. Each anemometer revolution was counted on an associated register to provide a visual indication of wind run. The registers were photographed at 60 minute intervals and the totals eventually transferred to cards for computer processing.

Instrumentation

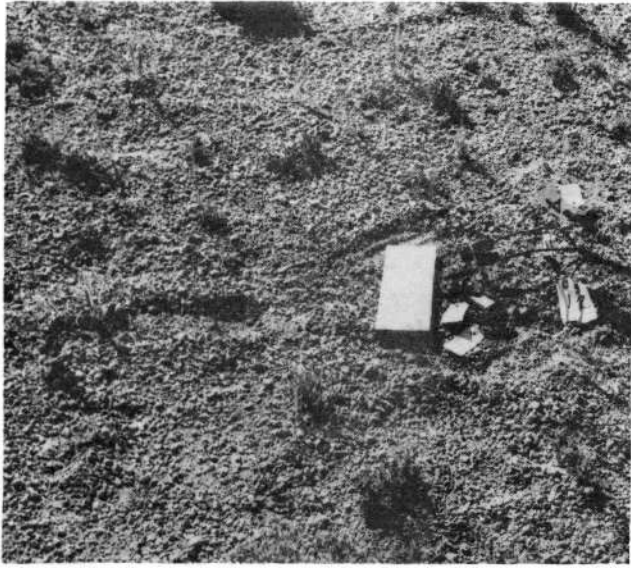
The micrometeorological instrument array at the site consisted of: three Kipp pyranometers (2 for $K\downarrow$, and 1 inverted for $K\uparrow$), two CSIRO net pyrradiometers (Q^*), one CSIRO pyrradiometer (obtaining $K\downarrow + L\uparrow$), all positioned 100 cm above the surface; five soil thermocouples (T) at depths of 1, 2, 5, 10, and 20 cm; one mast for dry-bulb temperature (T_d) and vapor pressure (e) measurements at heights of 20, 40, 80, 160, 240, and 320 cm; and one mast for windspeed (u) measurements at these same levels. Twenty-four channels of digital recorder capacity and six wind registers were required for this number of instruments.

Figure 2 shows several views of the instrumentation as it was installed at the pumice desert site. Signal cables leading to the trailer from these instruments were 75 meters in length.

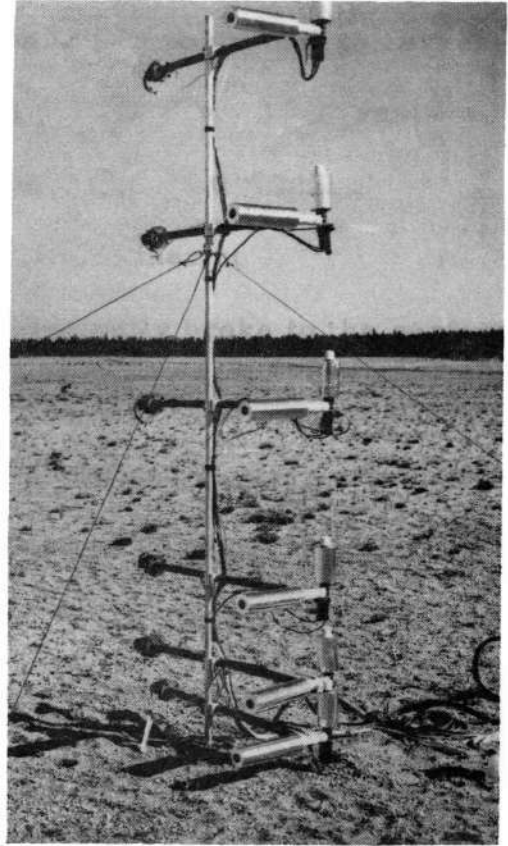
Care was taken in the installation and operation of all the radiometers to ascertain that they were horizontal and to insure that the supporting structures or other instruments did not obstruct the viewing area of the radiometers. Periodic checks were made for dew, frost, dust and internal moisture. One of the Kipp pyranometers was recorded on a strip chart recorder and used qualitatively to evaluate the suitability of the prevailing weather conditions, primarily the cloudiness, for steady state analysis.

Figure 2. Instrumentation at the pumice site.

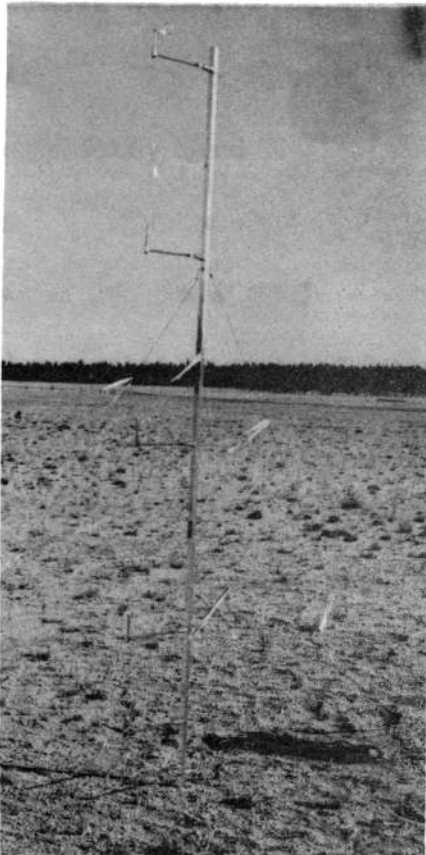
- (a) Close view showing the surface beneath which the soil thermocouples are buried. Connectors are held firm by the board. Thermocouples are placed under open soil (at left).
- (b) View of psychrometer mast with 6 levels of sampling. Air is drawn into nozzle at right and past the dry- and wet-bulbs by the fan at left. Water reservoir is upright section on each nozzle.
- (c) View of anemometer mast with 6 levels of sampling. The uniformity of the surface is evident in this and the above photographs.
- (d) View of the radiometer array. Two pyranometers are mounted in the white fixture, one being held inverted. The three pyrrometers extend toward the right, with the middle one being used for the all-wave incoming determination.



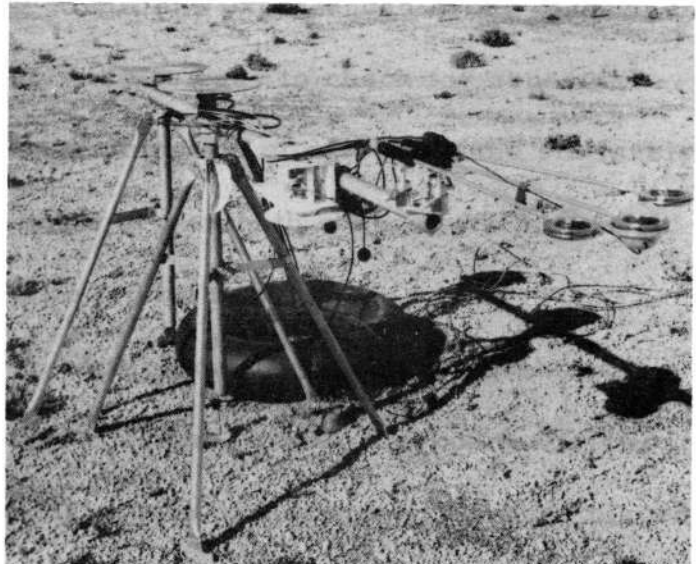
a



b



c



d

The five soil thermocouples were carefully positioned to correspond with the structural horizons in the pumice and with the gravimetric samples being taken for the determination of thermal characteristics. Measurements on the shallow (1 cm) thermocouple were later discarded because this instrument eventually broke to the surface of the soil and was exposed directly to solar radiation.

Six levels of dry bulb and wet bulb temperatures were measured using the ceramic wick psychrometer described in detail by Gay (1972) which is based on the design of Lourance (1967). Psychrometer difficulties were the most frequently experienced instrumental problem, as reliable, continuous measurements of wet bulb temperature are extremely hard to obtain. The problems encountered were due not only to the normal fouling of wicks with dust, or to air bubbles in the water, but also to the freezing conditions experienced every night on the pumice desert. Fortunately, it was easy to check for abnormal operation of a psychrometer by examination of data from the six levels of measurement. Normally, there is a smooth change of atmospheric moisture properties with distance from the surface.

Sensitive anemometers^{6/} were placed on the same levels as the psychrometers. Each anemometer assembly was checked for friction before each collection run and those with the least friction were placed

^{6/}C.W. Thornthwaite Associates, Centerton, New Jersey.

near the surface where windspeeds are least. Again, the regular change of windspeed with distance from the surface made it easy to screen the data to detect instrument malfunctions.

Measurement System Performance

Micrometeorological analyses of energy transfer require precise measurements because significant amounts of energy can be exchanged at relatively small potential differences. This is particularly true in the atmosphere where turbulent mixing contributes to the transfer process. Further, as emphasized by Smith (1970), it is essential that the investigator take rigorous precautions to insure that only high quality data is reported or analyzed.

Recent technological advances in data acquisition systems make it possible to collect field data with precisions previously obtainable only in the laboratory. These systems also permit rapid sampling of the large instrumentation arrays often required for micrometeorological studies. Of course, data handling and analysis is facilitated by the availability of computer assisted processing.

Though there is an ever-present possibility that measurement errors will degrade overall system performance, a complete evaluation of system errors is very difficult. Such an evaluation is restricted by the extent to which sensor integrity can be verified. Also, errors creep in from improper sensor operation or calibration,

as a result of instrument interactions, or because of the physical presence of the sensors in the environment. These problems must be considered and minimized through proper design of sensors and field experiments. Despite all preventive measures there will still be errors which cannot be eliminated.

It is useful to estimate the limits of measurement uncertainty as an aid in the interpretation of experimental results. This has been done here using as guidelines the instrument specifications, laboratory test results, and reference measurements in the field. The method used to obtain these estimates is explained in detail in Appendix IV.

The limits of performance as predicted by this method for each of the primary measurements used in this study are listed in Table 1. The listed uncertainty of windspeed measurements were not derived by this method. Instead they were developed from a discussion of anemometer errors by Halstead (1957), plus some additional conservatism on the part of the investigator. The errors in windspeed determination are primarily due to the response of the anemometers, rather than to the counting of the windspeed pulses.

Table 1. Overall system performance.

Typical Value	Uncertainty	Relative Error in Typical Value
Soil temperature, 15° C	-0.254° C, ±0.007° C	-1.7%
Dry bulb temperature, 15° C	-0.254° C, ±0.007° C	-1.7%
Dry bulb differential, 2.5° C	±0.010° C	±0.4%
Vapor pressure, 8.75 mb	-0.171 mb, ±0.016 mb	-2.0%
Vapor differential, 0.1 mb	±0.023 mb	±23%
Net radiation, 0.5 cal/cm ² min	±0.0001 cal/cm ² min	±0.02%
Surface temperature, 35° C (ε = 1)	±0.10° C	±0.3%
Windspeed, 200 cm/sec	±10 cm/sec	±5%
Windspeed differential, 100 cm/sec	±1 cm/sec	±1%

Mean Value Determination

The measurements employed in the analyses based on the eddy transfer equations should be mean values representing steady state conditions. The adequacy of the measurements in representing the desired mean value depends upon a number of factors, including the variability of the micrometeorological property, the response characteristics of the sensor and recorder, and the sampling scheme employed. The discussion presented in this section will substantiate the direct use of the measurements made for this study as mean values.

Sensor Response

The instantaneous value of an atmospheric property consists of a

mean value, presumed constant over a short time period considered here, and a deviation or fluctuation, which may add or subtract from the mean value (Webb, 1965). The deviation results from the eddying motion of the air in turbulent flow, and is associated with the transport of air parcels whose properties differ from those of the mean at the level of interest.

If a fast-response sensor is placed in such an environment, its signal output will vary almost exactly as the property being measured. The mean value of such a signal could be determined by continuous sampling measurement and rather elaborate numerical or electrical integration techniques. In contrast, the output of a slow-response sensor would reveal less fluctuation, as its slow response essentially performs the desired integration process. As a result, its output could be sampled less frequently. The use of a fast-response instrument introduces sampling problems where mean value determinations are needed.

Frequency of Samples

Experimental observations have suggested that the time period of the major fluctuations in atmospheric properties are close to 60 seconds (van der Hoven, 1957; McBean, 1968). In situations where this fluctuation appears in the sensor output the sampling rate would have to be rapid enough to describe the fluctuation mathematically in order

to numerically remove its effect and determine the mean. Shannon (1949) has provided sampling guidelines which indicate that under these circumstances a sampling rate of at least 30 seconds would be required. The number of successive samples necessary to achieve an estimate of the mean would depend upon the actual magnitude of the fluctuations in relation to the desired precision of the measurement.

Under typical conditions encountered in the atmosphere the requisite number of samples may well become prohibitive as well as being unrealistic in terms of the length of time that a constant mean value can be assumed. Consider as an example, a mean temperature of 19.6°C and with the fluctuations having an amplitude of 1°C . Using the statistical procedure outlined by Overton (1971), 100 samples of a random variable will be required to obtain a precision of 0.01°C . The variable may exhibit some periodicity, as indicated by van der Hoven (1957), but if this is not subject to mathematical characterization, one may have to operate as if the variable were random. Under the measurement conditions in this study, 50 minutes might elapse before 100 samples were obtained. During this time the mean would certainly have moved more than 0.01°C . Fast response sensors require more frequent, perhaps continuous samples to reduce the elapsed time to a period in which the mean is constant.

The Psychrometer Response

The temperature and vapor pressure sensors employed here (Gay, 1972) are designed with a relatively slow response time; they require approximately 70 seconds to reach 63% of a new value, which is slightly more than the period of the fluctuations. When the ratio of the sensor response time to the period of the fluctuations is 70/60, only 10% of the fluctuation magnitude will appear in the sensor output signal (Westman, 1956). If the sampling rate is random relative to the period of the fluctuation, the number of required samples drops dramatically. Overton's (1971) technique predicts that in this case only one sample is required to characterize the 19.6°C mean with a precision of 0.01°C.

The most significant aspect of this result is that a single measurement may be entirely adequate to determine the mean value of a property. Further, a series of such measurements will precisely describe the changes in that mean and thus permit the computation of an average value of the property over time. This becomes important when energy budget analyses are based on data that has been smoothed by averaging over a time period as long as an hour. This will be discussed further in the next section.

The wind speed measurements have a different basis than do the temperature and vapor values. Because the anemometers provide a

pulse output for each revolution the continuous accumulation of these pulses provides an integrated average wind flow.

Time Period of Analysis and Data Averaging

Three distinct methods of energy exchange analysis have been outlined for the estimation of the fluxes in Equation [1], depending upon whether energy transfer was by radiation, conduction, or convection. These methods employ relationships of properties that may be out of phase with the instantaneous values of the fluxes. For example, estimates of soil heat flux based on temperatures at various points in the soil profile will lag behind the flux taking place at the surface, because of the heat capacity of the soil.

Even the properties of the air require time to adjust to changes in convective transfer at the surface (Dyer, 1963). Radiant transfer, since it employs no medium, has no such lag. As a consequence it is necessary to process the data in a way that will minimize the effect of such phase differences.

Averaging Periods

The experience of others has revealed that a good correlation between energy budget components is obtained when flux density analyses are based on time-averaged values of meteorological properties (Tanner, 1967; Rider and Robinson, 1951). The time periods used

often vary from 1/2 to 1 hour in length. The analyses in this investigation are based on hourly averaged measurements.

The number of measurements needed to determine an average depends upon how the property is changing. Over a period of 1 hour, the mean air temperature or mean vapor pressure may undergo complex changes, depending upon the uniformity of the prevailing conditions, while the soil temperature may change slowly and smoothly. More measurements would be required to compute a precise average in the air than in the soil. These samples can be satisfactorily obtained by repeated measurements at intervals, providing that the interval length in each case depends upon the variability of the property.

Numerical Integration

It is usually convenient, for data collecting purposes, to establish regular, periodic measurements as was done here. However, if the interval between samples varies, it is no longer possible to employ simple averages. Instead, a method which weights the measurements according to the time interval they represent, called trapezoidal integration, has been selected for this investigation. The average hourly mean, \bar{y} , of a property is computed as

$$\bar{y} = \int_0^{60} y dt / \int_0^{60} dt . \quad [28a]$$

This can be approximated by

$$\bar{y} \approx (1/2)[(y_0+y_1)(t_1-t_0)+(y_1+y_2)(t_2-t_1)+\dots+(y_{n-1}+y_n)(t_n-t_{n-1})]/60 \quad [28b]$$

or, if the interval length is constant, by

$$\bar{y} \approx \Delta t(y_0+y_n+2 \sum_{i=1}^{i=n-1} y_i) / 120. \quad [28c]$$

The approximation becomes better and better as the time interval Δt decreases. The daytime interval was usually 5 minutes and the nighttime interval 10 minutes. Since windspeed data is collected as an integral, no further averaging procedure was applied to it.

Gradient Approximation and Similarity

The successful application of the aerodynamic transfer models depends upon the accurate mathematical characterization of the gradients (derivatives) of windspeed, temperature and vapor pressure with distance from the exchange surface. Numerous investigators have reported linear changes of these properties with the logarithm of distance from the surface (Webb, 1965). For computational purposes it has thus become common practice to approximate a gradient by

$$\partial \bar{y} / \partial z \approx (\bar{y}_1 - \bar{y}_2) / (z_1 z_2)^{1/2} \ln(z_1 / z_2) \quad [29]$$

where \bar{y} is the average value of the property at distance z (after Panofsky, 1965), $\partial\bar{y}/\partial z$ being associated with mean distance, $z_m = (z_1 z_2)^{1/2}$. This form has been adopted for the analyses (see Appendix III).

A profile plot of the log of the distance to the surface against the property is often made as an aid in the visualization of these gradients and as an indication of how well they are represented by Equation [29]. Figures 3, 4 and 5 are typical profiles of the data from this study. It is not intended to infer the interdependency of distance and the property from these plots. They merely indicate their relationship at a particular time, since the gradient is functionally dependent upon the rate of energy transfer from the surface to the atmosphere.

The examination of log profiles of the properties is helpful in the selection of those levels best suited for analysis. Instrument levels which exhibit departures from the general trend of values are suspect and should probably be discarded in the analysis. This is an important advantage that can be obtained by measuring at 3 or more levels. Some investigators (Morgan et al., 1971) have employed statistical fitting procedures to calculate gradients, certainly a desirable approach in some instances. However, even when it is possible to systematically remove or replace bad data, there are flux divergence and profile adjustment problems associated with gradient determinations (Dyer, 1963). These problems detract from the usefulness of

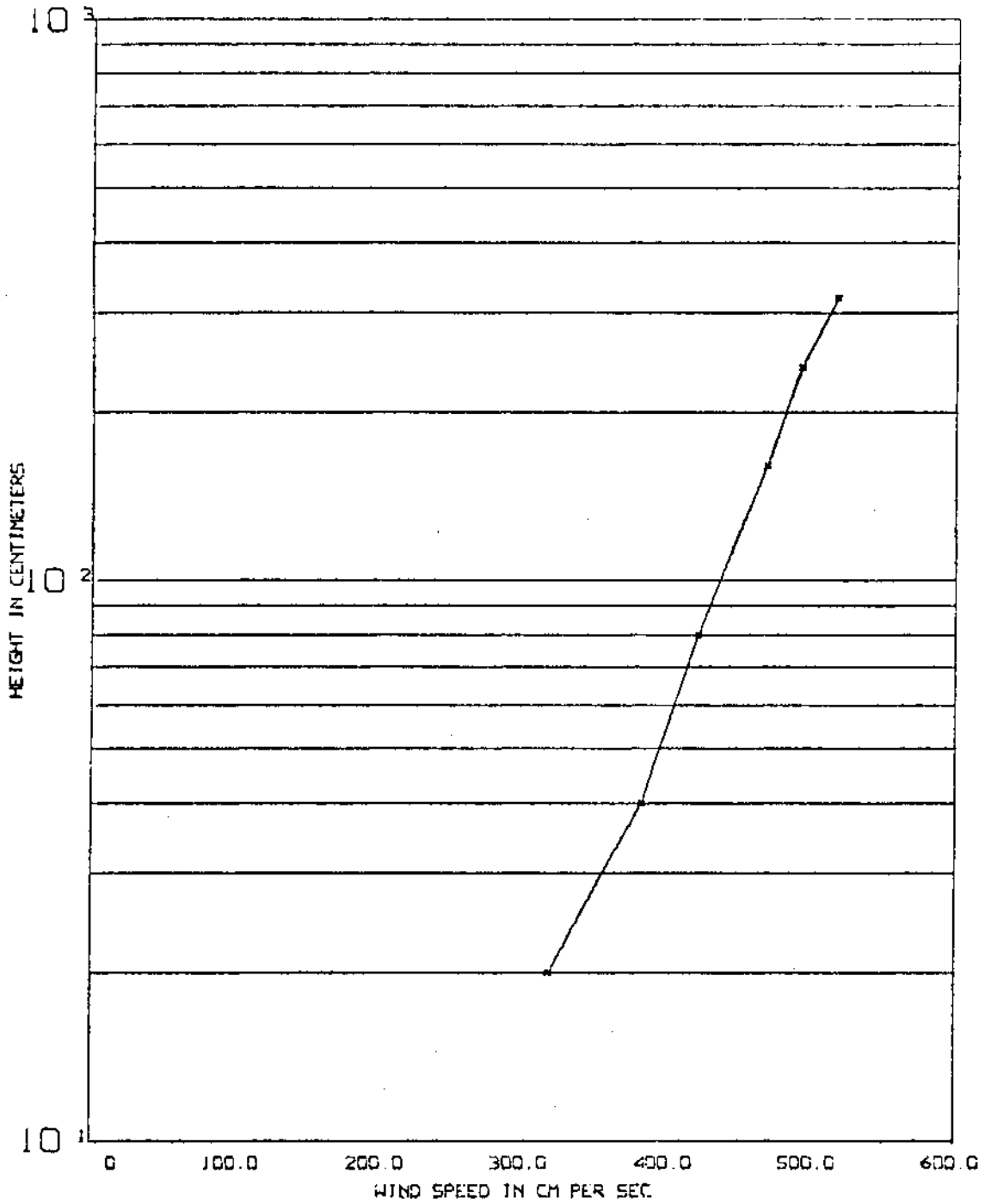


Figure 3. A representative midday windspeed profile from the pumice site. This plot used the hourly averaged data for hour 13 on 4 Sep 1969.

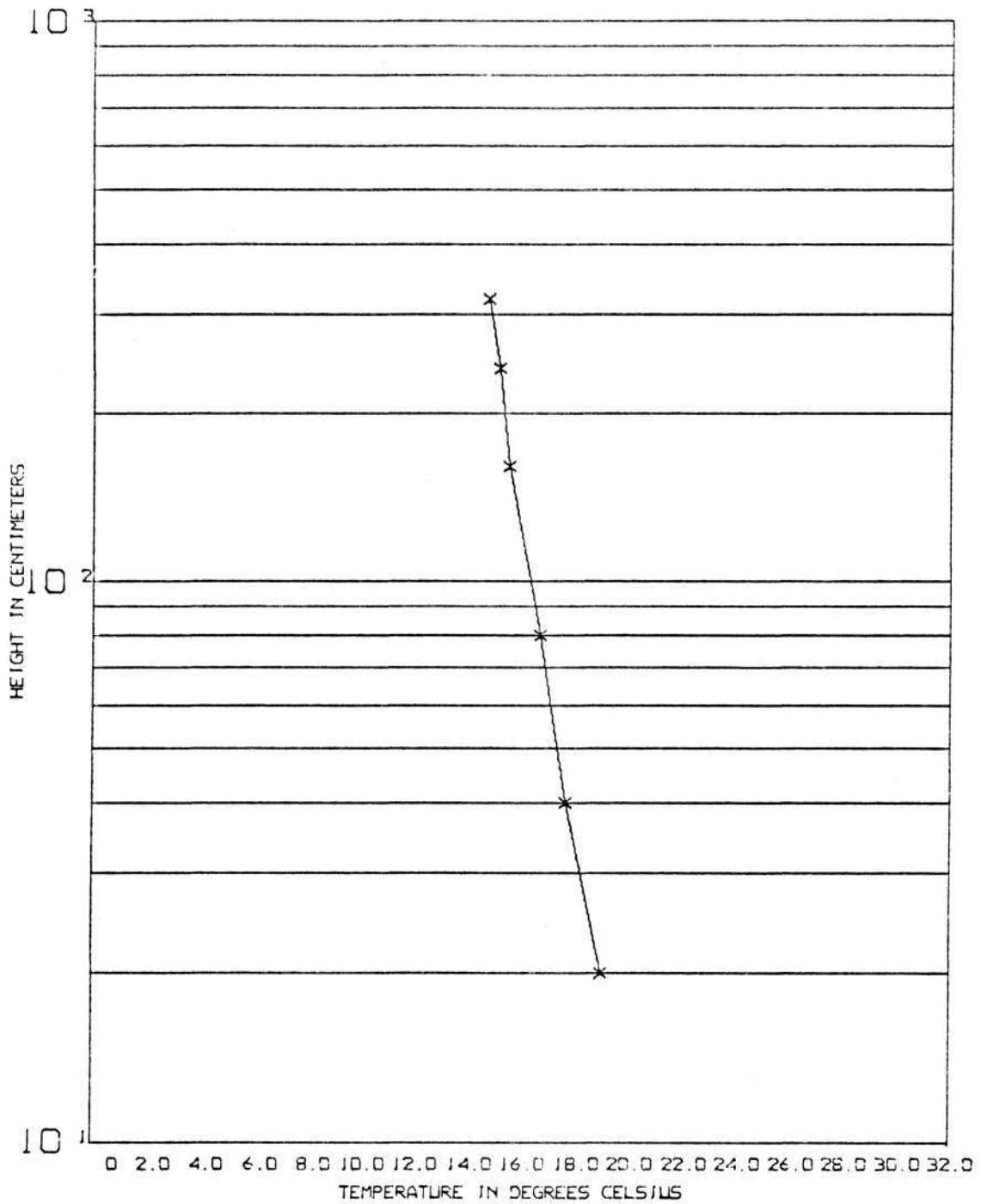


Figure 4. A representative midday temperature profile from the pumice site. This plot was made from hourly averaged data for hour 13 on 4 Sep 1969.

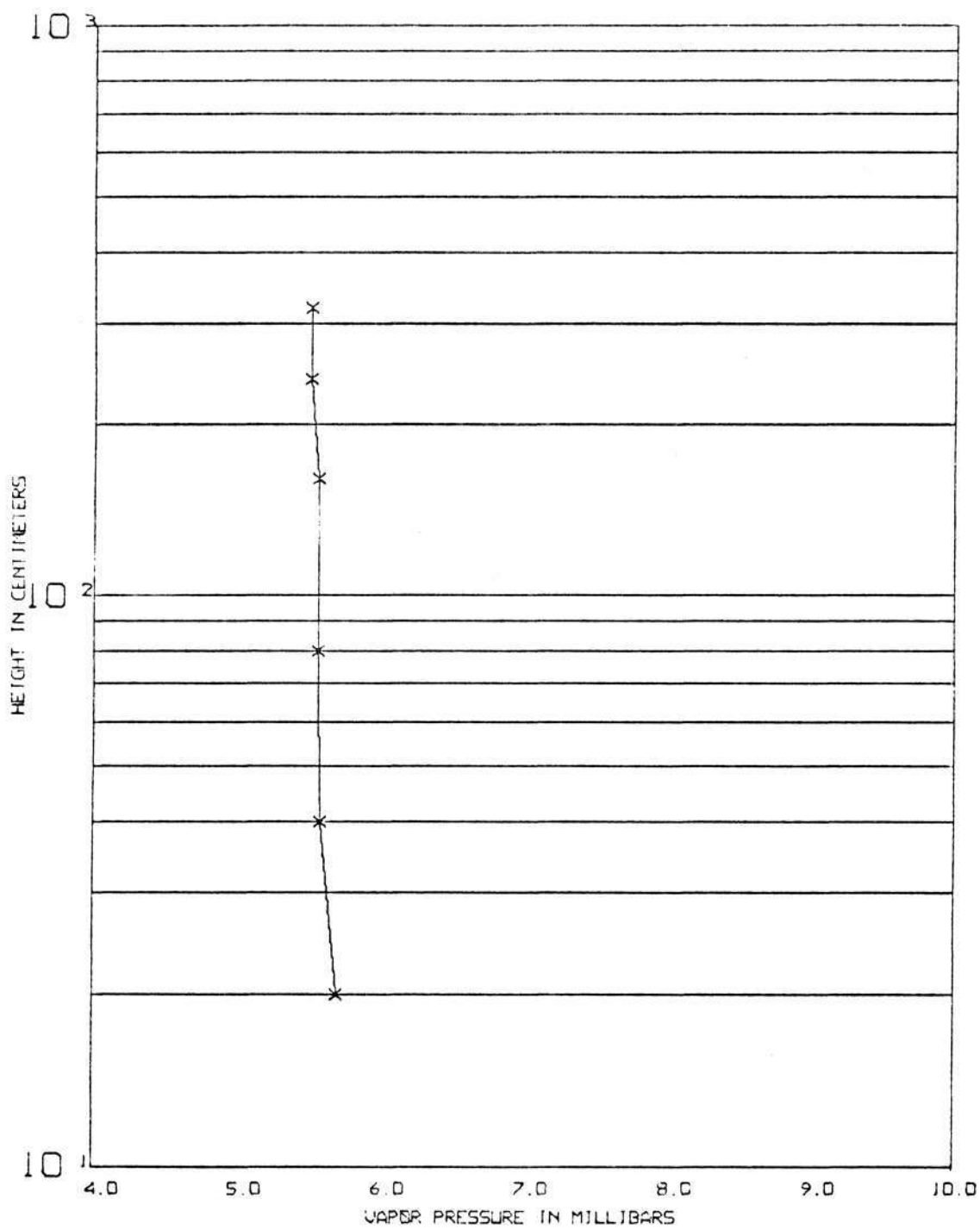


Figure 5. A representative midday vapor pressure profile from the pumice site. This plot was made from hourly averaged data for hour 13 on 4 Sep 1969.

the fitted gradients. In addition, other influences such as stability, become more important as the levels of the measurements become more widely spaced. The state of knowledge in turbulent transfer is still too incomplete to account for profile distortion from these cases.

Another valuable technique for examining data is plotting corresponding levels of two properties against each other (Tanner, 1963). This technique indicates the degree to which the change in each property is similar to the other with distance from the surface. A straight line relationship between two properties indicates that the transfer coefficient for them is the same, e.g., $K_H = K_V$.

The similarity test is very useful in identifying the times when this equality holds. The test is very helpful in developing Bowen ratio analyses. In other analyses, when equality between the turbulent transfer coefficients is not assumed, or $K_H \neq K_M$, the similarity test is theoretically not as useful since adjustment for this is often included in the stability correction. However, experience has shown that the similarity test is more sensitive than log profile plots for detecting malfunctioning instruments.

Application of this similarity test to the pumice desert data is provided in Figure 6. An error in psychrometric data is evident at the second level for hours 0, 1, and 8, 23, and 24 on the temperature and vapor pressure plot. The effect of stability is possibly exhibited on the temperature and windspeed plot between levels 1 and 2 in the

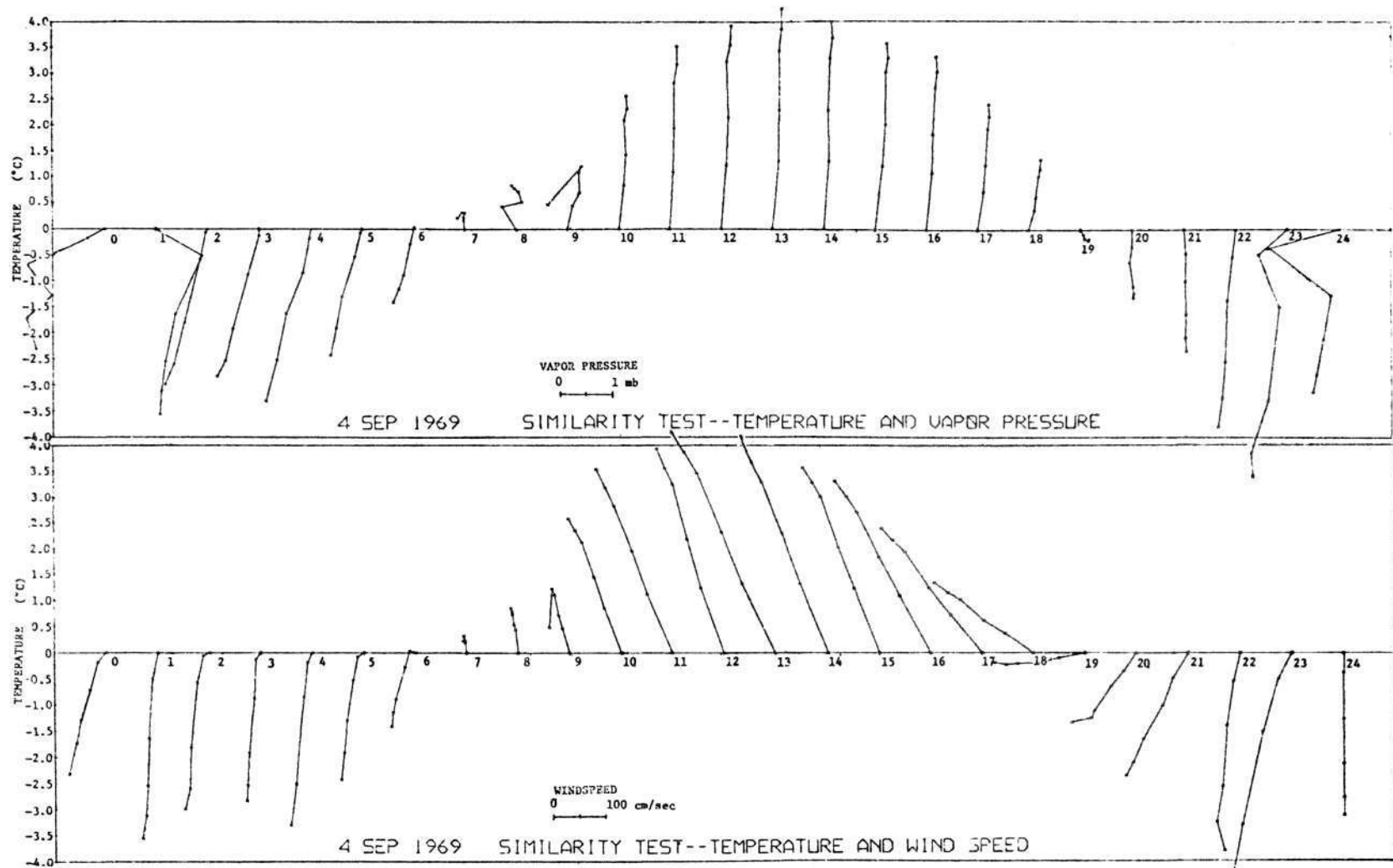


Figure 6. Relative similarity of properties at successive levels from the pumice surface. Level nearest surface is plotted on the center line. Plots begin at hour 0 and proceed through the day to hour 23 for Sep 1969, as shown, using hourly averaged data. Coordinates are computed by difference of the value at each level from the value at the first level.

early morning. The reversal in the temperature gradient at hour 9 was traced to instrument difficulties. Other irregularities are evident, but their interpretation is not so readily made. One must also consider the uncertainty of the measurements, which are roughly indicated by the size of the mark used to plot each data point.

If a straight line can be fitted, then there is no dissimilarity for practical purposes. On the basis of the similarity evident in Figure 6, instrument levels 2, 3, 4, 5, or 6 can be selected for the analysis of data taken on 4 September 1969. This same technique was used to select the best instrument levels on the other days of measurement.

Summary

This chapter has dealt with the methods used in this study to collect and process data for the micrometeorological analysis of the energy budget of a pumice surface. The site of the investigation has been described, as has the data acquisition and instrumentation system. The performance of that system and the suitability of the data for analysis have been evaluated.

IV. ENERGY BUDGET RESULTS

An energy budget analysis for the pumice desert has been completed on an hourly basis for three days during the summer of 1969, using a combination of the fundamental micrometeorological relationships set out in Chapter II, and the experimental methods discussed in Chapter III. Before presenting these results it will be helpful to show how this combination of theory and practice has led to the specific analysis used here.

First, consideration of the adequacy of the energy budget component evaluation will show that certain relationships, or models, should be given preference because of the prevailing micrometeorological conditions and data acquisition system performance while at the pumice site. The preferred relationships must then be adapted to these conditions. Finally, the results of the energy budget analysis will be presented in the form of hourly and daily component evaluations.

A discussion of these components will show seasonal variations in the energy budget. Characteristics of the pumice surface which play important roles in the partitioning of energy into its component parts will become evident. These characteristics are important in the micrometeorological interpretation of the results, and have implications to forestry in terms of the possible modification of the microclimate.

The data upon which the analyses are based are compiled in Appendix II. The analytical equations used are given in Appendix III. They are based upon the theoretical considerations of Chapter II and by the experimental conditions discussed in Chapter III and in this chapter.

The Uncertainty of Component Evaluation

The uncertainty associated with the evaluation of each energy budget component has been examined by extension of the method used earlier to assess overall measurement system performance (see Table 1). Basically, this method begins with the elemental measurement errors and considers their effect at each successive step in the flux evaluation process. The method can become quite involved, since some of the flux evaluations require numerous measurements of various kinds, which in turn may be combined in complex ways. Details of this method, with examples, can be found in Appendix IV.

Estimates of the average uncertainty associated with the evaluation of each of the energy budget components as determined by this method are presented in Table 2. These estimates reflect not only the performance of the data acquisition system but also the general nature of micrometeorological conditions encountered at the pumice site. These uncertainties would not necessarily be applicable to other situations, particularly with regard to the models used for the evaluation of

the sensible heat flux, H , and the latent heat flux, λE . For these models the prevailing temperature, vapor pressure, and windspeed gradients have a marked effect on the uncertainty figure. For example, a moist surface would probably increase the uncertainty associated with H and decrease that associated with λE . In other words, for surfaces having different characteristic magnitudes of the energy budget components, one should anticipate different relative uncertainties associated with their evaluation. Thus, the small relative uncertainty of the sensible heat component at the pumice surface is, in part, the consequence of the predominance of this mode of energy transfer there.

Table 2. Average uncertainty of flux density evaluation.

$\delta Q^*/Q^*$	$\delta G/G$	<u>Bowen Ratio Model</u>		<u>Aerodynamic Model</u>	
		$\delta H/H$	$\delta \lambda E/\lambda E$	$\delta H/H$	$\delta \lambda E/\lambda E$
<1%	<5%	9%	30%	3%	25%

As Table 2 shows, the relative uncertainties of the latent heat flux evaluations are largest by both the Bowen ratio and the aerodynamic models. The uncertainties of the net radiation and soil heat flux evaluations are negligible by comparison. Those for sensible heat flux are small or moderate. Before comparing the Bowen ratio model with the aerodynamic model it should be emphasized that the relative merits of these models, as indicated by the tabular values, involve

only their performance at the pumice site, and should not be interpreted as meaning that one model is theoretically better than the others.

In comparing models, it is seen that the uncertainty in evaluating the sensible heat transfer, H , by the Bowen ratio model is not as low as by the aerodynamic model. This is traceable to the dependency of the Bowen ratio evaluation on the determination of the vapor pressure gradient, which has a large uncertainty associated with it. Fortunately, the steep air temperature gradients, with which there is an associated low uncertainty, have the effect of restricting the uncertainty of the sensible heat flux evaluation to nearly the same uncertainty as the accompanying temperature gradient in both models as discussed in Appendix IV.

As noted above, direct evaluation of the latent heat flux by the Bowen ratio or the aerodynamic model is subject to the largest uncertainty of all the energy budget components. Thus, an improvement in the latent heat flux evaluation results from the use of Equation [1], which is rewritten to give λE as a residual:

$$\lambda E = -(Q^*+G+H). \quad [1]$$

Far less uncertainty (~10%) can be obtained in this way than by other means, under the conditions of this study. The main requirement is, of course, that all other energy budget components have been

satisfactorily accounted for. Evaluation by residual rather than from micrometeorological measurements, was the approach adopted for the latent heat flux component.

The Stability Correction Function

Calculation of λE as a residual requires the use of an aerodynamic model, Equation [18], for the evaluation of the sensible heat transfer, H . The stability correction required for this model was developed for this site according to Equation [22]. The required correction, ϕ , was developed as a function of the Richardson number (Ri) over a range of atmospheric stabilities. Fifty-two hourly analyses, covering the stability range $-0.01 < Ri < -10$, are plotted on Figure 7. The stability correction function which best fits these points is drawn on the figure; it has the formula:

$$\phi = (1 - 34Ri)^{0.55} . \quad [30]$$

This expression is based on λE evaluations which have been shown to have a possible uncertainty of 25%. Thus objections can be raised, but comparisons to correction functions proposed elsewhere tend to indicate that Equation [30] is of acceptable form. For example, Pruitt and Lourence (1966) developed a stability correction function to make their uncorrected aerodynamic estimates of λE fit the independent measurement of λE obtained from a lysimeter. Their

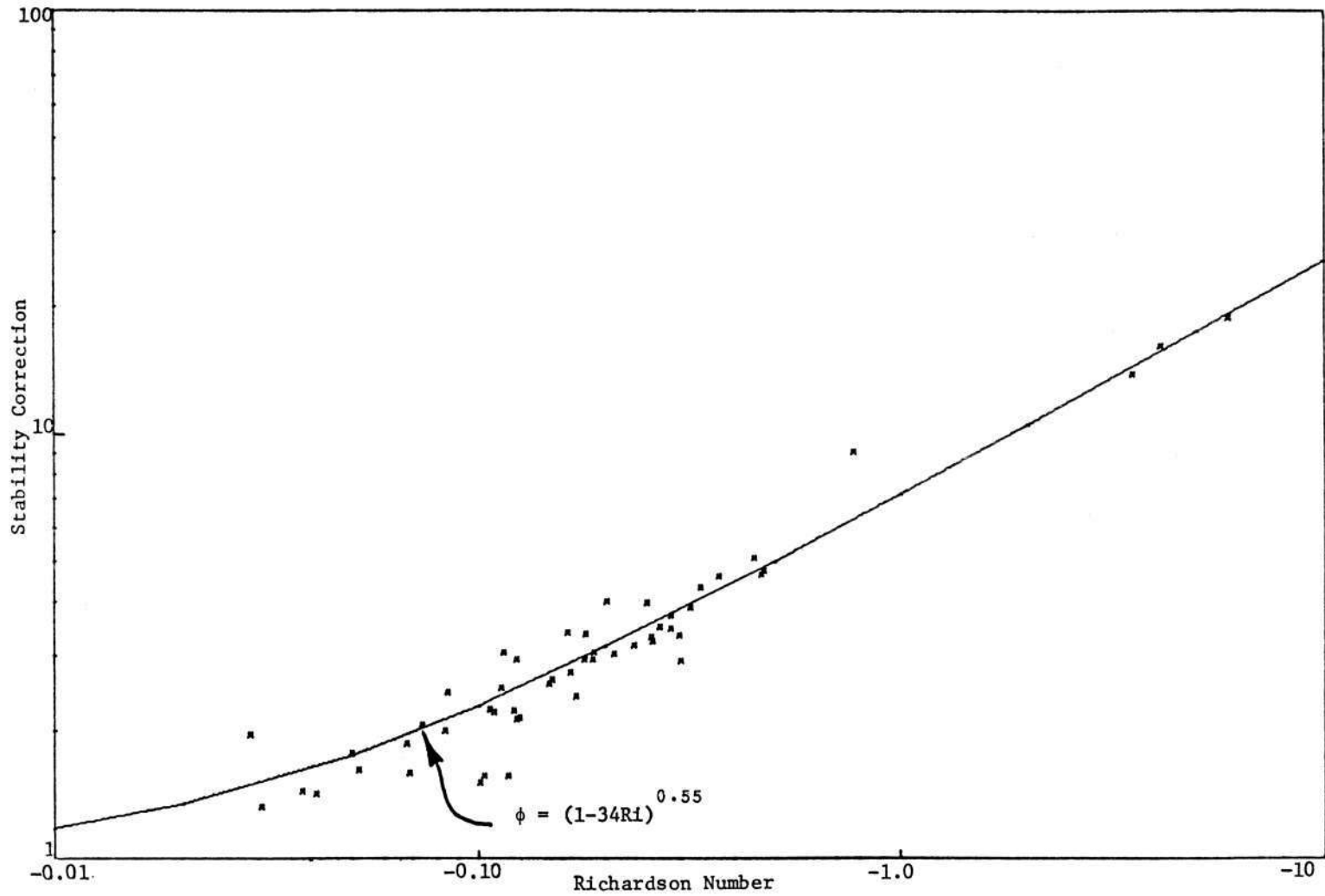


Figure 7. A stability correction function fitted to analyses from the pumice site data.

function is plotted in Figure 8; it closely parallels Equation [30], and has the formula

$$\phi = (1-50\text{Ri})^{0.5} \quad [31]$$

This correction function was also developed over a wide range of stabilities.

Other formulations of the correction function in the literature are not in such close agreement. Rarely, however, have other investigators encountered so wide a range of stabilities. Two other proposed formulations are drawn on Figure 8 for comparison with the expression developed here. These appeared in reports by Panofsky et al. (1960) and by Webb (1970):

$$\phi = (1-5\text{Ri})^2, \quad [32]$$

and

$$\phi = (1-18\text{Ri})^{0.5} \quad [33]$$

Significant departures between these four correction functions appear when $|\text{Ri}|$ becomes larger than -0.1. However, the similarity between Equation [31] and Equation [30] confirms that Equation [30] can be used to correct for stability in the evaluation of sensible heat transfer.

At night and at other times when the air temperature increases with distance from the surface the Richardson number becomes

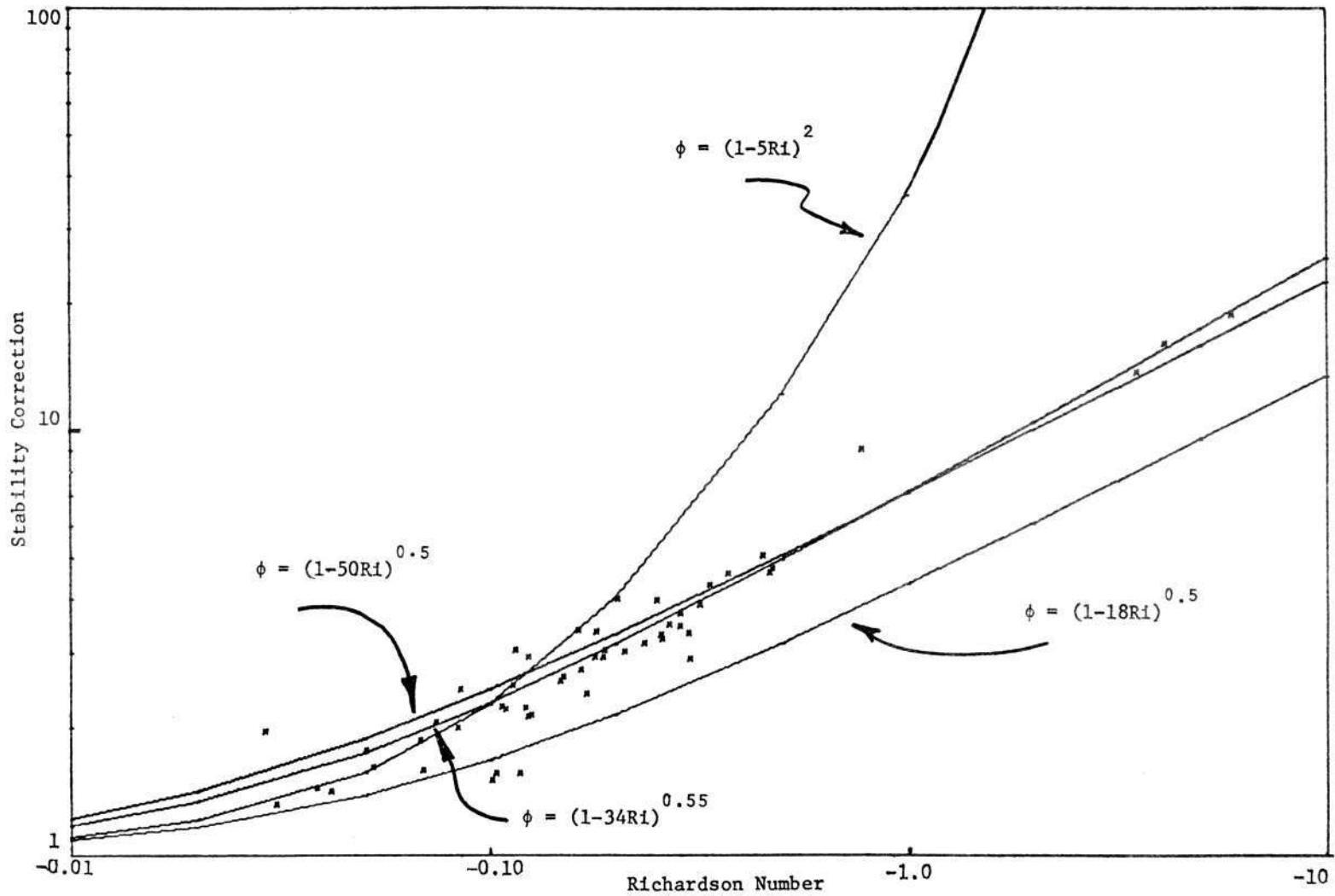


Figure 8. Comparison of the stability correction function developed for the pumice site, $[\phi = (1-34Ri)^{0.55}]$, to other forms appearing in the literature.

positive. It is an advantage to modify Equation [30] to handle both cases. Under the stable conditions found with $Ri > 0$, turbulence decays and may actually cease (Ellison, 1957). In this case, Equation [15], the basic turbulent transfer relationship, may not apply for evaluating energy transfers. The reduction in turbulence is also accompanied by a reduced rate of energy transfer to the air, since molecular diffusion is less effective than is convection in the transfer of energy. It has become a common procedure elsewhere (Holzman, 1943; Pruitt and Lourence, 1966) to modify the correction function to apply to stable (+Ri) cases by reversing the signs on both the coefficient of Ri and the exponent. The corresponding correction function utilized in this investigation for these cases is

$$\phi = (1+34Ri)^{-0.55} . \quad [34]$$

While this procedure is somewhat contrary to theory, it is felt that the net effect on component evaluation is probably minor because it is applied only at times when sensible and the latent heat fluxes are quite small. Experience has shown that at night, during times of +Ri, the net radiation, Q^* , is often balanced by the soil heat flux, G . This does not mean an absence of any sensible (H) or latent (λE) exchange but does suggest that their effect on the budget may cancel.

Hourly and Daily Component Evaluation

Days of Analysis

Data were collected at the pumice site during three expeditions in the summer of 1969. During these times there was no precipitation. Three days, 17 July, 13 August and 4 September, were selected for energy budget analyses out of the total of nine days spent at the site. The other days were not analyzed because of various instrumental difficulties or weather problems. It was further necessary to interpolate the analyses of sensible and latent heat for the hours from 1 to 6 on 13 August, because of inoperation of the air temperature system. Sensible heat flux for these hours is generally less than 2% of the mid-day rate, so this interpolation adds only a small additional uncertainty in the overall energy budget of that day.

Analytical Procedure

Since many possible avenues of analysis have been discussed, it seems appropriate to explicitly review the procedure employed. In its final form, the analytical procedure consisted of four basic steps, summarized as follows:

1. The net radiation flux density, Q^* , is computed for each sampled interval and time averaged, giving the average per-minute rate for the hour.

2. The per-minute rate of the soil heat flux density, G , is computed from time-averaged surface and soil temperatures.
3. The profiles of the time averaged windspeed and air temperature are examined together with the similarity plot of windspeed versus air temperature. From this examination a qualitative evaluation is made of the instrument levels most suitable for analysis. The Richardson number is determined for the chosen levels and an appropriate correction applied to the uncorrected aerodynamic estimate of sensible heat flux density for the same two levels. The result is the average per-minute rate for the hour.
4. The negative of the algebraic sum of steps 1, 2, and 3 is the residual value of the latent heat flux density, λE , for the hour, expressed as a per-minute rate.

The analytical equations used for these computations are given in Appendix III.

Tabulation of Results

Tables 3, 4, and 5 list the energy budget results by hourly periods for the three days analyzed. These results are also plotted as Figures 9, 10, and 11 for convenience in the following discussion of component relationships. Table 6 summarizes the daily energy budget by comparing the integral values of the components as they change

Table 3. Pumice surface energy budget by hour and day for 17 July 1969. Instrument levels: 80 and 320 cm.

Hour	Q* (cal/cm ² min)	G (cal/cm ² min)	H (cal/cm ² min)	λE (cal/cm ² min)
1	-0.0902	.0642	.0221	.0039
2	-0.0850	.0944	.0085	-0.0179
3	-0.0809	.0885	.0133	-0.0209
4	-0.0771	.0870	.0016	-0.0116
5	-0.0711	.0805	.0029	-0.0123
6	-0.0324	.0526	.0017	-0.0218
7	.0486	-0.0157	-0.0466	.0137
8	.1831	-0.0889	-0.0927	-0.0014
9	.3093	-0.1569	-0.1400	-0.0124
10	.4281	-0.1915	-0.2034	-0.0333
11	.5204	-0.1990	-0.2379	-0.0835
12	.5940	-0.1877	-0.3801	-0.0262
13	.6268	-0.1641	-0.3730	-0.0898
14	.6199	-0.1367	-0.4169	-0.0664
15	.5864	-0.0857	-0.4327	-0.0680
16	.5078	-0.0357	-0.4051	-0.0670
17	.4083	.0127	-0.3107	-0.1103
18	.2669	.0560	-0.2238	-0.0992
19	.1135	.0918	-0.0877	-0.1176
20	-0.0510	.1177	.0121	-0.1524
21	-0.1116	.1231	.0268	-0.0383
22	-0.1070	.1051	.0532	-0.0512
23	-0.1031	.0915	.0251	-0.0135
24	<u>-0.0966</u>	<u>.0778</u>	<u>.0236</u>	<u>-0.0048</u>
Integral (cal/cm ² day)	258	-7	-197	-54

Table 4. Pumice surface energy budget by hour and day for 13 August 1969. Instrument levels: 20 and 320 cm.

Hour	Q^* (cal/cm ² min)	G (cal/cm ² min)	H^1 (cal/cm ² min)	λE^1 (cal/cm ² min)
1	-0.0649	.0416	.0017	.0216
2	-0.0621	.0542	.0141	-0.0062
3	-0.0588	.0505	.0034	.0049
4	-0.0572	.0520	.0112	-0.0060
5	-0.0556	.0470	.0161	-0.0075
6	-0.0489	.0419	.0240	-0.0170
7	.0037	-0.0417	-0.0320	.0700
8	.1640	-0.0832	-0.0791	-0.0016
9	.3179	-0.1036	-0.1788	-0.0355
10	.4570	-0.0902	-0.3531	-0.0137
11	.5425	-0.1154	-0.4309	.0038
12	.5821	-0.1230	-0.4184	-0.0407
13	.5950	-0.1072	-0.4253	-0.0625
14	.5681	-0.0927	-0.4137	-0.0617
15	.5052	-0.0721	-0.4088	-0.0244
16	.4066	-0.0717	-0.3094	-0.0255
17	.3005	-0.0224	-0.2526	-0.0255
18	.1525	-0.0064	-0.1288	-0.0173
19	-0.0315	.0440	-0.0035	-0.0090
20	-0.0987	.0704	.0263	.0020
21	-0.0958	.0768	.0139	.0050
22	-0.0789	.0852	.0139	-0.0202
23	-0.0758	.0699	.0162	-0.0103
24	<u>-0.0703</u>	<u>.0657</u>	<u>.0073</u>	<u>-0.0027</u>
Integral (cal/cm ² day)	228	-14	-197	-17

¹ Values of H and λE are interpolated for hours 1 through 6.

Table 5. Pumice surface energy budget by hour and day for 4 September 1969. Instrument levels: 40 and 240 cm.

Hour	Q* (cal/cm ² min)	G (cal/cm ² min)	H (cal/cm ² min)	λE (cal/cm ² min)
1	-0.0723	.0555	.0011	.0156
2	-0.0695	.0718	.0047	-0.0070
3	-0.0667	.0630	.0017	.0020
4	-0.0649	.0631	.0034	-0.0016
5	-0.0577	.0556	.0041	-0.0020
6	-0.0452	.0440	.0040	.0028
7	-0.0100	.0000	-0.0079	.0179
8	.1223	-0.0655	-0.0298	-0.0270
9	.2505	-0.1022	-0.0866	-0.0618
10	.4803	-0.1114	-0.2336	-0.0352
11	.4977	-0.1019	-0.3798	-0.0159
12	.5566	-0.1118	-0.4447	-0.0001
13	.5961	-0.1000	-0.5228	.0266
14	.5645	-0.0962	-0.4587	-0.0096
15	.4914	-0.0776	-0.3712	-0.0425
16	.3959	-0.0359	-0.3483	-0.0117
17	.2571	.0002	-0.2341	-0.0232
18	.0897	.0240	-0.1010	-0.0127
19	-0.0722	.0679	.0087	-0.0044
20	-0.1250	.0895	.0162	.0193
21	-0.1145	.0808	.0337	-0.0000
22	-0.0988	.0971	.0080	-0.0063
23	-0.0900	.0126	.0695	.0078
24	<u>-0.0811</u>	<u>.0340</u>	<u>.0301</u>	<u>.0170</u>
Integral (cal/cm ² day)	194	-2	-180	-11

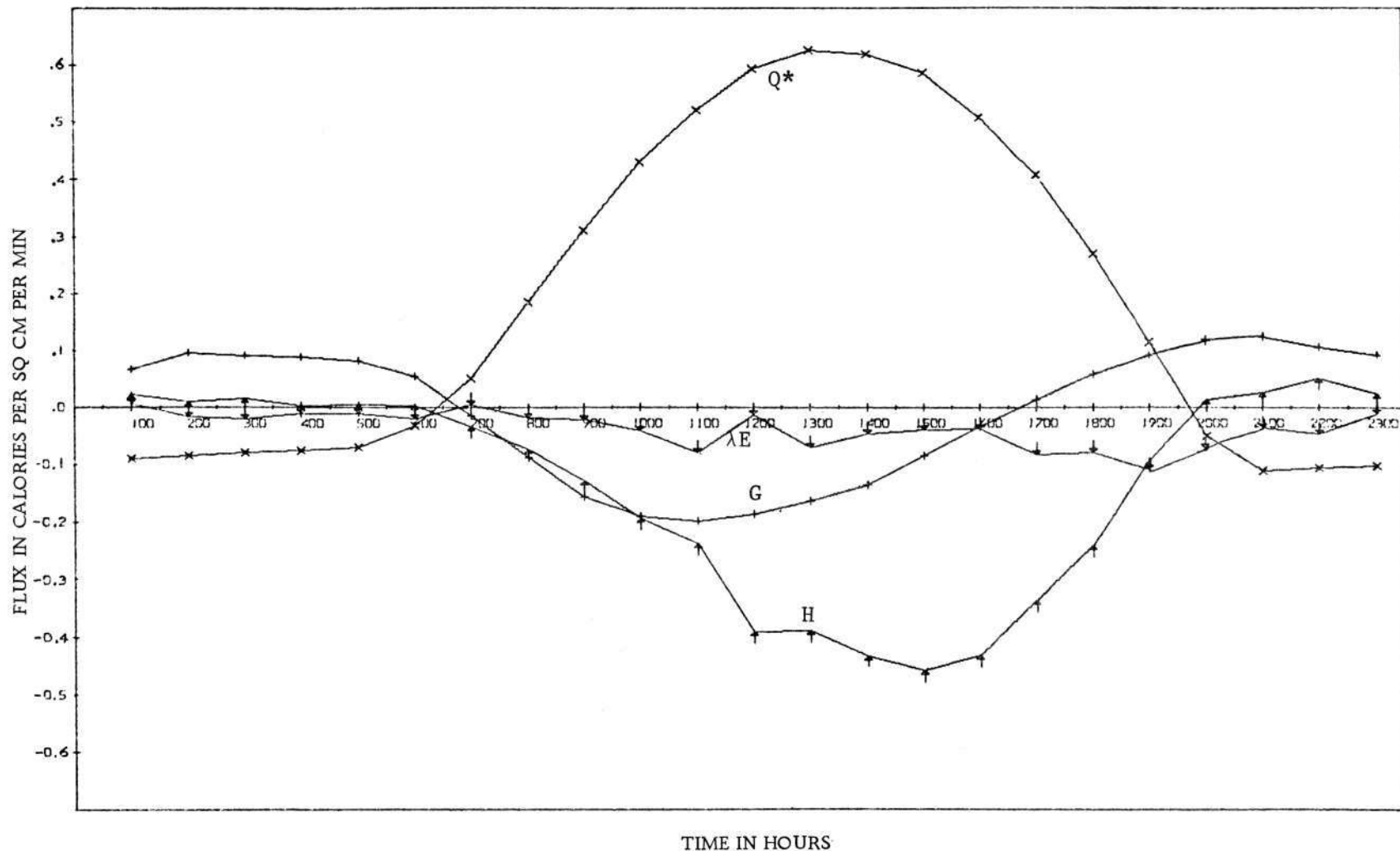


Figure 9. Pattern of energy budget components at the pumice site during 17 July 1969. Net radiation (Q*) is indicated by x; soil heat flux (G) by +; sensible heat flux (H) by †; and latent heat flux (λE) by ↓.

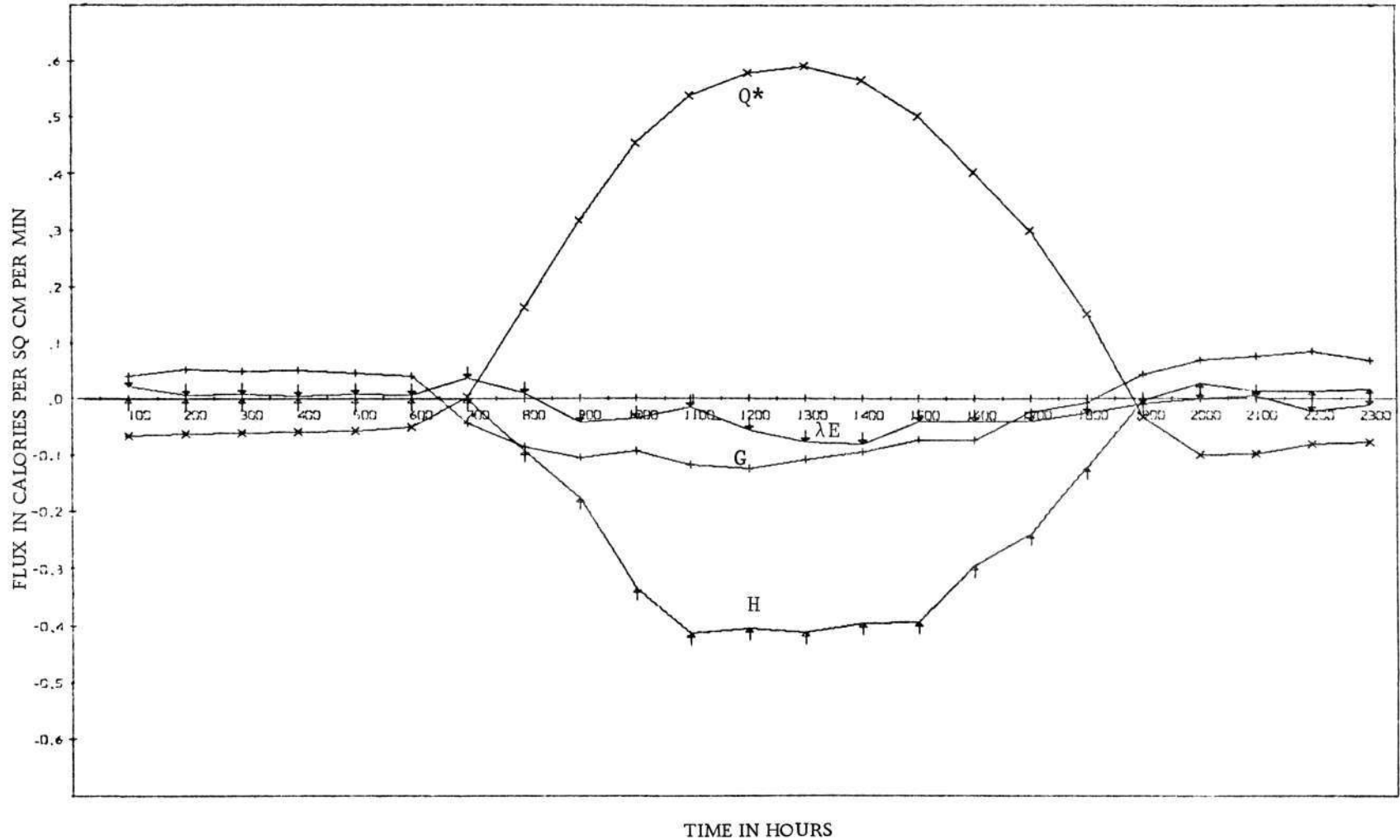


Figure 10. Pattern of energy budget components at the pumice site during 13 August 1969. Net radiation (Q^*) is indicated by x; soil heat flux (G) by +; sensible heat flux (H) by \uparrow ; and latent heat flux (λE) by \downarrow .

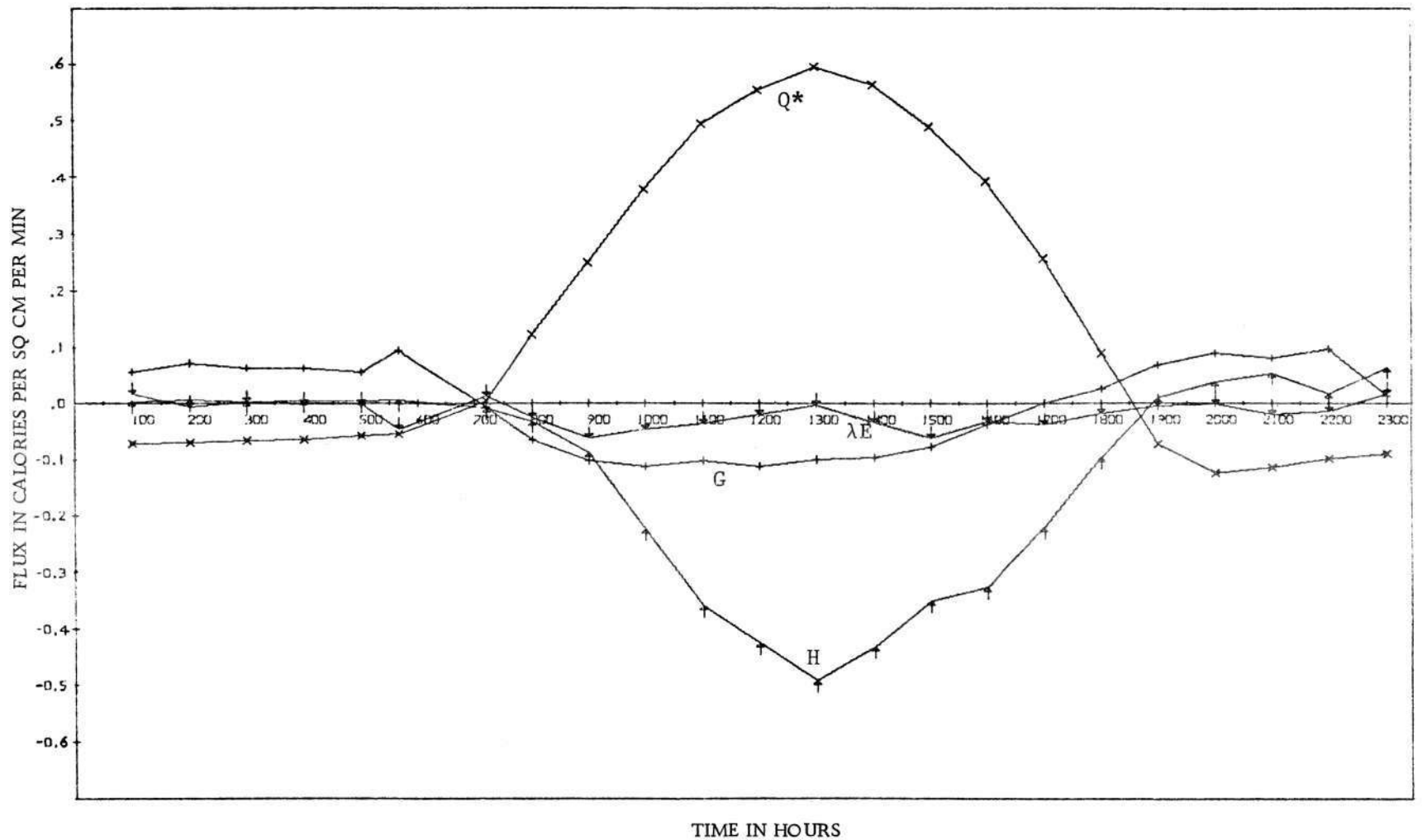


Figure 11. Pattern of energy budget components at the pumice site during 4 September 1969. Net radiation (Q^*) is indicated by x; soil heat flux (G) by +; sensible heat flux (H) by ↑; and latent heat flux (λE) by ↓.

from early to late summer.

Table 6. Daily integrals of the energy budget components.¹

	17 Jul 1969	13 Aug 1969	4 Sep 1969
Net radiation, Q^*	258	228	194
Soil heat flux, G	-7	-14	-2
Sensible heat, H	-197	-197	-180
Latent heat, λE	-54	-17	-11
Equivalent evaporation, ² cm/day	0.092	0.029	0.018

¹Tabular values in cal/cm^2 day, except as noted.

²Latent heat conversion based on the average temperature at the 2 cm depth in the soil, giving nominal values of 586, 586 and 592 cal/cm^3 of water evaporated, respectively.

Net Radiation

The Pattern and Magnitude of Net Radiation. As shown in Figures 9, 10, and 11 the pattern of net radiation at the pumice surface was very regular for each of the three days. Minimum net radiation occurs soon after sunset, and the value then increases gradually through the night until sunrise, when it begins to rise rapidly. The maximum is reached near solar noon, about 1300 hours local time. The smoothness and symmetry of these curves is indicative of the prevailing clear skies at the site. The seasonal changes in the net radiation evident in the tables is attributed to the seasonal reduction in the maximum zenith angle of the sun. A shift is also evident from the figures in the time when the curve crosses between positive and

negative flux values near sunrise and sunset, and the maximum net radiation progressively declines from 0.63 calories per square centimeter per minutes in July, to 0.59 calories per square centimeter per minute in September. There is a corresponding drop in the daily total, or integral, value of net radiation for the surface, as listed in Table 6.

The net radiation energy transfer to the surface for any hourly period is represented by the area between the curve and the axis. Over each 24 hour period it can be seen that the net radiation is predominantly positive, i. e. , toward the surface, so that it constitutes an energy source for the days studied. On 17 July 1969 the integral value of the net radiation was 258 calories per square centimeter per day. The values for 13 August 1969 and 4 September 1969 are 228 and 194 calories per square centimeter per day, respectively.

Albedo. The close correspondence between net radiation and the daily course of the sun illustrates the dependency of net radiation upon the availability of solar energy. However, the net radiation also depends upon the absorptive and emissive characteristics of the surface. For example, in mid-August 1969 measurements of net radiation over a nearby lodgepole forest supplied with essentially identical solar radiation showed a maximum flux of 0.97 calories per square centimeter per minute at noon, and an integral value of 385 calories per square centimeter per day (Gay, 1971b). In mid-August of 1971

measurements of net radiation over the marsh at Malheur Lake determined the maximum flux to be 0.94 calories per square centimeter per minute, with an integral value of 334 calories per square centimeter per day (Gay and Holbo, 1971). While this comparison is incomplete it is clear that the total radiant energy received by the pumice surface is not limited by availability of solar radiation over Central Oregon, but by surface characteristics.

The albedo, or relative reflectivity of the surface to solar energy, is the surface characteristic governing the disposition of solar energy. The measurement of net radiation does not describe this characteristic, and additional measurements were utilized (Equation [3]). The albedo of the pumice surface decreased slightly from 24% in July to 22% in September, probably because of the change in the zenith angle. Compared to other desert surfaces, this is fairly typical (Sellers, 1965). However, the albedo of the pumice surface is more than twice as large as the 9% albedos measured over the lodgepole forest or the marsh.

These contrasts in albedo are emphasized because the establishment of forests on the pumice surface would be accompanied by a change in this characteristic to a lower value. Whether or not this is required for the regeneration of forest is open for comparative examination at a later time. The obvious result of a lower albedo would be greater amounts of energy transfer to the surface from the sun. With

no other changes, this would lead to greater surface temperatures than are now experienced. Under natural circumstances the lower albedos are brought about by changes in other surface characteristics as well, which tend to act toward moderating surface temperatures. Forest regeneration practice would need to consider the overall effect of these influences. However, in so doing it would be recommended that an energy flow approach be taken, so that surface influences might be described quantitatively.

Soil Heat Flux

The Pattern and Magnitude of Soil Heat Flux. In Figure 9, 10, and 11 the pattern of the soil heat flux can be seen to be fairly regular for the three days of the study. Minima are achieved in the late morning hours and maxima in the late evening. This is out of phase with net radiation. This phase difference is due to the lag of deeper soil temperatures behind surface temperature. The extreme rates coincide with periods exhibiting the greatest net change in mean temperature in the soil profile, which are in the morning and evening.

From the figures it is unclear whether the soil is a source or a sink of energy to the surface, since the positive area approximately balances the negative area. The daily integral values listed at the bottom of Tables 3, 4, and 5 or in Table 6 show that the soil is an energy sink. The soil heat flux removed 7 calories per square

centimeter per day from the surface on 17 July, 14 calories per square centimeter per day on 13 August, and 2 calories per square centimeter per day on 4 September. Relative to the amount of energy supplied by net radiation to the surface on these days the losses were 3%, 6%, and 1%, respectively.

Volumetric Heat Capacity of the Pumice Soil. The volumetric heat capacity, C_i , of each layer of the pumice soil were obtained for implementation of Equation [6] to determine the soil heat flux.^{7/} Calculated values include the contribution of water in the soil profile. Table 7 lists the C_i values by increment from the surface.

Table 7. Volumetric heat capacities for the pumice soil profile.

Depth cm	17 July 1969 cal/°C cm ³	13 August 1969 cal/°C cm ³	4 September 1969 cal/°C cm ³
0- 2	0.1684	0.1673	0.1680
2- 5	0.4455	0.1673	0.1683
5-10	0.4400	0.3595	0.4392
10-20	0.4400	0.4008	0.3932

The changes at each level are due to seasonal changes in water content. The total water in the top 20 cm of pumice soil dropped steadily from 5.51 cm on 17 July, to 4.09 cm on 13 August, and to 3.93 cm by 4 September 1969.

^{7/} Personal communication: Dr. P.H. Cochran, USFS Silviculture Laboratory, Bend, Oregon.

Surface and Soil Temperature Regime. The importance of soil temperature as a factor in plant establishment is well documented in the literature (Vaartaja, 1954; Army and Hudspeth, 1960; Turner, 1965; Silen, 1960). The detailed soil temperature measurements made at the pumice site for the purpose of evaluating the soil heat flux are more easily interpreted from an environmental standpoint if they are plotted as temperature profiles at hourly intervals. Such a series of plots conveniently describes the daily course of temperature with depth. Surface and soil temperatures for the three days of the study are summarized in Figures 12, 13, and 14.

The most notable feature of these observations is the range of surface temperature, spanning nearly 50°C on each day. On 4 September 1969 not only does the surface temperature go below 0°C , but the temperature at 2 cm from the surface is also below 0°C for more than 8 hours. In contrast, temperatures at high as 35°C are common at this same depth, during the two earlier days of observation. It is interesting to note that smaller plants near the site were observed to position their roots strictly at distances in the neighborhood of 5 cm from the surface.

The plots verify the anticipated damping depth of the soils, showing approximately 2°C variation, or 5% of the surface temperature amplitude, at the 20 cm level.

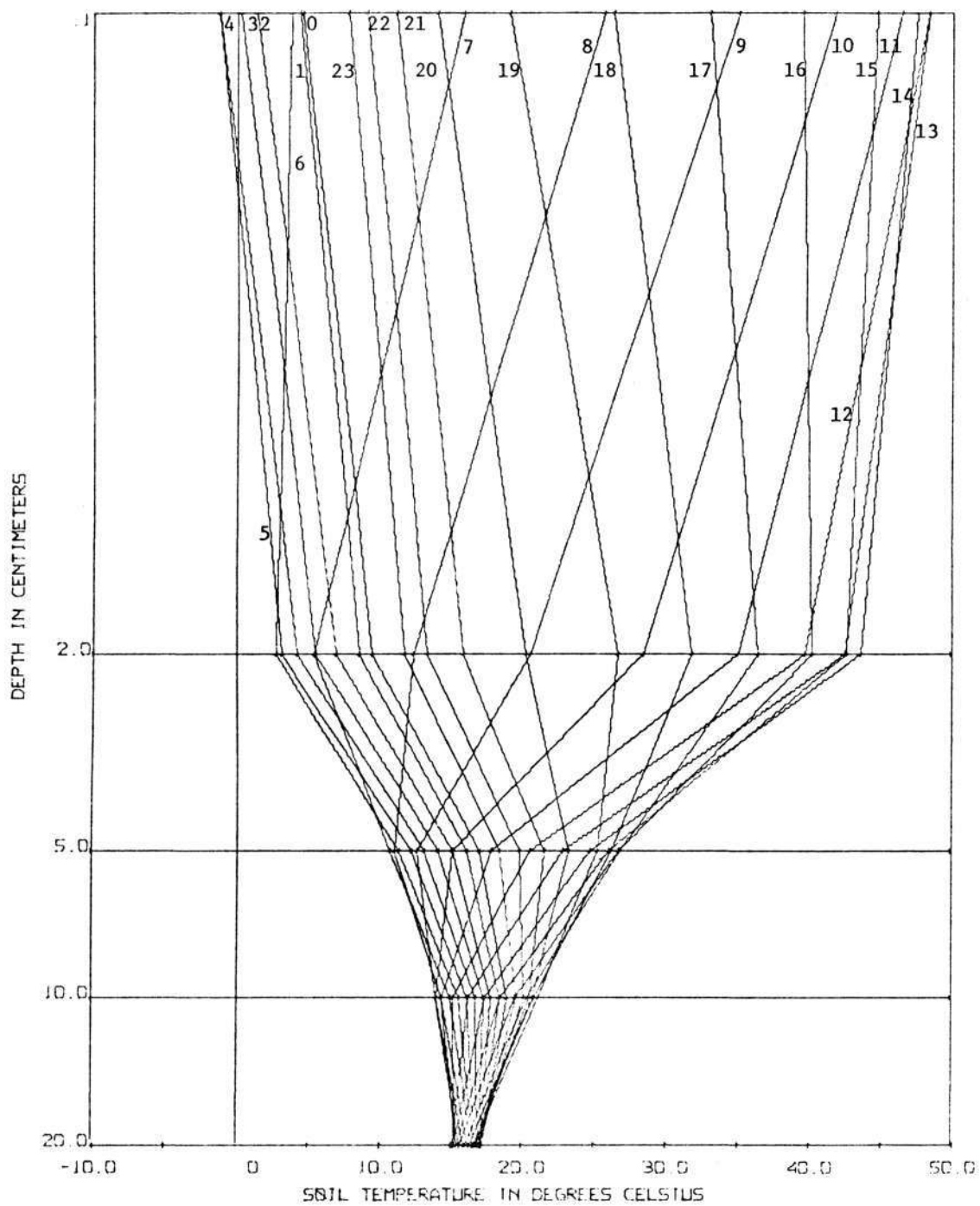


Figure 12. Soil temperature profiles during 17 July 1969 at the pumice site. Hour of record indicated near each profile.

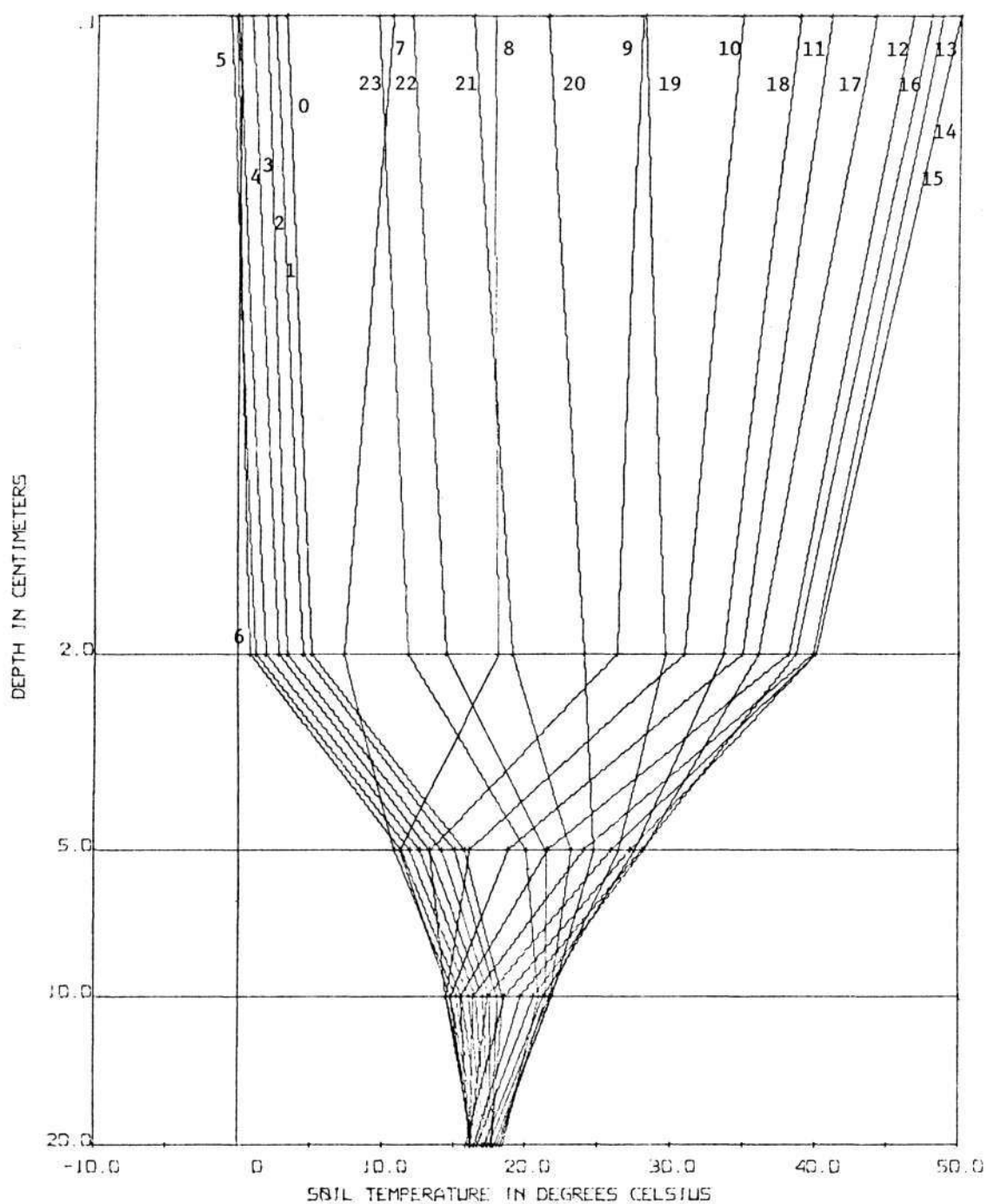


Figure 13. Soil temperature profiles during 13 August 1969 at the pumice site. Hour of record indicated near each profile.

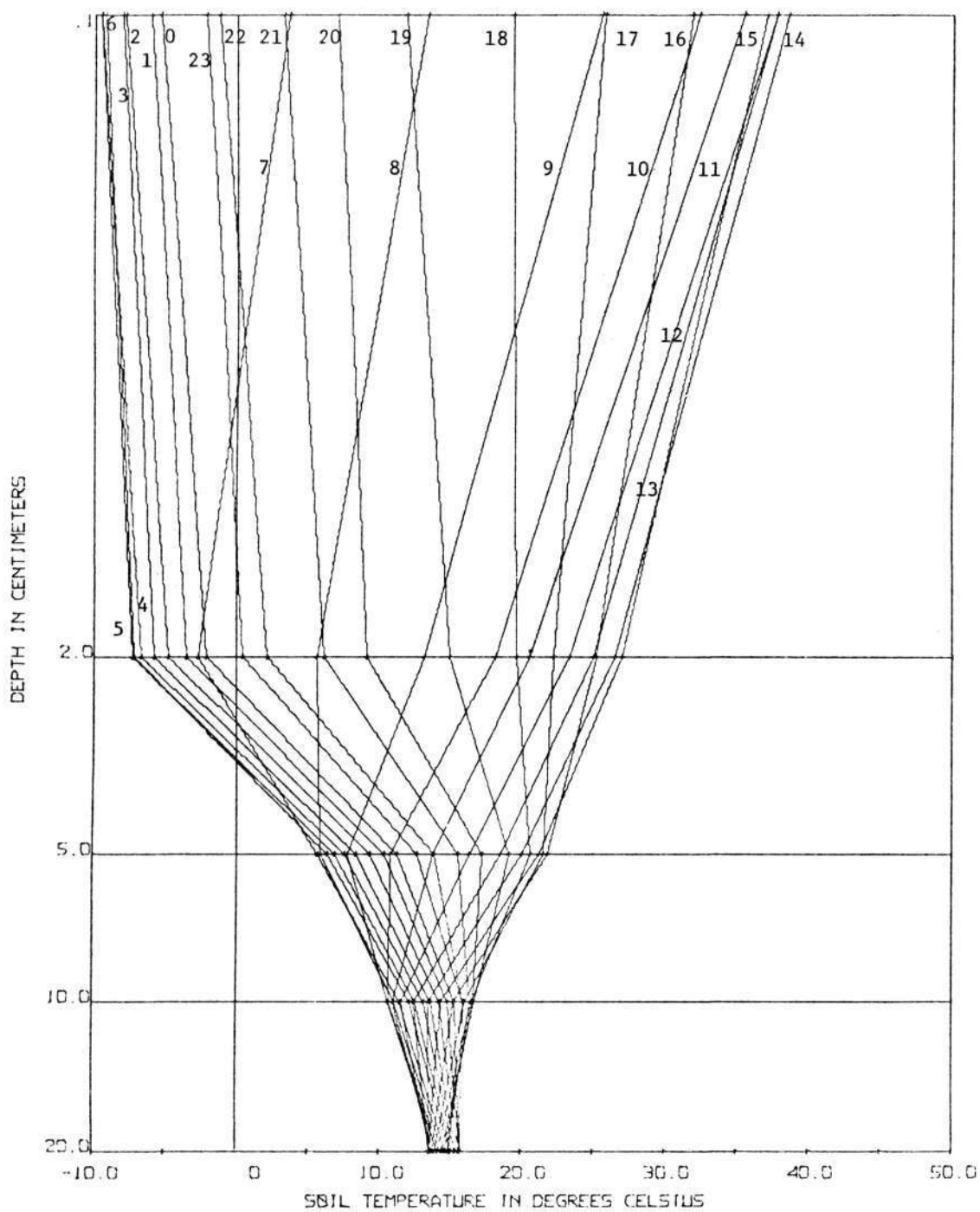


Figure 14. Soil temperature profiles during 4 September 1969 at the pumice site. Hour of record indicated near each profile.

Sensible Heat Flux

The Pattern and Magnitude of the Sensible Heat Flux. The pattern of the sensible heat flux, H , is somewhat irregular in Figures 9, 10, and 11, achieving large negative values near midday, depending upon both the temperature and the windspeed gradients. The values are directed toward the surface (positive) at night, but they remain small except when strong winds occur in the evening. On the whole, sensible heat flux removes energy from the surface. In fact, it is predominant among the energy budget components at the pumice site in this role. The daily integrals given in Tables 3, 4, and 5, or in Table 6 are all large and negative. For 17 July 1969 the sensible heat flux removed 197 calories per square centimeter per day. Losses for 13 August and 4 September were 197 and 180 calories per square centimeter per day, respectively. In terms of the energy supplied to the surface by net radiation, the relative amount of energy dissipated by the sensible heat flux on these three days was 76%, 86%, and 93%. The percentage amount increased as the summer waned and soil moisture declined.

The Roughness Length at the Pumice Site. The roughness length, z_0 , is comparable to the albedo and the volumetric heat capacity in that all three are surface characteristics which can be regarded as independent of the prevailing micrometeorological

conditions. Rough surfaces tend to slow windspeeds near them and thus increase windspeed gradients. As a result, the facility for energy transfer by turbulence is increased in proportion to the roughness length of the surface.

The roughness length of the pumice surface was determined through the application of Equation [25], using windspeed measurements during periods when temperature gradients were small. A value of 0.38 ± 0.03 centimeters was obtained, and a correlation coefficient of 0.99 was indicative of the merit of this figure. The small value is close to values reported for other similar surfaces, as summarized by Sellers (1965).

For the pumice surface, which dissipates such a significant proportion of its energy by sensible heat, it is interesting to postulate the effect of increased roughness on the microclimate, assuming that the other surface characteristics remain unchanged. Because of compensating effects between temperature and windspeed gradients the proportion of sensible heat flux could remain much the same, but proceed at reduced surface temperature extremes. This would be a desirable effect. If the deep soil temperature is about the same, the daily integral soil heat flux may remain much the same, although the reduced surface temperature amplitude may reduce the magnitude of this flux at any given time. An increase in net radiation would result in the daylight hours because of the lower surface temperatures,

which will probably not be offset by nighttime losses, giving more energy to the surface.

The Thickness of the Surface Boundary Layer. Concern with the thickness of the boundary layer, h , is related to the measurement levels used for flux analysis. The uniformity of the pumice surface satisfies most micrometeorological reservations about the site. However, the smoothness of the surface may result in a shallow boundary layer, invalidating certain measurement levels. Fortunately it is possible to evaluate this condition experimentally.

According to Equation [23] the practical limit of the boundary layer is 2000 times the surface flux density of momentum, using typical values of atmospheric characteristics. Since the momentum flux varies with the windspeed it is clear that the boundary layer must vary correspondingly. Windspeed measurements do not reflect the influence of the temperature gradient on momentum transfer, since the temperature gradient may act to enhance or suppress the transfer of momentum. Thus, in the application of Equation [23], allowance must be made for conservative momentum flux estimates in the daytime, and exaggerated estimates at night. This effect has been taken into account in the following results. Equation [15] was used for estimates of the momentum flux, substituting z_0 for one level, thus eliminating the need for two windspeed measurement levels. The 40 centimeter windspeed measurements were employed, because temperature

related effects are minimized when the distance to the surface is less than one meter (Webb, 1965).

The thickness of the boundary layer at the pumice site was found to exceed the highest measurement levels (320 cm) at all times when the windspeed at the 40 centimeter level was greater than 115 centimeters per second. From the data tabulation (Appendix II) it is seen that this condition is met during most daylight hours. Exceptions to this rule have been made for some mid-morning hours when instability of the air probably produced a boundary layer thicker than indicated by the windspeed measurements.

There were also times when the boundary layer was much less than 320 centimeters. These were mostly in the predawn hours. At these times the indicated boundary layer was only 20 centimeters or so. Obviously, the evaluation of sensible heat transfer made from measurements above that level can not adequately represent surface fluxes. In addition, it is questionable whether transfer models developed on the basis of turbulence would be applicable when windspeeds are so light. As a result, the magnitude of sensible heat flux estimates at these times are in error. Fortunately, the energy budget during these times is very nearly balanced between the net radiation and the soil heat flux. Also, at these times the estimated sensible heat flux is very small, so that the overall effect on the energy budget will be small, as well. For these reasons no analytical correction is

attempted for shallow boundary layer conditions at the pumice site.

Latent Heat Flux

The Pattern and Magnitude of the Latent Heat Flux. In Figures 9, 10, and 11, the magnitude of the latent heat flux, λE , at the pumice site is generally less than the other energy budget components, indicating its minor role in influencing the microclimate. The latent heat flux is nearly always negative excepting at dawn, when frost often forms on the surface. The irregular pattern of the latent heat flux may be due in part to the lumped uncertainty which this flux evaluation contains. When this is considered many of the peculiar variations can be smoothed.

The integral values of the magnitude of latent heat flux losses from the pumice surface for 17 July, 13 August, and 4 September 1969 are 54, 17, and 11 calories per square centimeter per day, respectively. These energy levels can be converted to evaporation equivalents, as is shown in Table 6. Water losses for the three days would be 0.092, 0.029, and 0.018 centimeters per day, in the same order. Relative to the amount of energy supplies to the surface by net radiation the dissipation of energy by evaporation was 21%, 7%, and 6% on the three days of the study.

Summary

The energy budget of a pumice desert surface has been analyzed for three clear summer days. The main features of the energy budget are: 1) Relatively low energy input to the surface by net radiation because of the high albedo; 2) Sizable hourly rates of soil heat flux which are, however, insufficient to keep soil and surface temperatures from reaching extreme values. Over the course of the day the soil heat flux returns almost as much energy to the surface as it removes; 3) The sensible heat flux removes the greatest proportion of the energy supplied to the surface by the net radiation component. This is accomplished through large negative magnitudes during the daylight hours. The magnitude of the sensible heat flux would probably remain large even if the surface were modified to reduce temperature extremes at the surface. 4) The latent heat flux has a minor effect on the surface microclimate because of its small magnitude at any time in the day. This component would be proportionately larger if more water were available, although even then energy relationships in the soil may suppress evaporation in the absence of a greater amount of living plant material to transfer water into direct contact with the air.

V. CONCLUSIONS

This study has been primarily concerned with the evaluation of the principal fluxes of thermal energy at the surface of a pumice desert. An energy budget framework was employed for the study, resulting in a description of the daily course of these energy fluxes. The conclusions which can be reached on the basis of these results can be grouped into three categories: 1) the applicability of micrometeorological relationships to the evaluation of energy budget components; 2) significant features of the energy budget of the pumice desert; and, 3) possibilities for environmental modification at the pumice surface.

The Applicability of Micrometeorological Relationships

The successful application of the micrometeorological relationships proposed in the literature depends upon the satisfaction of three conditions: 1) the representativeness of the relationships in characterizing the physical processes being evaluated from micrometeorological properties; 2) the fidelity with which the micrometeorological sensors represent these properties; and, 3) the accuracy and precision in measurement of the signals from these sensors.

The approach which has been taken in this study has been: 1) to accept the micrometeorological relationships as valid models for the evaluation of the physical processes, pending further experimental

verification; 2) to qualitatively screen the measurements by means of profiles and similarity plots for suitability to the application of these relationships; 3) to quantitatively evaluate the uncertainty in the measurements and the subsequent analyses; and then 4) to select the best combination of these relationships that yield the least uncertainty.

The energy budget analysis resulting from these considerations calculates the latent heat component as a residual in the energy budget equation, rather than by direct calculation, using either the Bowen ratio model or the aerodynamic model. The following discussion summarizes the essential considerations regarding the applicability of the micrometeorological relationships.

The Bowen Ratio Model

The Bowen ratio is the simplest to apply experimentally and analytically; neither windspeed measurements nor stability corrections are required. The major difficulty in this method is due to the sensors, it being difficult to achieve reliable gradient measurements of atmospheric vapor pressure. At the pumice site, this difficulty was accentuated by freezing conditions at night, and by the very slight vapor gradients in the daytime.

There are certain situations for which the Bowen ratio is analytically awkward. These are when either H or λE are equal in magnitude but opposite in direction, yielding $\beta = -1$, at which time

the Bowen ratio fails. These situations are transitory, being associated primarily with conditions during sunrise or sunset, and are seldom evident in hourly averaged data.

Other possible situations are when either $H = 0$, or $\lambda E = 0$. When $H = 0$, i. e., $\partial\theta = 0$, λE is simply equal in magnitude but opposite in direction to the available energy (Q^*+G). And, when $\lambda E = 0$, i. e., $\partial e = 0$, β is mathematically undefined, but obviously $H = -(Q^*+G)$ at those times.

The Aerodynamic Model

The aerodynamic model requires both windspeed measurements and a correction for stability. Thus, it is more complicated experimentally and analytically than the Bowen ratio. However, the aerodynamic model does provide a means of evaluating the sensible heat component without requiring the measurement of vapor pressure profiles. The lack of agreement in the literature as to the form of the stability correction further complicated application of this model. This problem was overcome in a unique fashion by using the energy budget equation as a defining equation for the stability correction. The close agreement of the resultant correction function with one well-substantiated form appearing in the literature confirms the usefulness of this approach, particularly for the evaluation of the sensible heat flux component.

A further requirement of the aerodynamic model is the existence of turbulent air flow in the surface boundary layer. This condition is commonly satisfied during the periods of higher windspeeds in the daylight hours, but records from the pumice site show very low windspeeds during some of the early morning hours. During these periods, turbulence may not be well developed, and the application of the aerodynamic model may be restricted.

Occasionally during these same hours, the estimated thickness of the boundary layer failed to extend across the two levels of measurement. Satisfactory aerodynamic flux analyses could not be made from the available measurements under such conditions. However, most hours in the day had windspeeds of sufficient intensity to create a boundary layer that extended beyond the highest measurement levels.

Fortunately, the magnitudes of the sensible and latent heat fluxes during these early morning hours are small, so that errors in their evaluation resulting from boundary layer problems are believed to have a negligible effect on the overall analysis.

Analytical Uncertainties

Important limitations on the accuracy of surface flux evaluations were associated with analytical uncertainties. These in turn relate to both the precision and accuracy of the measurements and the micro-meteorological conditions prevailing at the pumice site, particularly

with regard to the determination of vapor pressure gradients.

Vapor pressure gradients at the pumice site were quite small, because of the low rates of evaporation. When the vapor gradients are slight, the measurement uncertainties become larger. Micro-meteorological evaluation of the latent heat flux thus can include a sizeable uncertainty that averaged 25 percent at the pumice site. It should be noted that the average absolute value of the uncertainty is only $0.02 \text{ cal/cm}^2 \text{ min}$, or less. The uncertainties were minimized in the final analysis by obtaining the latent heat component as a residual in the energy budget equation.

Temperature gradients at the pumice site were generally large because of the high rates of sensible heat transfer. Thus, the uncertainty associated with the sensible heat flux analysis was relatively small, and this component was evaluated using the corrected aerodynamic model.

The uncertainty of evaluation of the net radiation and the soil heat flux were found to be negligible using the standard relationships.

Significant Features of the Energy Budget

At the pumice site net radiation, Q^* , was the main energy source to the surface. The net radiation for the pumice surface was smaller than that over nearby vegetated surfaces, partly because of the higher albedo of the desert surface. The pumice surface

temperatures ranged nearly 50°C during each of the three days of the study.

The rate of soil heat flux, G , away from the surface was greatest in the late morning hours. Maximum rates of soil heat flux toward the surface occurred shortly after sunset. Over an entire 24-hour period the soil heat flux returned nearly as much energy to the surface as it had removed. Harsh environmental temperatures were observed in the soil to a depth of 2 cm.

The sensible heat flux, H , to the air was the main energy sink. On a daily basis the sensible heat flux accounted for the disposal of between 76% and 93% of the energy supplied by net radiation, increasing in proportion later in the summer. Steep air temperature gradients that frequently exceeded 4°C in the boundary layer from 20 cm to 320 cm of the surface were associated with the high rates of sensible energy transfer. High air temperatures were not measured, however, even though the surface temperatures sometimes exceeded 50°C .

Latent heat transfer, λE , was of less importance as a dissipator of energy. The magnitude of this component was not very large initially, and it declined to rather small values as moisture was depleted from the surface soil layer. Had more water been available, it would probably have been evaporated preferentially to the dissipation of thermal energy by either sensible or soil heat fluxes. At the

pumice site the latent energy component was limited by drying of the surface soil and by the lack of active plant tissue for transport of moisture from the soil depths to sites of energy exchange. However, except for leaves very near the hot surface it is unlikely that adapted plants would exhibit high evaporation rates for temperature control because of the moderate air temperatures. On the other hand, unadapted plants would perhaps transpire excessively in response to the characteristically low atmospheric water vapor content.

Possibilities for Environmental Modification

The methods by which environmental modification can be brought about at pumice surfaces will no doubt involve changes in surface characteristics such as the volumetric heat capacity of the soil, the albedo, the roughness length, or perhaps the availability of moisture. The anticipated effect of changes in these characteristics has been discussed by Cochran (1969). Environmental modification has not been a central objective of this study, but rather the energy budget has been examined as a means of characterizing the microclimate of a surface, for which purpose it holds considerable promise. Energy budget analysis is regarded as a way to reduce complex microclimatological relationships into a form that readily enables the comparison of different surfaces. The extent to which the microclimate of a pumice surface may be modified remains to be demonstrated by experiment.

Summary

The major contribution of this study is the quantification of the principal energy transfers at a pumice surface. The success of this study depended upon the collection of precise microclimatological data in the field and its analysis by micrometeorological relationships developed from theory. One important aspect of the analysis was the development of a unique stability correction specifically for this study, that appears to be generally applicable to other surface as well. This was necessitated by the lack of a general theory extending over a wide stability range. A second important aspect was the adaption and application of a method for assessing the uncertainty of measurement and analysis.

The significant features of the pumice energy budget and the associated surface characteristics were found to be: 1) a high proportion of energy going into sensible heat transfer; 2) a high albedo causing the energy input to the surface to be less than maximum; and 3) low evaporation rates due to the dry surface. These results were not unexpected. Moreover, this study has demonstrated the applicability of micrometeorological theory in characterizing complex microclimatological relationships and presenting them in a simple, readily comparable form using the energy budget framework.

The possibilities for environmental modification of the pumice

surface have not been explored. However, there must be a way to capitalize or optimize what has obviously occurred naturally by succession or by accident in making the environment suitable for the establishment of the forests which surround the pumice surface. The energy budget is regarded as one way to make a systematic approach to understanding these environmental relationships.

BIBLIOGRAPHY

- Army, T. J. and E. B. Hudspeth, Jr. 1960. Alteration of the micro-climate of the seed zone. *Agron. J.* 52:17-22.
- Batchelor, G. K. 1953. The conditions for dynamical similarity of motions of frictionless perfect-gas atmosphere. *Quart. J. Roy. Meteorol. Soc.* 79:224-235.
- Baumgartner, A. 1956. Investigations on the heat and water economy of a young forest. Translated from: *Untersuchungen über den Wärme-und Wasserhaushalt eines jungen Waldes. Ber. Deut. Wetterdienstes* 5:4-53. CSIRO Translation 3760, Melbourne, Australia. 1958.
- Bavel, C. H. M. van, L. J. Fritschen, and R. J. Reginato. 1963. Surface energy balance in arid lands agriculture 1960-1961. ARS-USDA Production Research Report No. 76. 46 p.
- Bowen, I. S. 1926. The ratio of heat losses by conduction and by evaporation from any water surface. *Phys. Rev.* 27:779-787.
- Carson, J. E. 1961. Soil heat flux measurement. In: *Soil temperature and weather conditions.* Argonne National Laboratory. ANL-6470. 156 p.
- Cochran, P. H. 1969. Thermal properties and surface temperatures of seedbeds. Pacific Northwest Forest and Range Experiment Station, USDA, Portland, Oregon. 19 p.
- Cochran, P. H., L. Boersma, and C. T. Youngberg. 1967. Thermal properties of a pumice soil. *Soil Sci. Soc. Amer. Proc.* 31:454-459.
- Deacon, E. L. 1949. Vertical diffusion in the lowest layers of the atmosphere. *Quart. J. Roy. Meteorol. Soc.* 75:89-193.
- Denmead, O. T. 1969. Comparative micrometeorology of a wheat field and a forest of *Pinus radiata*. *Agr. Meteorol.* 6:357-371.
- Denmead, O. T. and I. C. McIlroy. 1970. Measurements of non-potential evaporation from wheat. *Agr. Meteorol.* 7:285-302.
- Dyer, A. J. 1967. The turbulent transport of heat and water vapor in an unstable atmosphere. *Quart. J. Roy. Meteorol. Soc.* 93:501-508.

- Ellison, T.H. 1957. Turbulent transport of heat and momentum from an infinite rough plane. *J. Fluid. Mech.* 2:456-466.
- Fritschen, L.J. 1963. Construction and evaluation of a miniature net radiometer. *J. Appl. Meteorol.* 2:165-172.
- Funk, J.P. 1959. Improved polythene-shielded net radiometer. *J. Sci. Instr.* 36:267-270.
- Funk, J.P. 1960. Measured radiative flux divergence near the ground at night. *Quart. J. Roy. Meteorol. Soc.* 86:382-389.
- Gates, D.M. 1965. Energy, plants, and ecology. *Ecology* 46:1-13.
- Gay, L.W. 1971a. An environmental data acquisition system. National Conference on the Forest Weather and Associated Environments May 18-20, 1971. Atlanta, Ga. 8 numb. leaves. (mimeographed). Abstracted in *Bull. Amer. Meteorol. Soc.* 52:202-203.
- Gay, L.W. 1971b. Forest climatology studies at Oregon State University. *Proc. Ore. Acad. of Sci.* 7:11-23.
- Gay, L.W. 1972. On the construction and use of ceramic-wick psychrometers. In: *Psychrometry in Water Relations Research*, ed. by Brown, R.W., B.P. van Haveren, and H.H. Wiebe. Utah Agricultural Expt. Station, Logan. (In Press).
- Gay, L.W. and H.R. Holbo. 1971. Evapotranspiration study - Malheur Lake, Silvies River Drainage. Oregon State University, Corvallis. Final Report, Corps of Engineers. Contract No. DACW 68-72-C-0032. 21 numb. leaves. (mimeographed).
- Geiger, R. 1966. *The climate near the ground.* Harvard University Press, Cambridge, 611 p.
- Halstead, M.H. 1957. Wind profile instrumentation. In: *Exploring the atmosphere's first mile, Vol. I*, ed. by Lettau, H.H., and B. Davidson. Pergamon, New York. 376 p.
- Hermann, R.K. 1968. A watering experiment with sown ponderosa pine in Central Oregon. *Northwest Sci.* 42:47-52.

- Hermann, R.K. 1970. Planting in pumice and root development of ponderosa pine. In: Regeneration of ponderosa pine, ed. by Hermann, R.K. School of Forestry, Oregon State University, Paper 681:50-53.
- Holzman, B. 1943. The influence of stability on evaporation. *Ann. New York Acad. Sci.* 44:13-18.
- Horn, E.M. 1968. Ecology of the pumice desert, Crater Lake National Park. *Northwest Sci.* 42:141-149.
- Hoven, Isaac van der. 1957. Power spectrum of horizontal wind speed in the frequency range from 0.0007 to 900 cycles per hour. *J. Meteorol.* 14:160-164.
- Industrial Development Research Council. 1968. Registered community audit. A study conducted for the Bend, Oregon, Chamber of Commerce. Atlanta, Georgia. 4 numb. leaves. (mimeographed).
- Lemon, E.R. 1965. Micrometeorology and the physiology of plants in their natural environment. Chapter 2, Plant Physiology, Volume 4, Part A, Academic Press, New York. 452 p.
- Lettau, H.H. 1959. Research problems in micrometeorology. University of Wisconsin, Madison. Final Report, USAEC Contract No. DA-36-039-SC-80063. 85 p.
- Lourence, F.J. 1967. Instrumentation development and calibration. Chapt. II, Part III, University of California, Davis. Final Report, USAEC Contract No. DA-02-086-AMC-0447(E). 84 p.
- Lowry, W.P. 1969. Weather and life. Academic Press, New York, 305 p.
- Lumley, J.L. and H.A. Panofsky. 1964. The structure of atmospheric turbulence. Interscience, New York, 239 p.
- McBean, G.A. 1968. An investigation of turbulence within the forest. *J. Appl. Meteorol.* 7:410-416.
- McIlroy, I.C. and D.E. Angus. 1964. Grass, water and soil evaporation at Aspendale. *Agr. Meteorol.* 1:201-224.

- Miller, D.H. 1955. Snow covered and climate in the Sierra Nevada, California. Univ. Calif. Publ. Geog. 11:1-218.
- Morgan, D.L., W.O. Pruitt, and F.J. Lourence. 1971. Analysis of energy, momentum, and mass transfers above vegetative surfaces. Chapt. I, and Appendix B. University of Clifornia, Davis. Final report, USAEC. Contract No. DA-AMC-28-043-68-G10. 128 p.
- Munn, R.E. 1966. Descriptive micrometeorology. Academic Press, New York, 245 p.
- Murray, F.W. 1967. On the computation of saturation vapor pressure. J. Appl. Meteorol. 6:203-204.
- Namken, L.N., C.J. Gerard, and R.G. Brown. 1968. Evapotranspiration of cotton and estimation methods. Agron. J. 60:4-7.
- Overton, W.S. 1971. A note on necessary sample size for precision of estimated mean. Department of Statistics, Oregon State University, Statistical Note. 8 p.
- Panofsky, H.A., A.K. Blackadar, and G.E. McVehil. 1960. The diabatic wind profile. Quart. J. Roy. Meteorol. Soc. 86:390-398.
- Panofsky, H.A. 1963. Determination of stress from wind and temperature measurements. Quart. J. Roy. Meteorol. Soc. 89:85-94.
- Panofsky, H.A. 1965. Reanalysis of Swinbank's Kerang observations. In: Flux of heat and momentum in the planetary boundary layer of the atmosphere. Chapter IV, Pennsylvania State University, College Park. Air Force Cambridge Research Laboratories. Final Report No. 65-531. 140 p.
- Paulson, C.A. 1970. The mathematical representation of wind speed and temperature profiles in the unstable atmospheric surface layer. J. Appl. Meteorol. 9:857-861.
- Prandtl, L. 1952. Essentials of fluid dynamics. Blackie, London. 452 p.

- Priestley, C.H.B. and W.C. Swinbank. 1947. Vertical transport of heat by turbulence in the atmosphere. *Proc. Roy. Soc., A*, 189:543-561.
- Pruitt, W.O. and F.J. Lourence. 1966. Tests of aerodynamic, energy balance and other evaporation equations over a grass surface. In: *Investigations of energy momentum and mass transfers near the ground. Chapter IV, University of California, Davis. Final Report, USAEC Contract No. DA-AMC-28-043-65-G12. 259 p.*
- Rauner, Yu. L. 1960. The heat balance of forests. *Izvestiya Akademii Nauk SSSR. Seriya Geograficheskaya* 1:49-59. Translated by Israel Prog. Sci. Transl. No. 1342. U.S. Dept. Comm. Washington, D. C.
- Reifsnyder, W.E. and H.W. Lull. 1965. Radiant energy in relation to forests. *USDA Tech. Bull. No. 1344. 111 p.*
- Richardson, L. F. 1920. The supply of energy from and to atmospheric eddies. *Proc. Royal Soc., A*, 97:354-373.
- Rider, N.E. and G.D. Robinson. 1951. A study of the transfer of heat and water vapour above a surface of short grass. *Quart. J. Roy. Meteorol. Soc.* 77:375-401.
- Scarborough, J.B. 1966. *Numerical mathematical analysis. Johns Hopkins Press. 6th ed. 600 p.*
- Sellers, W.D. 1965. *Physical climatology. Univ. of Chicago Press, Chicago. 272 p.*
- Shannon, C.E. 1949. A mathematical theory of communication. *Bell System Tech. J.* 27:379-423; 623-565.
- Silen, R.R. 1960. Lethal surface temperatures and their interpretation for Douglas-fir. Unpublished Ph.D. thesis on file at Oregon State University, Corvallis. 170 numb. leaves.
- Smith, L.P. 1970. The difficult art of measurement. *Agr. Meteorol.* 7:281-283.
- Sternes, G.L. 1969. Climate of Bend, Oregon. In: *Climatology of the United States. No. 20-35. U.S. Dept. Comm., ESSA.*

- Suomi, V.E., M. Fransilla, and N.F. Islitzer. 1954. An improved net-radiation instrument. *J. Meteorol.* 11:276-282.
- Swinbank, W.C. and A.J. Dyer. 1967. An experimental study in micro-meteorology. *Quart. J. Roy. Meteorol. Soc.* 93:494-500.
- Tanner, C.B. 1963. Basic instrumentation and measurements for plant environment and micrometeorology. University of Wisconsin, Madison. *Soils Bulletin* 6. 358 p.
- Tanner, C.B. 1967. Measurement of evapotranspiration. In: *Irrigation of agricultural lands*, ed. by Hagan, R.M., H.R. Haise, and T.W. Edminster. *Agronomy* 11:534-574.
- Tanner, C.B. 1968. Evaporation of water from plants and soil. In: *Water deficits and plant growth*, Vol. I, ed. by Kozlowski, T.T. Chapter 4. Academic Press, New York. 390 p.
- Thornthwaite, C.W. and B. Holzman. 1939. The determination of evaporation from land and water surfaces. *Monthly Weather Rev.* 67:4-11.
- Turner, J.C. 1965. Some energy and microclimate measurements in a natural arid zone plant community. *UNESCO Arid Zone Res.* 25:63-70.
- Vaartaja, O. 1954. Factors causing mortality of tree seeds and succulent seedlings. *Acta Forestalia Fennica* 62:1-34.
- Wagg, J.W.B. and R.K. Hermann. 1962. Artificial seeding of pine in Central Oregon. *Oregon State University Forest Research Lab. Note* 47. 47 p.
- Webb, E.K. 1965. Aerial microclimate. In: *Agricultural meteorology*, ed. by Waggoner, P.E. *Meteorol. Monogr.* 6:27-58.
- Webb, E.K. 1970. Profile relationships: The log-linear range, and extension to strong stability. *Quart. J. Royal Meteorol. Soc.* 96:67-90.
- Westman, H.P. (ed.). 1956. Reference data for radio engineers. *International Telephone and Telegraph Corp.* New York. 4th ed. 1121 p.

- Wijk, W.R. van and D.A. de Vries. 1963. Periodic temperature variations in a homogeneous soil. In: Physics of plant environment, ed. by Wijk, W.R. van. Wiley, New York. 382 p.
- Woods, F.W. 1960. Energy flow silviculture - a new concept for forestry. Soc. Amer. For. Proc. 60:25-28.
- Youngberg, C.T. and C.T. Dryness. 1964. Some physical and chemical properties of pumice soils in Oregon. Soil Sci. 97:391-399.

APPENDICES

APPENDIX I

Symbols and Definitions

<u>Symbol</u>	<u>Definition</u>
A	psychrometric constant, $^{\circ}\text{C}^{-1}$; constant temperature offset, $^{\circ}\text{C}$
B	amplitude of the time-dependent temperature offset, $^{\circ}\text{C}$
C	volumetric heat capacity of the soil, $\text{cal}/\text{cm}^3\text{ }^{\circ}\text{C}$
C_p	specific heat of the air, $0.24 \text{ cal}/\text{gm}^{\circ}\text{C}$
E	water vapor flux density, $\text{gm}/\text{cm}^2 \text{ min}$
G	soil heat flux density, $\text{cal}/\text{cm}^2 \text{ min}$
H	sensible heat flux density, $\text{cal}/\text{cm}^2 \text{ min}$
K_{\downarrow}	incoming shortwave radiation flux density, $\text{cal}/\text{cm}^2 \text{ min}$
K_{\uparrow}	outgoing shortwave radiation flux density, $\text{cal}/\text{cm}^2 \text{ min}$
K_H	eddy diffusivity of heat, cm^2/sec
K_M	eddy diffusivity of momentum, cm^2/sec
K_V	eddy diffusivity of vapor, cm^2/sec
L_{\downarrow}	incoming longwave radiation flux density, $\text{cal}/\text{cm}^2 \text{ min}$
L_{\uparrow}	outgoing longwave radiation flux density, $\text{cal}/\text{cm}^2 \text{ min}$
L_g	outgoing longwave surface radiation flux density, $\text{cal}/\text{cm}^2 \text{ min}$
M	unspecified measurement
N	average count rate of anemometer revolutions, counts/min
Q^*	net all-wave radiation flux density, $\text{cal}/\text{cm}^2 \text{ min}$
Ri	Richardson number

<u>Symbol</u>	<u>Definition</u>
T	soil temperature, °C
T _d	dry bulb temperature, °C
T _h	hemisphere temperature of the pyrrometer, °C
T _r	thermocouple reference junction temperature, °C
T _w	wet bulb temperature, °C
TS	surface temperature, °C
V	measured signal value, millivolts
a	radiometer calibration coefficient, millivolts cm ² min/cal; coefficient in the thermocouple equation, 0.0438
b	coefficient in the thermocouple equation, 0.4377
c	constant of integration; coefficient in the thermocouple equation, 22.7
d	damping distance in the soil, cm
e	vapor pressure of water in the air, mb
e _s	saturation vapor pressure at the wet bulb temperature, mb
g	acceleration due to gravity, 980 cm/sec ²
h	thickness of the boundary layer, cm
k	von Karman's constant (0.4)
p	atmospheric pressure, mb
r	reflected longwave radiation flux density, cal/cm ² min
s	standard deviation from sample mean
t	time, sec, min, hr, or day
u	horizontal windspeed, cm/sec

<u>Symbol</u>	<u>Definition</u>
x	volume fraction of a soil increment
y	mean value of property
\bar{y}	time average value of a property
z	vertical distance to the exchange surface, cm
z_0	roughness length, cm
α	albedo; coefficient in the stability correction function
β	Bowen ratio
Γ	adiabatic lapse rate, $-0.0001^\circ\text{C}/\text{cm}$
γ	exponent in the stability correction function
Δ	difference between values, either in space or time
δ	error coefficient
ϵ	emissivity; ratio of molecular weights of water to air, 0.622
θ	potential temperature, $T_d + \Gamma z$, $^\circ\text{C}$
λ	latent heat of vaporization of water, $\text{cal}/\text{gm}^\circ\text{C}$
ρ	density of the air, $1.02 \times 10^{-3} \text{ gm}/\text{cm}^3$
σ	Stefan-Boltzmann constant, $8.27 \times 10^{-11} \text{ cal}/\text{cm}^2 \text{ }^\circ\text{K min}$
τ	momentum flux density, dyne/cm^2
ϕ	stability correction
ω	angular frequency, $2\pi f$

APPENDIX II

Data Tabulation

Table II-1. Microclimate measurements at the pumice site, 17 July 1969.

HR	W* LY/MIN	SOIL TEMPERATURES DEGREES C					AIR TEMPERATURES DEGREES C						VAPOR PRESSURE MILLIBARS						WIND SPEED CM/SEC					
		100CM	SURFACE	2CM	5CM	10CM	20CM	40CM	80CM	160CM	240CM	320CM	20CM	40CM	80CM	160CM	240CM	320CM	20	40	80	160	240	320
1	-0.090	4.47	8.59	16.25	18.60	17.35	6.41	6.67	7.35	8.06	8.49	8.91	7.34	7.37	7.41	7.48	7.48	7.47	61	77	94	116	134	146
2	-0.095	1.43	6.37	15.21	18.04	17.30	2.29	2.39	3.04	4.06	4.78	5.17	6.48	6.54	6.66	6.83	6.84	6.85	48	64	83	105	111	114
3	-0.081	.33	5.56	14.19	17.46	17.20	.61	.71	1.13	2.06	2.67	3.15	5.91	5.94	6.07	6.25	6.27	6.39	46	60	75	96	103	113
4	-0.077	-1.15	4.32	13.20	15.87	17.18	-1.34	-1.15	-0.75	.04	.65	1.10	5.33	5.38	5.51	5.69	5.86	5.96	35	45	56	68	71	70
5	-0.071	-1.21	3.19	12.29	16.29	16.92	-2.22	-2.24	-1.90	-1.43	-1.21	-0.96	5.45	5.20	5.10	5.21	5.29	5.35	28	37	44	54	61	66
6	-0.032	3.85	2.76	11.43	15.73	16.80	-1.96	-2.02	-2.02	-1.78	-1.61	-1.43	5.90	5.83	5.01	5.49	5.06	5.12	26	34	46	56	63	65
7	.343	15.82	5.47	11.89	15.12	16.70	3.47	3.16	3.03	2.95	2.92	2.76	5.15	5.46	6.52	6.04	6.43	6.49	33	36	38	39	40	38
8	.183	25.66	12.43	11.09	14.50	16.42	10.89	10.54	10.29	10.07	9.74	9.83	7.29	7.29	7.19	7.13	7.09	7.12	48	53	56	59	60	58
9	.309	35.05	20.65	12.73	14.12	16.10	16.13	15.41	14.97	14.65	14.40	14.31	6.73	6.77	6.65	6.58	6.65	6.62	74	87	87	93	95	96
10	.429	41.88	28.47	15.23	14.12	15.83	18.89	18.01	17.43	16.95	16.63	16.56	17.07	16.34	5.97	5.91	5.94	5.88	106	122	130	139	142	144
11	.520	46.47	35.15	17.99	14.51	15.56	21.47	20.54	19.77	19.02	18.60	18.78	19.95	19.49	5.26	5.12	5.03	5.17	143	167	178	193	200	205
12	.594	48.36	39.81	20.69	15.31	15.39	23.84	22.50	21.47	20.36	20.03	20.09	6.32	6.16	5.99	5.73	5.83	5.87	191	228	249	271	281	289
13	.627	49.40	42.56	23.05	16.39	15.30	24.37	23.09	22.02	21.25	20.74	20.66	6.88	6.38	6.30	6.35	6.29	6.19	209	252	275	302	315	323
14	.620	47.64	43.72	24.93	17.55	15.38	25.46	24.13	23.00	22.16	21.65	21.53	7.33	6.45	6.40	6.41	6.33	6.24	217	263	290	317	330	338
15	.585	44.79	42.67	25.25	18.70	15.56	26.21	24.93	23.79	22.93	22.38	22.27	7.48	6.29	6.15	6.18	6.09	6.02	264	326	360	397	413	423
16	.508	39.67	40.28	26.89	19.71	15.81	26.07	24.87	23.84	23.01	22.48	22.39	7.34	5.75	5.65	5.66	5.57	5.45	255	315	350	388	407	418
17	.408	33.14	36.47	26.96	20.50	16.17	25.53	24.59	23.71	23.03	22.65	22.52	7.24	5.23	5.15	5.16	5.07	4.95	294	369	416	468	491	504
18	.267	26.40	31.90	26.41	21.04	16.53	23.96	23.32	22.75	22.22	21.89	21.82	7.94	5.83	5.78	5.78	5.71	5.56	301	380	431	485	510	527
19	.113	19.15	26.77	25.41	21.34	16.87	21.83	21.57	21.34	21.11	20.90	20.89	8.54	6.54	6.48	6.50	6.43	6.30	295	376	426	483	513	531
20	-0.051	14.05	20.32	23.37	20.89	16.82	17.65	17.73	17.86	17.94	17.94	17.97	5.65	5.86	5.69	5.70	5.61	5.48	246	313	359	412	433	456
21	-0.112	11.09	15.91	21.67	20.68	17.03	13.85	14.28	14.77	15.29	15.56	15.71	5.86	6.09	5.93	5.90	5.81	5.68	133	169	199	276	284	264
22	-0.107	9.05	13.38	20.02	20.29	17.21	11.90	12.41	13.02	13.70	14.09	14.33	6.47	6.67	6.52	6.50	6.40	6.30	137	173	215	250	274	290
23	-0.103	7.84	11.81	19.61	19.77	17.32	10.56	10.96	11.40	11.81	12.06	12.25	7.21	7.38	7.31	7.33	7.27	7.19	106	135	160	197	212	225
0	-0.135	5.89	10.34	17.63	19.33	17.35	8.12	8.51	9.05	9.60	9.99	10.29	7.39	7.48	7.43	7.50	7.45	7.40	0	0	0	0	0	0

Table II-2. Microclimate measurements at the pumice site, 13 August 1969.

HR	W LY/MIN	SOIL TEMPERATURES DEGREES C					AIR TEMPERATURES DEGREES C						VAPOR PRESSURE MILLIBARS						WINDSPEED CM/SEC					
		150CM	SURFACE	2CM	5CM	10CM	20CM	40CM	80CM	160CM	240CM	320CM	20CM	40CM	80CM	160CM	240CM	320CM	20	40	80	160	240	320
1	-0.065	2.34	4.49	14.99	18.03	17.72	0	0	0	0	0	0	0	0	0	0	0	41	54	68	78	83	87	
2	-0.062	1.66	3.44	14.10	17.50	17.65	0	0	0	0	0	0	0	0	0	0	0	35	46	56	69	76	78	
3	-0.059	.70	2.81	13.31	16.98	17.56	0	0	0	0	0	0	0	0	0	0	0	33	43	51	57	62	63	
4	-0.057	-0.31	1.95	12.57	16.47	17.43	0	0	0	0	0	0	0	0	0	0	0	30	38	47	54	58	56	
5	-0.056	-1.77	1.23	11.89	15.99	17.29	0	0	0	0	0	0	0	0	0	0	0	29	37	45	52	55	57	
6	-0.049	-2.43	.75	11.27	15.53	17.13	0	0	0	0	0	0	0	0	0	0	0	29	37	46	55	56	50	
7	.004	10.51	7.34	11.79	15.10	17.00	0	0	0	0	0	0	0	0	0	0	0	38	41	44	45	47	45	
8	.164	17.56	18.04	11.24	14.75	16.91	13.20	12.56	12.40	12.15	12.13	12.10	9.73	9.80	9.53	9.54	9.47	9.49	45	49	50	52	53	52
9	.318	27.85	26.26	17.33	14.42	16.71	19.12	17.92	17.69	17.28	17.12	17.02	9.59	9.78	9.42	9.44	9.35	9.34	138	157	168	184	192	196
10	.457	34.67	31.87	16.02	14.38	16.41	23.53	22.06	21.48	20.78	20.41	20.24	9.05	9.16	8.97	9.35	8.90	8.89	246	284	313	347	364	374
11	.542	41.85	34.91	18.66	14.70	16.23	26.27	24.54	23.74	22.96	22.56	22.46	8.71	8.65	8.55	9.62	8.53	8.50	212	243	264	286	297	316
12	.582	46.57	38.12	21.52	15.39	16.11	27.65	25.96	25.11	24.45	24.00	23.91	8.11	8.22	8.15	10.25	8.12	8.09	209	239	259	281	289	299
13	.535	48.71	39.78	23.96	16.32	16.06	28.68	26.99	26.16	25.49	24.99	24.90	8.02	8.09	8.10	11.27	8.05	7.92	198	226	245	264	274	284
14	.568	51.65	42.05	25.86	17.30	16.11	30.18	28.52	27.69	27.04	26.56	26.46	7.64	7.85	7.94	12.38	7.74	7.65	208	241	263	286	298	311
15	.535	47.32	39.95	27.16	18.52	15.83	31.12	29.54	28.73	28.01	27.60	27.42	7.15	7.29	7.24	13.46	7.14	7.02	191	221	241	262	273	282
16	.407	47.86	38.59	27.99	19.57	16.45	31.11	29.75	29.04	28.48	28.16	28.04	6.98	7.06	6.99	14.65	6.88	6.79	195	226	245	267	275	286
17	.331	47.96	35.95	28.09	20.49	16.60	31.08	29.93	29.18	28.86	28.56	28.42	7.09	7.00	6.69	15.87	6.83	6.73	212	246	275	296	305	325
18	.153	38.67	33.58	27.49	21.19	17.06	29.93	29.13	28.82	28.50	28.31	28.25	7.39	7.29	7.24	16.73	7.17	7.08	184	216	238	262	276	283
19	-0.071	27.96	29.62	26.43	21.64	17.42	26.61	26.48	26.60	26.59	26.55	26.54	8.77	8.77	8.75	17.30	8.68	8.62	218	259	282	300	300	363
20	-0.033	21.31	23.97	24.74	21.81	17.76	22.97	23.21	23.62	23.89	24.01	24.08	9.30	9.35	9.35	16.65	9.33	9.28	177	212	241	277	286	307
21	-0.096	16.13	19.04	23.36	21.71	18.04	18.81	19.38	20.29	21.02	21.39	21.68	9.39	9.46	9.41	15.53	9.51	9.50	87	108	126	144	154	158
22	-0.073	11.83	14.39	21.43	21.37	18.24	13.17	13.48	14.34	15.01	15.61	16.11	9.08	9.14	9.14	12.59	9.18	9.21	59	77	89	110	122	130
23	-0.076	3.55	11.82	19.97	20.91	18.39	11.53	11.73	12.61	13.52	14.29	14.92	9.11	9.26	9.36	12.17	9.40	9.37	74	92	110	130	146	148
0	-0.074	3.55	10.63	13.33	20.50	18.46	10.30	10.54	11.37	12.57	13.39	14.01	9.07	9.14	9.20	11.71	9.36	9.30	0	0	0	0	0	0

Table II-3. Microclimate measurements at the pumice site, 4 September 1969.

HR	Q* LY/MIN 100CM	SOIL TEMPERATURES DEGREES C					AIR TEMPERATURES DEGREES C						VAPOR PRESSURE MILLIBARS						WINDSPEED CM/SEC					
		SURFACE	2CM	5CM	10CM	20CM	20CM	40CM	80CM	160CM	240CM	320CM	20CM	40CM	80CM	160CM	240CM	320CM	20	40	90	160	240	320
1	-0.072	-6.15	-3.49	1.31	14.81	15.69	-6.45	-5.96	-4.81	-3.90	-3.34	-2.90	4.66	3.77	4.29	4.49	4.57	4.60	37	48	55	58	62	68
2	-0.069	-7.88	-4.83	9.26	14.22	15.58	-7.46	-7.42	-6.89	-5.66	-4.86	-4.48	3.43	3.47	3.58	3.89	4.10	4.27	33	45	57	70	72	82
3	-0.067	-9.13	-5.75	8.33	13.62	15.44	-8.27	-8.15	-7.39	-6.34	-5.72	-5.43	3.22	3.21	3.43	3.74	3.89	4.04	32	42	46	56	53	62
4	-0.065	-9.59	-6.70	7.51	13.06	15.28	-9.82	-9.65	-8.98	-8.18	-7.30	-6.51	2.92	2.94	3.08	3.39	3.58	3.80	32	41	48	57	64	75
5	-0.058	-9.61	-7.28	6.75	12.50	15.09	-9.74	-9.67	-9.22	-8.45	-7.83	-7.31	2.93	2.96	3.07	3.33	3.44	3.55	45	56	66	78	84	90
5	-0.054	-9.30	-7.23	6.33	12.13	14.96	-9.32	-9.36	-9.05	-8.43	-8.19	-7.91	2.95	2.94	3.03	3.15	3.24	3.35	41	53	62	80	85	87
7	.013	3.61	-2.73	5.63	11.38	14.66	-6.04	-6.22	-6.27	-6.35	-6.36	-6.26	3.69	3.71	3.71	3.69	3.74	3.83	31	34	35	37	38	39
8	.122	13.35	5.62	5.84	10.97	14.53	1.73	1.29	1.20	1.00	.94	.88	4.22	4.48	4.11	4.16	4.25	4.29	50	56	58	61	63	64
9	.251	25.47	13.09	7.73	10.60	14.30	10.11	9.65	9.40	9.01	8.89	9.63	4.68	4.57	4.44	4.45	4.40	5.06	98	112	118	127	132	137
10	.381	32.31	18.09	10.72	10.56	14.05	14.26	13.41	12.81	12.14	11.91	11.67	5.93	5.84	5.79	5.82	5.77	5.78	188	221	241	254	277	290
11	.498	35.36	23.48	13.68	10.91	13.81	15.81	14.70	13.84	12.98	12.62	12.27	5.70	5.64	5.62	5.61	5.56	5.56	255	304	335	370	386	404
12	.557	37.73	23.31	16.30	11.54	13.63	17.43	16.19	15.25	14.18	13.87	13.50	5.42	5.32	5.28	5.30	5.23	5.22	235	280	316	334	350	365
13	.596	37.71	24.95	18.49	12.38	13.51	19.00	17.68	16.68	15.54	15.12	14.72	5.69	5.57	5.56	5.56	5.50	5.50	318	382	421	468	493	517
14	.565	38.48	26.46	20.02	13.36	13.49	19.72	18.40	17.41	16.41	16.03	15.70	5.68	5.57	5.58	5.54	5.49	5.51	281	336	370	417	428	447
15	.491	35.95	26.96	21.21	14.33	13.55	19.58	18.35	17.56	16.56	16.30	16.10	6.12	5.98	5.92	5.90	5.85	5.89	249	297	327	362	377	395
16	.396	31.78	25.15	21.79	15.22	13.69	19.12	18.04	17.28	16.41	16.10	15.80	6.27	6.15	6.12	6.08	6.03	6.06	293	354	393	435	456	478
17	.257	25.66	22.21	21.60	15.96	13.88	17.43	16.71	16.19	15.49	15.27	15.04	5.94	5.82	5.78	5.74	5.70	5.72	299	359	401	448	472	494
18	.090	19.33	19.64	20.57	16.46	14.10	15.81	15.44	15.21	14.79	14.66	14.47	5.63	5.52	5.49	5.43	5.41	5.39	268	323	364	409	433	460
19	-0.072	11.79	14.91	19.09	16.68	14.37	12.68	12.77	12.87	12.89	12.90	12.86	5.65	5.59	5.58	5.51	5.49	5.50	229	279	316	360	381	403
20	-0.125	7.00	9.14	17.24	16.65	14.59	9.12	9.46	9.76	10.22	10.37	10.44	5.69	5.70	5.75	5.67	5.66	5.68	138	164	197	220	226	265
21	-0.115	3.21	6.10	15.47	16.36	14.77	5.79	6.27	6.80	7.44	7.89	8.15	5.76	5.73	5.74	5.73	5.74	5.72	91	121	141	179	199	213
22	-0.099	-1.31	2.12	13.90	15.90	14.89	1.06	1.61	2.45	3.62	4.31	4.86	5.06	5.13	5.22	5.27	5.33	5.41	52	66	79	88	100	85
23	-0.090	-2.19	.41	12.63	15.93	15.72	-0.37	.14	1.15	2.94	3.95	4.55	4.87	5.43	5.03	5.25	5.59	5.58	78	104	135	175	195	212
0	-0.085	-3.57	-1.07	11.75	15.54	15.77	-2.83	-2.45	-1.56	-0.70	-0.05	.30	4.24	5.62	4.39	4.54	4.68	4.74	0	0	0	0	0	0

APPENDIX III

Analytical Equations

This section details computational relationships by which micrometeorological data is obtained from voltage (V) and pulse count measurements, and how this data is employed for the estimation of the energy fluxes. The symbols used in this section are consistent with the text and are defined elsewhere. Duplication is avoided in instances where computational technique has been explained in the text.

Basic Data

1. Radiation flux density.

$$a) Q^* = (V/a)_{Q^*}$$

$$b) K\downarrow = (V/a)_{K\downarrow}$$

$$c) K\uparrow = (V/a)_{K\uparrow}$$

$$d) (K\downarrow + L\uparrow) = (V/a)_{(K\downarrow + L\downarrow)} + \sigma(T_h + 273.16)^4$$

2. Temperature.

a) $T = V/n(V/n(0.0438V/n - 0.4377) + 22.7) + T_r$ is a cubic polynomial fitting a standard Celsius conversion table for compensated copper-constantan thermocouples, where V is entered in millivolts below the reference and n is the number of series connected thermocouples.

- b) For the hemisphere temperature, T_h , on a pyrrometer (see 1.d), above) and for soil temperature, T ,
 $n = 1$.
- c) For the dry-bulb temperature, T_d , $n = 2$.
- d) And, since the wet-bulb temperature depends upon four junctions between the dry- and wet-bulbs, as well as two junctions for the dry-bulb, the relationship becomes:

$$T_w = \left(\frac{V_d}{2} + \frac{V_w}{4}\right) \left(\frac{V_d}{2} + \frac{V_w}{4}\right) (0.0438 \left(\frac{V_d}{2} + \frac{V_w}{4}\right) - 0.4377) + 22.7) + T_r$$

3. Windspeed.

- a) The anemometer provides a pulse signal each revolution. The pulses are counted and the average count rate, N , is computed for the sampled interval:
 $N = \text{total counts} / \text{length of interval in minutes.}$
- b) Two linear equations fit the manufacturer's conversion table for the anemometers:
- 1) $N \leq 210: \bar{u} = 2.501N + 13.62$
 - 2) $N > 210: \bar{u} = 2.361N + 42.61$

Derived Data

1. Surface Temperature.

See text Equations [3 and 4].

2. Potential Temperature (for computational purposes).

$$\theta = T_d + \Gamma z$$

3. Latent Heat of Vaporization.

$$\lambda = (597 - 0.563 T_w)$$

4. Vapor Pressure.

$$a) e = e_s - Ap(T_d - T_w)$$

$$b) e_s = 6.1078 \exp(17.269 T_w / (T_w + 237.3)),$$

Tetens formulation where $T_w > 0$ (Murray, 1967).

$$c) A = 0.697 \times 10^{-3} (1 + 1.15 \times 10^{-3} T_w)$$

Computational Models

1. Soil Heat Flux Density.

$$G = \frac{1}{2(t' - t)} \{ C_1 [(\bar{T}_S - \bar{T}_S') + (\bar{T}_1 - \bar{T}_1')] (z_1) \\ + C_2 [(\bar{T}_1 - \bar{T}_1') + (\bar{T}_2 - \bar{T}_2')] (z_2 - z_1) \\ + C_3 [(\bar{T}_2 - \bar{T}_2') + (\bar{T}_3 - \bar{T}_3')] (z_3 - z_2) \\ + C_4 [(\bar{T}_3 - \bar{T}_3') + (\bar{T}_4 - \bar{T}_4')] (z_4 - z_3) \},$$

where the prime indicates the value at the end of the averaging period.

2. Bowen Ratio.

$$\beta = C_p p (\bar{\theta}_1 - \bar{\theta}_2) / \lambda \epsilon (\bar{e}_1 - \bar{e}_2)$$

3. Uncorrected Aerodynamic Sensible Heat Flux Density.

$$H = \rho C_p k^2 (60 \text{ sec/min}) (\bar{\theta}_1 - \bar{\theta}_2) (\bar{u}_1 - \bar{u}_2) / (\ln z_1 / z_2)^2$$

4. Uncorrected Aerodynamic Latent Heat Flux Density.

$$\lambda E = \rho \lambda k^2 (60 \text{ sec/min}) (\bar{e}_1 - \bar{e}_2) (\bar{u}_1 - \bar{u}_2) / (\ln z_1 / z_2)^2$$

5. Richardson Number.

$$Ri = \left(\frac{g}{(\bar{\theta}_1 - \bar{\theta}_2)^{1/2} + 273.16} \right) \left(\frac{(\bar{\theta}_1 - \bar{\theta}_2) (z_1 z_2)^{1/2} (\ln z_1 / z_2)}{(\bar{u}_1 - \bar{u}_2)^2} \right)$$

6. Stability Correction Term.

$$\text{a) if } Ri \leq 0, \quad \phi = (1 - 34Ri)^{0.55}$$

$$\text{b) if } Ri > 0, \quad \phi = (1 + 34Ri)^{-0.55}$$

APPENDIX IV

The Uncertainty of Measurement and Analysis

A general technique for the evaluation of the uncertainties of measurements and of analyses has been used to aid in the interpretation of this research. Techniques of this type are not common in micrometeorological studies, and a method for the objective assessment of errors has long been needed. The methods employed in this section are adapted from Numerical Mathematical Analysis by Scarborough (1966). Application to the various measurement and analytical equations used in this research will be shown by way of examples. The development begins with an exposition of the basic method, and then continues with the successive assessment of the uncertainties associated with the measured micrometeorological properties. This provides a basis for the estimation of uncertainties associated with the analyses of the various energy budget components. The results of these calculations were summarized earlier in Chapter III, Table 1, Overall System Performance, and in Chapter IV, Table 2, Average Uncertainty of Flux Density Evaluation.

The Basic Relationships

A measurement or estimation, M , can be expressed in a general way as some function of the variables, y_i , which contribute

to its determination:

$$M = (y_1, y_2, \dots, y_n).$$

Errors in the variables, δy_i , produce error, δM , in the measurement, so that the determination is actually

$$M + \delta M = (y_1 + \delta y_1, y_2 + \delta y_2, \dots, y_n + \delta y_n). \quad [\text{IV-1}]$$

The measurement error, δM , can be isolated by expanding this function using Taylor's Theorem, ignoring the small terms in the series, and then subtracting Equation [IV-1], to yield:

$$\delta M = \delta y_1 \partial M / \partial y_1 + \delta y_2 \partial M / \partial y_2 + \dots + \delta y_n \partial M / \partial y_n. \quad [\text{IV-2}]$$

This is the general formula for computing the error of a function having absolute errors δy_i . It is interesting to note that this formula is the total differentiation of the function, M .

When δy_i is not considered an absolute limit but rather a randomly distributed uncertainty or probable error, the overall error, δM , is more adequately represented by a comparably derived formula based upon the principle of least squares:

$$\delta M = [(\delta y_1 \partial M / \partial y_1)^2 + (\delta y_2 \partial M / \partial y_2)^2 + \dots + (\delta y_n \partial M / \partial y_n)^2]^{1/2}. \quad [\text{IV-3}]$$

Relative error is often a useful index to the error of measurement.

The relative error of y_i is the ratio of $\delta y_i/M$. Correspondingly, the relative error of M expressed in Equation [IV-2] is

$$\begin{aligned} \delta M/M &= (\delta y_1/M)(\partial M/\partial y_1) + (\delta y_2/M)(\partial M/\partial y_2) \\ &+ \dots + (\delta y_n/M)\partial M/\partial y_n. \end{aligned}$$

When δy_i is randomly distributed as in Equation [IV-3], the relative error is

$$\begin{aligned} \delta M/M &= [(\delta y_1/M)^2(\partial M/\partial y_1)^2 + (\delta y_2/M)^2(\partial M/\partial y_2)^2 \\ &+ \dots + (\delta y_n/M)^2(\partial M/\partial y_n)^2]^{1/2} \end{aligned}$$

The following formulae illustrate some of the ways by which derivatives may be calculated:

- 1) When the functional relationship of M is a product, such as

$$M = (\text{constant})y_1^m y_2^n y_3^p,$$

then the derivatives, $\partial M/\partial y_i$, are:

$$\partial M/\partial y_1 = mM/y_1 = (\text{constant})y_1^{m-1} y_2^n y_3^p;$$

$$\partial M/\partial y_2 = nM/y_2 = (\text{constant})y_1^m y_2^{n-1} y_3^p;$$

and

$$\partial M/\partial y_3 = pM/y_3 = (\text{constant})y_1^m y_2^n y_3^{p-1}.$$

- 2) When the functional relationship is a series of sums of products, then the derivatives are calculated accordingly. For example:

$$M = y_1^3 + y_1^2 + y_1$$

$$\partial M / \partial y_1 = 3y_1^2 + 2y_1 + 1.$$

- 3) However, if the function is a sum of independent variables, then the derivatives are all equal to 1.

Measurement Considerations

The following treatment assumes that the sensor is perfectly calibrated, that it faithfully represents the property to be evaluated, and therefore the uncertainty of measurement depends on the performance of the data acquisition system. Of course, measurements are subject to both systematic and random errors. These two classes of errors contribute to the uncertainty of measurement in different ways. Systematic errors reduce accuracy, while random errors reduce precision.

In some instances the effects of systematic errors are minimized if the analysis requires only knowledge of differences in value. For example, offsets in temperature measurement due to systematic errors common to both sensors are cancelled if temperature differences are measured. Thus if the random errors are small, the

measured temperature difference may faithfully represent the true temperature difference, even though the individual measurements were quite inaccurate in absolute terms.

Measurement System Specifications

The extent to which uncertainties in measurement influence the determination of micrometeorological properties ultimately rests with the performance of the data acquisition system. The manufacturer's specifications for their equipment can be used to determine the expected performance limits. These limits can then be tested and confirmed by the user. The specifications of the system used in this study are summarized in Table IV-1.

Table IV-1. Performance specifications of the data acquisition system. *

Conditions	Accuracy	Precision
Daily calibration, Ambient temperature 24° C to 26° C, and 1/6 second per reading	±0.007% of scale ±0.004% of reading ±4 microvolts	±0.001% of scale

* VIDAR 520 Integrating Digital Voltmeter and VIDAR 610 Scanner with VISCAN 3 gold reed switches.

The total error is the sum of the errors in accuracy and in precision of measurement and depends on the voltmeter scale and on the value of the reading; thus it is not a fixed amount. Note that

accuracy is specified to be within 4 microvolts at best, regardless of scale of reading. As may be expected, the accuracy of this system is not nearly as good as its precision.

In the absence of additional confirmation of these specifications it may not be possible to distinguish between systematic and random measurement errors. Consequently, the total error in any given measurement may have to be calculated in consideration of its probability of occurrence, rather than as an absolute offset. On the other hand, if the precision of measurement is sufficiently good and test data is available it may be possible to isolate systematic errors, which will result in reduced error, particularly for comparative (difference) measurements. Because the actual magnitude of the errors remains somewhat uncertain under all conditions, they may be appropriately termed uncertainties.

In the absence of test data the expected performance limits can be calculated from specifications. The range of input signals commonly encountered is from near 0 to almost 100 mV. For a signal of 2 mV the uncertainty related to its measurement is obtained as follows:

- 1) State the voltage measurement in general terms:

$$V = f(\text{signal} + \text{accuracy term} + \text{precision term}).$$

- 2) Because the errors are not absolutely known the uncertainty is best expressed in least squares form:

$$\delta V = [(\delta \text{ signal})^2 + (\delta \text{ accuracy})^2 + (\delta \text{ precision})^2]^{1/2} .$$

3) a. If the signal is without error in representing the variable,
then $\delta \text{ signal} = 0$.

b. Decomposing δ accuracy into its parts, according to the specifications for the equipment, gives:

$$\delta \text{ accuracy} = (\delta \text{ scale} + \delta \text{ reading} + 4 \text{ microvolts}),$$

or

$$(0.00007 \times 10 \text{ mV} + 0.00004 \times 2 \text{ mV} + 0.004 \text{ mV}) = 0.00478 \text{ mV}.$$

c. Decomposing δ precision the same way gives:

$$\delta \text{ precision} = (\delta \text{ scale}) = 0.00001 \times 10 \text{ mV} = 0.0001 \text{ mV}.$$

4) The calculated total uncertainty in measuring the 2 mV signal is thus:

$$\delta V = [0 + (0.00478 \text{ mV})^2 + (0.00001 \text{ mV})^2]^{1/2} = 0.00478 \text{ mV}.$$

Note that the largest part of this uncertainty is due to the 4 microvolt (0.004 mV) inaccuracy limit.

Figure IV-1 illustrates the calculated uncertainty limit (upper curve) for the system. The jump at 30 mV is due to the change in scale of the voltmeter, which affects the least significant digit of the measurement. The lower curve will be discussed in the next section.

Measurement System Performance

Test data for evaluating the performance of the measurement system was obtained only for temperature. However, it will be shown how this data can be used to calculate the random errors of voltage

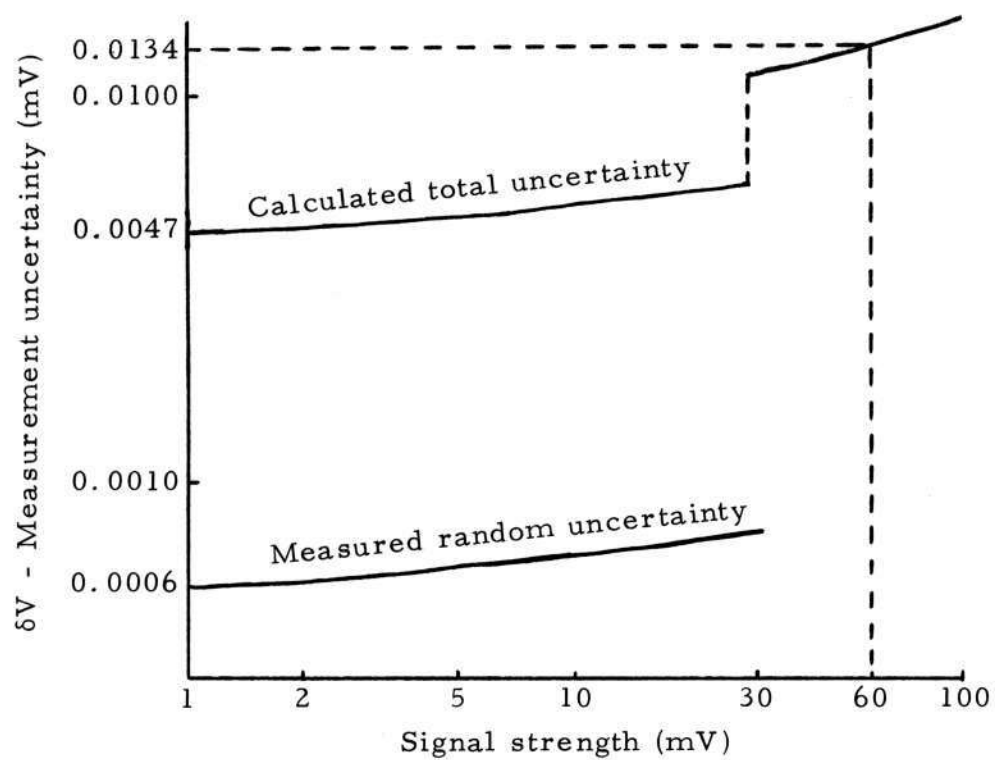


Figure IV-1. Uncertainty of voltage measurement.

measurement, for which the uncertainties inherent in most of the other measurements and analyses can be estimated.

Every temperature determination depends on the measurement of the thermocouple signal, the reference junction temperature, and the various connectors and cables through which the signal passes. Errors associated with temperature determination can originate in any one of these sources. Evaluation of these errors becomes possible when an independent temperature standard, such as an ice bath, is included in the experimental design.

For temperature determinations thermocouple voltage measurements are made with respect to a similar thermocouple junction maintained at a reference temperature. A nominal value of 65.00°C was used for this study, which was checked periodically with a high resolution mercury thermometer. Since the range of temperatures measured were below the reference temperature the polarities of the thermocouple voltage signals were made negative.

The manufacturer's specifications for the reference junction are that it will exhibit no more than $\pm 0.05^{\circ}\text{C}$ temporal variation from the set point temperature, and no more than $\pm 0.05^{\circ}\text{C}$ spatial variation between the 48 junction circuits incorporated within it. Laboratory tests have confirmed that the spatial variation is less than 0.01°C (Gay, 1972).

System performance was evaluated during field measurement,

by monitoring an ice bath with a single thermocouple (identical to the soil temperature thermocouples) which was otherwise subject to all measurement system errors. The ice was made from distilled water, then crushed and mixed with distilled water in a thermos. The equilibrium temperature of this mixture is very close to 0°C , by definition. Any differences from zero are useful in the evaluation of the prevailing systematic and random errors over the observation period.

Figure IV-2 shows a plot of the variation in the measured temperature of the ice bath as a function of time (dashed line) during the 4 September 1969 observation period. The general shape of the temperature curve appears to contain three parts:

- 1) An offset of the data from 0°C , which obviously represents the largest part of the measurement inaccuracy. This offset includes the uncertainty in knowing the actual temperature of the reference junction, the effect of any spurious voltages generated in the cables, connectors or switches in the temperature signal path, and any calibration errors in the voltmeter.
- 2) A time varying change in the offset. This part could be due to temperature effects on the above factors, including temporal changes in the reference junction.
- 3) A random scatter of the data about the regular pattern

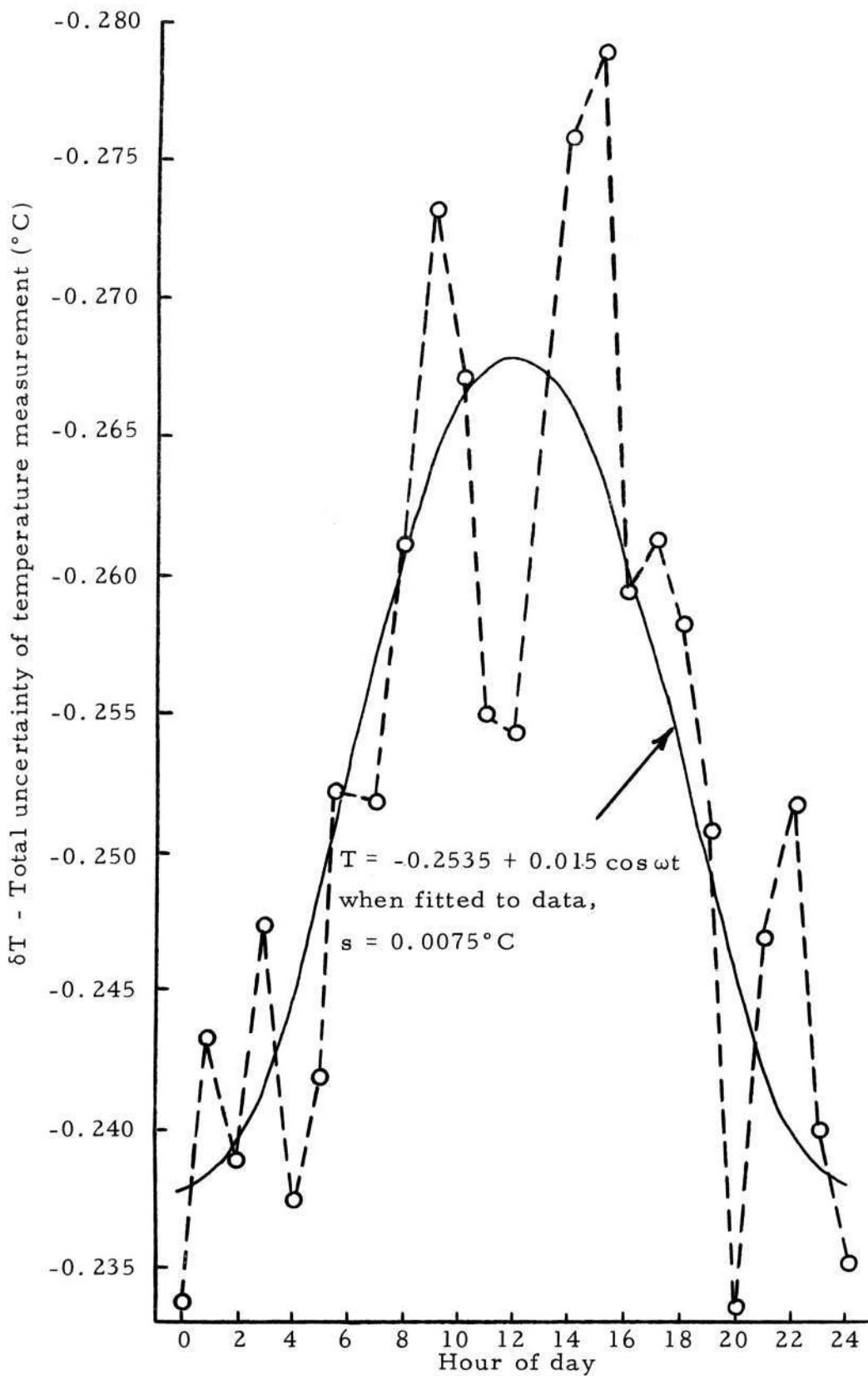


Figure IV-2. Pumice site ice bath data--4 September 1969.

described above, representing the uncertainty in measurement precision and thus the limit in system resolution.

Since the temperature of the ice bath is known (0°C) the presence of these three parts is a direct measurement of the total uncertainty of temperature determination:

$$\delta T = \text{offset error} + \text{time variation error} \\ + \text{random measurement error.}$$

The ice bath data can be fitted to a periodic function (solid line), and the offset and time-wise errors can be found as parameters in the function. The random measurement errors will be expressed by the standard deviation, s , of the data from the fitted function. Figure IV-2 suggests a trigonometric function of the form:

$$T = A + B \cos \omega t + s.$$

The limit of δT corresponding to a 0.95 probability would be given by:

$$\delta T = A + B \cos \omega t + 1.96s.$$

For the ice bath data $A = -0.2535^{\circ}\text{C}$, $B = 0.015^{\circ}\text{C}$, and $s = 0.0075^{\circ}\text{C}$.

The random voltage measurement uncertainty may now be determined. The functional relationship of T as a function of V ,

in millivolts, for a single copper-constantan thermocouple is

$$T = V(V(aV-B)+c) + T_r, \quad [\text{IV-4}]$$

where $a = 0.0438$, $b = 0.4377$ and $c = 22.7$. Normally T_r would be 65.00°C , but in this case it can be regarded as also including systematic errors A and $B \cos \omega t$, which are constant at any given time.

According to Equation [IV-2] the uncertainty in the temperature measurement is:

$$\delta T = \delta V(\partial T/\partial V). \quad [\text{IV-5}]$$

Conversely:

$$\delta V = \delta T/(\partial T/\partial V).$$

Differentiating Equation [IV-4] gives:

$$\partial T/\partial V = 3aV^2 - 2bV + c \quad [\text{IV-6}]$$

Taking $\delta T = 1.96\text{ s}$, and computing $\partial T/\partial V$ over the range of voltages usually encountered shows that

$22.7^\circ\text{C/mV} \leq \partial T/\partial V \leq 26.5^\circ\text{C/mV}$. A value of 25°C/mV may be taken as typical. Solving Equation [IV-5] gives

$$\delta V = 1.96 \times 0.0075/25 = 0.00059 \text{ mV}.$$

This figure is slightly more than one-tenth as large as the

calculated uncertainty limit of 0.00478 mV presented earlier. For comparison, the measured value of this uncertainty is drawn as the lower curve of Figure IV-1. This indicates that a significant portion of the uncertainty is systematic in nature. It is of interest to note that the difference is close to the 4 microvolt accuracy specification listed on Table IV-1. Therefore, this larger portion of the uncertainty becomes important mainly when the absolute value must be known, and may be relatively unimportant when differences in value are of primary interest.

Uncertainty of Radiation Determinations

Unfortunately, it was not possible to have test data on a voltage standard. As a result the uncertainty calculations for radiation are based upon the total expected uncertainty as calculated from the measurement system specifications. It will be seen that the uncertainty of radiation determinations is quite small, anyway.

Most of the radiant flux density estimates are made by applying a calibration coefficient to the simple measurement of the voltage output of the sensor in order to transform the reading into appropriate units. The procedure for Q_{\uparrow} is similar, except that another term must be included to compensate for the radiation from the heat sink on the underside of the instrument.

The uncertainty of the net radiometer for typical midday

conditions is:

Given 1) $Q^* = (V/a)_{Q^*}$,

and 2) $Q^* = 1 \text{ cal/cm}^2 \text{ min}$, $a = 60 \text{ mV cm}^2 \text{ min/cal}$,

$V = 60 \text{ mV}$, and $\delta V = 0.0134 \text{ mV}$ (see Figure IV-1).

The uncertainty of Q^* is $\delta Q^* = \delta V(\partial Q^*/\partial V)$, and $\partial Q^*/\partial V = 1/a$,
 $\delta Q^* = 0.013 \times 1/60 = 0.00022 \text{ cal/cm}^2 \text{ min}$, or $\delta Q^*/Q^* = 0.022\%$.

Figure IV-3 graphically depicts the measurement uncertainty as developed on a plot of the instrument response curve.

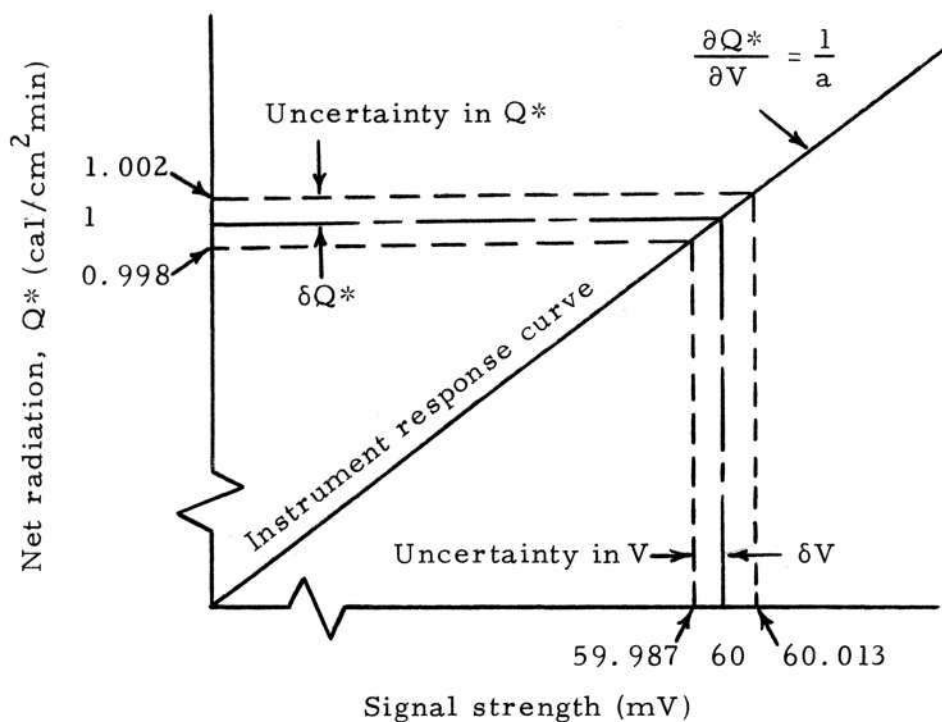


Figure IV-3. Measurement uncertainty of net radiation for an instrument having calibration coefficient, a , of $60 \text{ mV cm}^2 \text{ min/cal}$.

Similar calculations for $K\downarrow$ and $K\uparrow$ suggest their relative error to be slightly larger ($\approx 0.05\%$) primarily because of smaller values of the calibration coefficient, a , for the instruments used.

The allwave incoming flux density, $Q\downarrow = K\downarrow + L\downarrow$, results from the relationship

$$Q\downarrow = (V/a)_{Q\downarrow} + L(T_h),$$

where $L(T_h)$ is the compensation term for longwave radiation to the underside of the instrument. Therefore, for this measurement the uncertainty of $Q\downarrow$ can be written

$$\delta Q\downarrow = \{[\delta V(\partial Q\downarrow/\partial V)]^2 + [\delta T_h(\partial L/\partial T_h)]^2\}^{1/2},$$

where, from the Stefan-Boltzmann law,

$$L = \sigma(T_h + 273.16)^4 \text{ cal/cm}^2 \text{ min},$$

and

$$\partial L/\partial T_h = 4\sigma(T_h + 273.16)^3 \text{ cal/cm}^2 \text{ min } ^\circ\text{C}.$$

If $Q\downarrow = 1.8 \text{ cal/cm}^2 \text{ min}$, $a = 60 \text{ mV cm}^2 \text{ min/cal}$, $T_h = 25^\circ\text{C}$ and $\delta T_h = -0.25^\circ\text{C}$, the result is $\delta Q\downarrow = 0.0008 \text{ cal/cm}^2 \text{ min}$, or about 0.04%.

The radiometric surface temperature is based upon the relationship

$$L\uparrow = Q\downarrow - K\uparrow - Q^*.$$

Consequently, the uncertainty is

$$\delta L \uparrow = [(\delta Q \downarrow)^2 + (\delta K \uparrow)^2 + (\delta Q^*)^2]^{1/2} \approx 0.0009 \text{ cal/cm}^2 \text{ min.}$$

A typical value for $L \uparrow$ is $0.65 \text{ cal/cm}^2 \text{ min.}$, so that the relative error is around 0.15%. Employing the Stefan-Boltzmann law the surface temperature is

$$TS + 273.16 = (L \uparrow / \epsilon \sigma)^{1/4},$$

and the uncertainty is

$$\begin{aligned} \delta TS &= \delta L \uparrow (\partial TS / \partial L \uparrow) = (0.0009 \times 298) / (4 \times 0.65) \\ &\approx 0.10^\circ \text{C.} \end{aligned}$$

If the surface emissivity is 0.9, then $L \uparrow$ is only 0.58, and the uncertainty increases to 0.11°C.

Uncertainty of the Temperature and Vapor Pressure Measurements

It has previously been shown that the measured temperature using a single thermocouple may be in error by as much as $-0.2535 \pm 0.015 \pm 0.0075(1.96)^\circ \text{C.}$ This uncertainty estimate is not applicable in instances where temperature differences are of interest. This is due to the systematic errors in the measurement, which cancel out unless the differences are taken over time. The random errors must be treated in least squares fashion, however:

$$\begin{aligned}
\delta(T_1 - T_2) &= \delta T_1 - \delta T_2 \\
&= (A+B \cos \omega t + 1.96s)_1 - (A+B \cos \omega t + 1.96s)_2 \\
&= [(1.96s_1)^2 + (1.96s_2)^2]^{1/2} \\
&= 0.021^\circ \text{C}.
\end{aligned}$$

Over periods of an hour the maximum difference in the $B \cos \omega t$ term is 0.006°C , which could increase the uncertainty to 0.027°C , if not taken into account (see Figure IV-2).

Dry-Bulb Temperatures

When the sensor employs two series-connected thermocouples, as in the dry-bulb instrument, the uncertainty changes because the response curve is different. The functional relationship for the dry-bulb sensor using two thermocouples is:

$$T_d = (V/2)[(V/2)(a(V/2) - b) + c] + T_r .$$

The derivative of this relationship is

$$\partial T_d / \partial V = (1/8)(3aV^2 - 4bV + 4c) .$$

The value of this derivative is close to 12.5°C/mV for typical values of V , and is only half that of a single junction thermocouple. Thus, the random uncertainty of the dry-bulb measurement (see Equation [IV-5]) is:

$$\begin{aligned}\delta T_d &= \delta V(\partial T_d / \partial V) \\ &= 0.00059(12.5) = 0.0074^\circ \text{C},\end{aligned}$$

the value of δV having been calculated on page 125.

For two such sensors the random uncertainty in knowing their temperature difference is:

$$\begin{aligned}\delta(T_1 - T_2) &= [(\delta T_1)^2 + (\delta T_2)^2]^{1/2} \\ &= \sqrt{2}(0.0074) = 0.010^\circ \text{C}.\end{aligned}$$

Wet-Bulb Temperature. The wet-bulb temperature depends on 4 series-connected thermocouples referenced to the dry-bulb temperature. The functional relationship for the wet-bulb is:

$$T_w = (V/4)[(V/4)(a(V/4)-b)+c] + T_d,$$

and its derivative is:

$$\partial T_w / \partial V = (1/64)(3aV^2 - 8bV + 16c).$$

Typically, $\partial T_w / \partial V = 5.8^\circ \text{C mV}$ as a result of the greater voltage output of the 4-junction thermocouple. The random uncertainty of wet-bulb measurement would be:

$$\begin{aligned}
\delta T_w &= [(\delta V(\partial T_w / \partial V))^2 + (\delta T_d)^2]^{1/2} \\
&= [(\delta V(\partial T_w / \partial V))^2 + (\delta(\partial T_d / \partial V))^2]^{1/2} \\
&= [(0.00059 \times 5.8)^2 + (0.00059 \times 12.5)^2]^{1/2} \\
&= 0.0081^\circ \text{C}.
\end{aligned}$$

Vapor Pressure. Vapor pressure, e , determinations depend upon the measured wet- and dry-bulb temperatures. For flux analysis only vapor pressure differences are used, so that the random uncertainties of the dry-bulb (0.0074°C) and wet-bulb (0.0081°C) are of primary interest.

The vapor pressure of water in the air is given by the relationship:

$$e = e_s - Ap(T_d - T_w), \quad [\text{IV-7}]$$

where

$$e_s = 6.1078 \exp(17.269T_w / (T_w + 237.3)),$$

and

$$A = 0.697 \times 10^{-3} (1 + 1.15 \times 10^{-3} T_w).$$

In general form, the random uncertainty of a vapor pressure determination would be:

$$\delta e = [(\delta T_w (\partial e / \partial T_w))^2 + (\delta T_d (\partial e / \partial T_d))^2]^{1/2}.$$

The necessary derivatives, from Equation [IV-7], are:

$$\frac{\partial e}{\partial T_w} = \frac{6.1078[\exp(17.269T_w)/(T_w + 237.3)](17.269 \times 237.3)}{T_w^2 + 2T_w \cdot 237.3 + (237.3)^2} + Ap$$

$$\simeq 0.442 \exp(17T_w/247) + 1.09$$

$$\simeq 1.72 \text{ mb}/^\circ\text{C};$$

and

$$\partial e/\partial T_d \simeq -Ap \simeq -1.09 \text{ mb}/^\circ\text{C}.$$

The resultant uncertainty is:

$$\delta e = [(0.0081 \times 1.72)^2 + (0.0074 \times (-1.09))^2]^{1/2}$$

$$= 0.016 \text{ mb},$$

and the corresponding random uncertainty of a difference in vapor pressure determination would be:

$$\delta(e_1 - e_2) = [(\delta e_1)^2 + (\delta e_2)^2]^{1/2}$$

$$= \sqrt{2}(0.016) = 0.023 \text{ mb}.$$

Uncertainty of the Soil Heat Flux Analysis

The evaluation for soil heat flux, G , uses measured soil (T) and surface (T_S) temperatures. The uncertainty of the soil heat flux evaluation is thus related to the uncertainty of these measurements. The evaluation also depends upon knowledge of the volumetric heat capacity (C) of the soil and of the placement (z) of the

sensors from the surface. As has already been stated, it is assumed, for purposes of this discussion, that constants such as these are known without error.

Essentially, the soil heat flux analysis used in this study consists of computing the rates of transfer across four soil layers, which are then added to give the total:

$$G = G_1 + G_2 + G_3 + G_4.$$

The determination of G_i at each level requires two temperature difference measurements taken over time in addition to the appropriate constants. The determination of G_1 uses surface temperature measurements, for which the uncertainty of the difference over time is: $\delta(\Delta T) = 0.14^\circ\text{C}$. The remaining computations use soil temperature measurements which have a maximum uncertainty of a difference determination over time of: $\delta(\Delta T) = 0.027^\circ\text{C}$.

The above relationship for soil heat flux theoretically extends to the depth beyond which no energy is transferred. Thus, at the lowest level $\Delta T = 0$, so that the following uncertainty equation has only one difference determination associated with the last term:

$$\begin{aligned} \frac{\delta G}{G} = & \left[\left(\frac{\delta(\Delta TS)}{G} \frac{\partial G_1}{\partial \Delta TS} \right)^2 + \left(\frac{\delta(\Delta T)}{G} \frac{\partial G_1}{\partial \Delta T_1} \right)^2 \right]^{1/2} \\ & + \left[\left(\frac{\delta(\Delta T)}{G} \frac{\partial G_2}{\partial \Delta T_1} \right)^2 + \left(\frac{\delta(\Delta T)}{G} \frac{\partial G_2}{\partial \Delta T_2} \right)^2 \right]^{1/2} \\ & + \left[\left(\frac{\delta(\Delta T)}{G} \frac{\partial G_3}{\partial \Delta T_2} \right)^2 + \left(\frac{\delta(\Delta T)}{G} \frac{\partial G_3}{\partial \Delta T_3} \right)^2 \right]^{1/2} \\ & + \left[\frac{\delta(\Delta T)}{G} \frac{\partial G_4}{\partial \Delta T_3} \right]. \end{aligned}$$

This equation simplifies in form, showing that the apportioning term, $|G_1/G|$, can be factored out of each term in square brackets:

$$\begin{aligned} \frac{\delta G}{G} = & \frac{G_1}{G} \left[\left(\frac{\delta(\Delta TS)}{\Delta TS} \right)^2 + \left(\frac{\delta(\Delta T)}{\Delta T_1} \right)^2 \right]^{1/2} + \frac{G_2}{G} \left[\left(\frac{\delta(\Delta T)}{\Delta T_1} \right)^2 + \left(\frac{\delta(\Delta T)}{\Delta T_2} \right)^2 \right]^{1/2} \\ & + \frac{G_3}{G} \left[\left(\frac{\delta(\Delta T)}{\Delta T_2} \right)^2 + \left(\frac{\delta(\Delta T)}{\Delta T_3} \right)^2 \right]^{1/2} + \frac{G_4}{G} \left[\frac{\delta(\Delta T)}{|\Delta T_3|} \right]. \end{aligned}$$

Other simplifications can also be made for computational purposes by factoring out $\sqrt{2} \delta(\Delta T)$ from the middle terms.

For 0900 hours of 4 Sep. 1969 the total and term wise values of the soil heat flux were: $G = -0.1022$, $G_1 = -0.0549$, $G_2 = -0.0394$, $G_3 = -0.0276$, and $G_4 = 0.0197$. The units of G are $\text{cal/cm}^2 \text{min}$. At this time the approximate temperature differences were: $\Delta TS = 12^\circ \text{C}$, $\Delta T_1 = 7.5^\circ \text{C}$, $\Delta T_2 = 2^\circ \text{C}$, and $\Delta T_3 = 0.4^\circ \text{C}$.

Computing the relative uncertainty from these values it is found that $\delta G/G \simeq 4.3\%$. This amount may be taken as nominal for the soil heat flux analysis.

The Uncertainty of the Bowen Ratio Model

Application of the Bowen ratio depends upon temperature difference measurements, vapor pressure difference measurements, net radiation measurements and soil heat flux evaluations. Thus, an increasing number of terms enter into the uncertainty calculation as flux analysis proceeds. These introduce not only the uncertainty of knowing the micrometeorological properties, but also the functional dependence of the flux on these properties as depicted by the model.

The Bowen ratio is calculated:

$$\beta = (pC_p / \lambda \epsilon)(\Delta \theta / \Delta e).$$

The random uncertainty of the Bowen ratio is:

$$\delta \beta = \{ [(\delta(\Delta \theta)(\partial \beta / \partial \Delta \theta))]^2 + [\delta(\Delta e)(\partial \beta / \partial \Delta e)]^2 \}^{1/2}.$$

The random uncertainties of the temperature and vapor pressure differences were calculated earlier as:

$$\delta(\Delta \theta) = 0.010^\circ \text{C},$$

and

$$\delta(\Delta e) = 0.023 \text{ mb.}$$

The derivatives of β with respect to $\Delta\theta$ and Δe are simply:

$$\partial\beta/\partial\Delta\theta = \beta/\Delta\theta,$$

and

$$\partial\beta/\partial\Delta e = \beta/\Delta e.$$

Latent heat transfer is calculated according to this relationship when using the Bowen ratio:

$$\lambda E = -(Q^*+G)/(1+\beta).$$

The random uncertainty of this calculation would taken the form:

$$\delta\lambda E = [(\delta Q^* \frac{\partial\lambda E}{\partial Q^*})^2 + (\delta G \frac{\partial\lambda E}{\partial G})^2 + (\delta\beta \frac{\partial\lambda E}{\partial\beta})^2]^{1/2}.$$

The necessary derivatives are:

$$\partial\lambda E/\partial Q^* = -1/(1+\beta),$$

$$\partial\lambda E/\partial G = -1/(1+\beta),$$

and

$$\partial\lambda E/\partial\beta = (Q^*+G)/(1+\beta)^2.$$

The uncertainty equation can be stated:

$$\delta\lambda E = \frac{1}{1+\beta} [(\delta Q^*)^2 + (\delta G)^2 + (\delta\beta)^2 \frac{(Q^*+G)^2}{(1+\beta)^2}]^{1/2} .$$

The Bowen ratio solution for sensible heat transfer is:

$$H = -(Q^*+G)\beta/(1+\beta) .$$

The development is the same as above, substituting H for λE and producing these derivatives:

$$\partial H/\partial Q^* = -\beta/(1+\beta),$$

$$\partial H/\partial G = -\beta/(1+\beta),$$

and

$$\partial H/\partial\beta = -(Q^*+G)/(1+\beta)^2 .$$

The uncertainty equation for sensible heat transfer becomes:

$$\delta H = \frac{1}{1+\beta} [\beta^2 (\delta Q^*)^2 + \beta^2 (\delta G)^2 + (\delta\beta)^2 \frac{(Q+G)^2}{(1+\beta)^2}]^{1/2}$$

It is difficult to generalize with regard to the magnitude of the Bowen ratio uncertainties encountered at the pumice site. In relative terms it has been found that the uncertainty of the latent heat component ranged from about 10% to as much as 50% when vapor pressure differences were exceedingly small. The corresponding uncertainty range of the sensible heat component was from 3% to 15%. Average values of 30% for $\delta\lambda E/\lambda E$ and 9% for $\delta H/H$ can be taken as

representative.

The Uncertainty of the Correction Function, ϕ

The correction function depends on the stability parameter Ri , which in turn depends upon measurements of temperature and wind-speed. The form of the correction function is:

$$\phi = (1 \pm \alpha Ri)^{\pm \gamma} .$$

The uncertainty of this function is:

$$\delta\phi = |\delta Ri (\partial\phi / \partial Ri)| .$$

The uncertainty of Ri takes the form:

$$\delta Ri = \{ [\delta(\Delta\theta) \frac{\partial Ri}{\partial \Delta\theta}]^2 + [\delta(\Delta u) \frac{\partial Ri}{\partial \Delta u}]^2 \}^{1/2}$$

The derivatives of Ri are:

$$\partial Ri / \partial \Delta\theta = Ri / \Delta\theta,$$

and

$$\partial Ri / \partial \Delta u = -2Ri / \Delta u.$$

The derivative $\partial\phi / \partial Ri$ makes use of the relation:

$$\frac{d \log u}{dx} = \frac{1}{u} \frac{du}{dx} ,$$

defining $u = \phi$, and $x = Ri$:

$$1) \frac{\partial \log \phi}{\partial \phi} = \frac{1}{\phi}$$

$$2) \log \phi = \gamma \log(1 - \alpha Ri)$$

$$3) \frac{\partial [\gamma \log(1 - \alpha Ri)]}{\partial Ri} = \frac{-\gamma \alpha}{(1 - \alpha Ri)}$$

$$4) \partial \log \phi = \frac{\partial \phi}{\phi} = \frac{-\gamma \alpha \partial Ri}{(1 - \alpha Ri)}$$

$$5) \therefore \frac{\partial \phi}{\partial Ri} = \frac{-\phi \gamma \alpha}{(1 - \alpha Ri)} .$$

The entire uncertainty statement is thus:

$$\delta \phi = \left[\left(\frac{\delta(\Delta \theta) Ri}{\Delta \theta} \right)^2 + \left(\frac{\delta(\Delta u) Ri}{\Delta u} \right)^2 \right]^{1/2} \left[\frac{-\phi \gamma \alpha}{(1 - \alpha Ri)} \right] .$$

In general the uncertainty of the correction function has been found to be in the range of 1% to 2% of the value of the correction function.

The Uncertainty of the Corrected Aerodynamic Model

The stability corrected aerodynamic analysis for latent heat transfer is basically:

$$\lambda E = f(\Delta e, \Delta u, \phi).$$

A corresponding statement for sensible heat transfer is:

$$H = f(\Delta \theta, \Delta u, \phi).$$

Both of these forms assume a suitable mathematical description of micrometeorological properties with distance from the surface, and that ϕ includes correction for both profile distortion and eddy diffusivity.

The applicable uncertainty equations are:

$$\delta\lambda E = [(\delta(\Delta e) \frac{\partial\lambda E}{\partial\Delta e})^2 + (\delta(\Delta u) \frac{\partial\lambda E}{\partial\Delta u})^2 + (\delta(\phi) \frac{\partial\lambda E}{\partial\phi})^2]^{1/2} .$$

and

$$\delta H = [(\delta(\Delta\theta) \frac{\partial H}{\partial\Delta\theta})^2 + (\delta(\Delta u) \frac{\partial H}{\partial\Delta u})^2 + (\delta(\phi) \frac{\partial H}{\partial\phi})^2]^{1/2} .$$

The derivatives are simply formed:

$$\begin{aligned} \frac{\partial\lambda E}{\partial\Delta e} &= \frac{\lambda E}{\Delta e} & \frac{\partial H}{\partial\Delta\theta} &= \frac{H}{\Delta\theta} \\ \frac{\partial\lambda E}{\partial\Delta u} &= \frac{\lambda E}{\Delta u} & \frac{\partial H}{\partial\Delta u} &= \frac{H}{\Delta u} \\ \frac{\partial\lambda E}{\partial\phi} &= \frac{\lambda E}{\phi} & \frac{\partial H}{\partial\phi} &= \frac{H}{\phi} . \end{aligned}$$

As a result of these derivatives it is seen that the relative uncertainty is quite readily determined:

$$\frac{\delta\lambda E}{\lambda E} = [(\frac{\delta(\Delta e)}{\Delta e})^2 + (\frac{\delta(\Delta u)}{\Delta u})^2 + (\frac{\delta(\phi)}{\phi})^2]^{1/2} .$$

and

$$\frac{\delta H}{H} = [(\frac{\delta(\Delta\theta)}{\Delta\theta})^2 + (\frac{\delta(\Delta u)}{\Delta u})^2 + (\frac{\delta(\phi)}{\phi})^2]^{1/2} .$$

For the conditions of the pumice site it has been found that the uncertainty in the latent heat flux evaluation averages about 25%. For sensible heat an average figure of 3% or less is representative.